

**UCLA**

**UCLA Electronic Theses and Dissertations**

**Title**

NFκB RelA dynamic control in early B lymphopoiesis and aging

**Permalink**

<https://escholarship.org/uc/item/6mv359fs>

**Author**

Lin, Yu-Sheng

**Publication Date**

2019

Peer reviewed|Thesis/dissertation

UNIVERSITY OF CALIFORNIA

Los Angeles

NF $\kappa$ B RelA dynamic control in early B lymphopoiesis and aging

A dissertation submitted in partial satisfaction of  
the requirement for the degree Doctor of Philosophy  
in Microbiology, Immunology, and Molecular Genetics

by

Yu-sheng Lin

2019

©Copyright by

Yu-sheng Lin

2019

## ABSTRACT OF THE DISSERTATION

NF $\kappa$ B RelA dynamic control in early B lymphopoiesis and aging

by

Yu-sheng Lin

Doctor of Philosophy in Microbiology, Immunology, and Molecular Genetics

University of California, Los Angeles, 2019

Professor Alexander Hoffmann, Chair

Aging and inflammation have been shown to reduce the supply of functional B-cells; the prevailing explanation is that hematopoietic differentiation decisions are skewed towards the myeloid lineage. Here, we have addressed how inflammaging may affect B-lymphopoiesis itself. Using a new NF $\kappa$ B reporter mouse, we uncovered dramatic dynamics in RelA control during early B lymphopoiesis in young but not in all aged mice. When genetically perturbing NF $\kappa$ B RelA dynamics with specific I $\kappa$ B mutants, we found severe, cell-intrinsic defects in B lymphopoiesis, that could not be attributed to a differentiation block or reduced cell survival. Careful quantification of B-lymphoid progenitors allowed us to fit a mathematical model of the differentiation pathway, which led to the seemingly paradoxical prediction – confirmed *ex vivo* – that mutant B-cell progenitors ‘rush through’

the differentiation pathway. Further analysis revealed the differentiation hypermorph leads to diminished mature cell populations given that differentiation pauses are essential for population expansion. Transcriptomic profiling at single-cell resolution revealed RelA dynamic dysregulation resulted in an accelerated progression of transcriptomic cell states that are not in sync with the classically defined progenitors and – importantly – overridden preBCR checkpoint. As this is a major quality control step to ensure proper immunoglobulin heavy chain recombination, the mutant triggers premature  $\kappa$ -light chain recombination, resulting in B-cells with nonfunctional immunoglobulin. Our findings establish a new paradigm for how aging and inflammation impact humoral immunity via dysregulation of RelA dynamics: accelerated differentiation diminishes the size and the quality of the B-cell pool available for adaptive immune responses.

The dissertation of Yu-sheng Lin is approved.

Kenneth Dorshkind

Kathrin Plath

April Pyle

Fuyuhiko Tamanoi

Alexander Hoffmann, Committee Chair

University of California, Los Angeles

2019

## DEDICATION

To my family, especially my father, who has spent unconditioned love and efforts on guiding me throughout education and life. Your ethics and perseverance have always inspired me.

To my wife, who always brings laughter to me and stands with me no matter any adversity in life. You have supported and motivated me to be a better man. Thank you for the patience and the faith in me.

To my grandparents, Chuan-gong Lin and Bao-chin Lin- Tsai, who had endured war and poverty but still believed knowledge and education are the key to a better life. They devoted themselves in making it happen. May they rest in peace.

To Dr. Ning-sun Yang, who advised me during the time I was an undergraduate student, you have educated me on the social responsibilities of being a scientist and the importance of critical thinking. Thank you for enlightening me in the scientific career.

To my thesis advisor, Dr. Alexander Hoffmann, who has always impressed me with constant passion in science and rigorous standards before reaching scientific conclusion.

Thank you for the training and the confidence in me.

## TABLE OF CONTENTS

ABSTRACT OF THE DISSERTATION .....	ii
COMMITTEE PAGE .....	iv
DEDICATION .....	v
TABLE OF CONTENTS.....	vi
LIST OF FIGURES .....	viii
LIST OF SUPPLEMENTARY TABLES .....	x
ACKNOWLEDGEMENTS .....	xi
VITA.....	xiii
Chapter 1: General Introduction.....	1
Hematopoiesis, aging, and inflammation.....	2
B lymphopoiesis in mouse bone marrow .....	2
Checkpoints in early B lymphopoiesis.....	5
NF $\kappa$ B signaling systems .....	6
NF $\kappa$ B and early B lymphopoiesis .....	8
Focus of study .....	9
Chapter 2: NF $\kappa$ B RelA dynamic control in early B lymphopoiesis and aging .....	10
Abstract.....	11
Results.....	13
RelA protein expression is dynamically regulated during the early stages of healthy B lymphopoiesis .....	13
Genetic dysregulation of RelA dynamics leads to severe B lymphopenia.....	18
RelA dynamics control early B lymphopoiesis in a cell lineage-intrinsic manner.....	24
Unbiased, quantitative phenotyping with a mathematical model of early lymphopoiesis .....	27

<i>Ex vivo</i> differentiation system confirms model predictions of accelerated differentiation .....	32
Single-cell RNAseq analysis reveals uncoordinated progression of transcriptomic states .....	34
Immunoglobulin expression profiling reveals that RelA dysregulation overrides the pre-BCR developmental checkpoint .....	38
Discussion .....	41
Supplementary tables .....	44
Material and methods .....	58
Material details .....	58
Method details .....	59
Key resource table .....	72
Acknowledgement .....	80
Chapter 3: Conclusion and Future Directions .....	81
Conclusion .....	82
Future Directions .....	84
References .....	86

## LIST OF FIGURES

Figure 1. Stages of B lymphopoiesis in mouse bone marrow. ....	3
Figure 2. Overview of NFκB signaling. ....	6
Figure 3. Comparison between canonical and non-canonical NFκB signaling. I .....	8
Figure 4. NFκB RelA protein expression is dynamically regulated along the stages of early B lymphopoiesis. ....	14
Figure 5. NFκB RelA dysregulation during aging correlates with reduced bone marrow B cell output. ....	16
Figure 6. RelA protein is differentially expressed in Fraction B between normal and dysregulated RelA group in aging. ....	17
Figure 7. Genetic dysregulation of RelA dynamics leads to severe B lymphopenia in the spleen. ....	19
Figure 8. Genetic dysregulation of RelA dynamics leads to severe B lymphopenia originating in the bone marrow. ....	21
Figure 9. The developmental phenotype caused by dysregulated RelA is bone marrow cell-intrinsic. ....	25
Figure 10. The developmental phenotype caused by dysregulated RelA is not majorly contributed by bone marrow cell-extrinsic factors. ....	26
Figure 11. Dysregulation of RelA dynamics do not lead to increased apoptotic rate in Fraction C and C', while various proliferation markers do not provide quantitative and conclusive results. ....	28
Figure 12. Mathematical modeling suggests increased differentiation rates in Fraction C and Fraction C' could lead to diminished B cell outputs in mouse bone marrow with dysregulated RelA dynamics. ....	29

Figure 13. Mathematical model fitting with different homogeneous net proliferation rates also suggest increased differentiation rates in Fraction C and Fraction C' could lead to diminished B cell outputs in mouse bone marrow with dysregulated RelA dynamics.....30

Figure 14. Facilitated transition between Fraction B and Fraction D in native phenotype can be recapitulated ex vivo. ....33

Figure 15. Increased NFκB transcriptional activity by RelA dynamics dysregulation result in a Fraction B showing transcriptional signatures of later developmental stages. ....35

Figure 16. Despite the similarity in marker gene expression, clusters in *WT* and *IκBε<sup>-/-</sup>IκBβ<sup>-/-</sup>IκBa<sup>+/-</sup>RelA<sup>V/+</sup>* mouse bone marrow still shows differential gene expression patterns.....37

Figure 17. RelA dynamics dysregulation overrides the immunoglobulin heavy chain recombination checkpoint while prematurely activate immunoglobulin light chain recombination mechanism, resulting in diminished pre-B cell outputs with non-functional immunoglobulin gene expression.....39

Figure 18. Inability to finish recombination of immunoglobulin heavy chain in mouse bone marrow with dysregulated RelA dynamics is not due to deficiency in recombinase RAG2 and RAG1 expression. ....40

Figure 19. Schematics demonstrating how dysregulation in RelA dynamic controls impacts early B lymphopoiesis by rushing the Fraction B to Fraction D transition and results in diminished B cell repertoire. ....83

LIST OF SUPPLEMENTARY TABLES

Table 1. Input Progenitor Cell Number .....44

Table 2. Inferred Input Net Proliferation Rate(g) .....45

Table 3. Differentiation Rate from model fitting with progenitor cell number with inferred input net proliferation rate .....46

Table 4. Differentiation Rate from model fitting with progenitor cell number with homogeneous net proliferation rate = 0.5 .....47

Table 5. Differentiation Rate from model fitting with progenitor cell number with homogeneous net proliferation rate = 1 .....48

Table 6. Residence Time from model fitting with progenitor cell number with inferred input net proliferation rate .....49

Table 7. Residence Time from model fitting with progenitor cell number with homogeneous net proliferation rate = 0.5 .....50

Table 8. Residence Time from model fitting with progenitor cell number with homogeneous net proliferation rate = 1 .....51

Table 9. Cumulative characteristic time(AU time) of Cell Flux from model fitting with progenitor cell number with inferred input net proliferation rate.....52

Table 10. Relative cell flux rate(1/AU time) of Cell Flux from model fitting with progenitor cell number with inferred input net proliferation rate.....53

Table 11 Cumulative characteristic time(AU time) of Cell Flux from model fitting with progenitor cell number with homogenous net proliferation rate = 0.5 .....54

Table 12 Relative cell flux rate(1/AU time) of Cell Flux from model fitting with progenitor cell number with homogenous net proliferation rate = 0.5 .....55

Table 13 Cumulative characteristic time(AU time) of Cell Flux from model fitting with progenitor cell number with homogenous net proliferation rate = 1 .....56

Table 14 Relative cell flux rate(1/AU time) of Cell Flux from model fitting with progenitor cell number with homogenous net proliferation rate = 1 .....57

## ACKNOWLEDGEMENTS

Accomplishment of the dissertation and the thesis studies would not be possible without the help, encouragement, and contribution from many advisors and colleagues.

I would like to first my thesis advisor and principal investigator, Prof. Alexander Hoffmann, whose mentorship, enthusiasm in science, and support for exploring new idea have provided me a role model for my scientific career. When I first joined the lab as a volunteer in 2010, I was soon inspired by his constant excitement on scientific discoveries and how this solid excitement is able to motivate the people around to pushing forward at the frontier of systems biology.

I want to sincerely thank the members of my thesis committee, Prof. Kenneth Dorshkind, Prof. Kathrin Plath, Prof. April Pyle, and Prof. Fuyuhiko Tamanoi, for their constructive feedbacks and insightful suggestions for my thesis project.

I would also like to acknowledge the funding resource from UCLA Warsaw fellowship and National Institute of Health grant R01 AI132731 for the support on my thesis research.

I would also especially thank my colleague, Dr. Yi Liu, for being a close mentor on my thesis project and scientific training. He has taught me flow cytometry, coding, and the use of other data analysis tools, which is essential for almost all the figures in this dissertation.

I would also like to acknowledge current members in the Signaling Systems Lab: Dr. Kim Anh Ngo, who joined the graduate program the same year as I did, has provided encouragement and feedback for me to make progress toward the completion of the dissertation. Dr. Stefanie Luecke has constantly cared about the wellness of me being a graduate student and helped me proof-reading my dissertation. Dr. Diane Lefaudeux has introduced me to R and constantly helping me with troubleshooting codes. Dr. Marie Oliver

Metzig, Dr. Koushik Roy, Dr. Ying Tang, and Katherine Sheu have provided useful feedbacks in the cell fate subgroup meeting. Adewunmi Adelaja and Dr. Quen Cheng have provided insights in the clinical aspects. Dr. Catera Wilder and Xiaofei Lin have been the center of the lab community that foster positive connections in the working environment. Ning Wang and Dr. Anup Mazumder have provided critical feedback on cell signaling.

In addition to the help and company of current lab member, I would also like to acknowledge previous lab members: Emily Yu Hsin Chen, for being an old friend and colleague that helped me overcome lots of obstacles in academic or personal life. Dr. Riku Fagerlund, for showing me good science and good life can be a feasible combination. Dr. Sho Ohta, for showing me the ideal attitude for scientist: stringent analysis can lead to robust scientific discovery. Dr. Simon Mitchell, for introducing me into the world of coding, which I am still benefited from every single day. Dr. Bryce Alves and Dr. Jonathan Almaden, for introducing me to T and B cell biology field. Dr. Vincent Feng-Sheng Shih and Dr. Christine Shiang-Ling Cheng, for helping me settling down as a foreign graduate student and showing me the perseverance on pursuing good science. Dr. Max Shokirev and Dr. Paul Loriaux, for inspiring me on using computational modeling on cell fate interpretation and prediction. Dr. Karen Fortmann, Dr. Diana Rios, Dr. Rachel Tsui, Dr. Andrew Caldwell, Dr. Jeremy Davis-Turak, Dr. Kristyn Feldman, Bing Xia, and Brian Kim, for their encouragement and friendship.

## VITA

### Education

- 2011-2014 Master of Science, Department of Chemistry and Biochemistry, University of California San Diego, San Diego, California, United State of America
- 2005-2009 Bachelor of Science, Department of Life Science, National Taiwan University, Taipei, Taiwan

### Fellowships and Award

- 2018 Warsaw Fellowship, Department of MIMG, UCLA
- 2018 Top Poster Award, I3T retreat, David Geffen School of Medicine, UCLA
- 2015 Sidney Rittenberg Award, Department of MIMG, UCLA

### Publications

**Yu-sheng Lin**, Yi Liu, Ying Tang, Arnav Mehta, Jennifer K King, May Paing, Dinesh S. Rao, and Alexander Hoffmann, Age-associated dysregulation of RelA dynamics diminishes early B lymphopoiesis, *In preparation*

Yi C. Liu, **Yu-sheng Lin**, Koushik Roy, Supriya Sen, Dinesh S. Rao and Alexander Hoffmann, NF  $\kappa$  B system regulated Flt3-mediated hematopoiesis, *In preparation*

Koushik Roy, Simon Mitchell, Yi Liu, Sho Ohta, **Yu-sheng Lin**, Marie Oliver Metzigg, Stephen L Nutt and Alexander Hoffmann, The switch from B-cell proliferation to plasma cell differentiation phases requires dynamic NF  $\kappa$  B/cRel downregulation, *Immunity*,

Accepted on December 2018

Riku Fagerlund, Marcelo Behar, Karen T. Fortmann, **Y. Eason Lin**, Jesse D. Vargas, and Alexander Hoffmann, Anatomy of a negative feedback loop: the case of I $\kappa$ B $\alpha$ , J R Soc Interface. 2015 Sep 6;12(110):0262

Tsung-Feng Wu, Tony Minghung Yen, Yuanyuan Han, Yu-Jui Chiu, **Eason Y.-S. Lin** and Yu-Hwa Lo, A light-sheet microscope compatible with mobile devices for label-free intracellular imaging and biosensing, Lab Chip. 2014 Sep 7;14(17):3341-8

### **Oral Presentations**

**Yu-sheng Lin**, Yi Liu, Ying Tang, Arnav Mehta, Jennifer K King, May Paing, Dinesh S. Rao, and Alexander Hoffmann, Age-associated dysregulation of RelA dynamics diminishes early B lymphopoiesis, La Jolla Immunology Conference 2019

**Yu-sheng Lin**, Yi Liu, Arnav Mehta, Jennifer K King, May Paing, Dinesh S. Rao, and Alexander Hoffmann, RelA dynamics alter developmental pacing in early B lymphopoiesis, Immunology LA 2018

**Yu-sheng Lin**, Yi Liu, Arnav Mehta, and Alexander Hoffmann, RelA dynamics alter developmental pacing in early B lymphopoiesis, Oral Presentation, Southern California Biomedical Sciences Graduate Symposium 2017

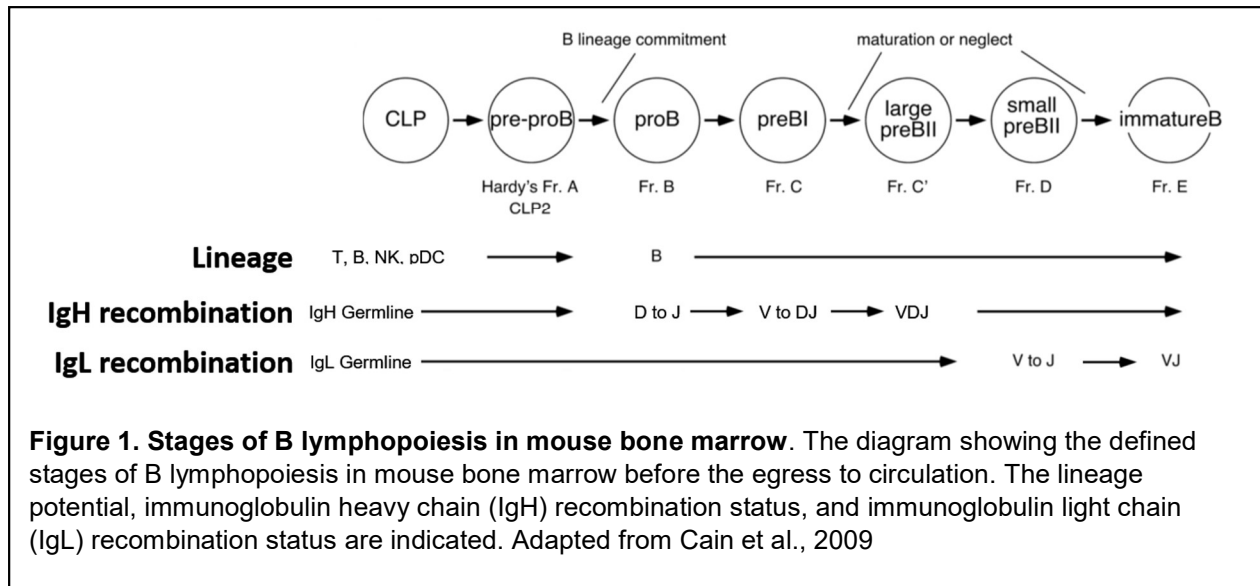
# Chapter 1: General Introduction

## **Hematopoiesis, aging, and inflammation**

Hematopoiesis is a continuous and constant process which requires the involvement of heterogeneous stem cells and progenitors that can eventually lead to outputs of differentiated effector cells in different lineages (Orkin et al., 2008; Doulatov et al., 2012; Busch et al., 2015; Pietras et al., 2015; Velten et al., 2017). Maintenance of homeostasis in hematopoietic outputs is crucial for establishing functional immune systems, while the perturbation on the homeostasis by stress such as inflammation and aging can potentially lead to diseased outcomes (Orkin et al., 2008; Chung and Park, 2017; Pietras, 2017; Haas et al., 2018). Among the generation of all lineages of immune effector cells, aging and inflammation have been shown to result in reduction in lymphoid lineage outputs and repertoire (Van der Put et al., 2003; Linton and Dorshkind., 2004; Guerrettaz et al., 2008; Cain et al., 2009; Dorshkind et al., 2009; Beerman et al., 2010a; Frasca et al., 2011; Melamed and Scott, 2012), which can be associated with reduced responsiveness to vaccination, more vulnerability to infection, and higher propensity to mortality (Larbi et al., 2008; Frasca et al., 2011; Pera et al., 2015; Ciabattini et al., 2018). The prevailing explanation for the reduction in lymphoid lineage development is that aging and inflammation bias hematopoietic development towards the myeloid lineage (Beerman et al., 2010b; Chung and Park, 2017; Pietras, 2017), however, whether aging and inflammation impact the development of naïve lymphocytes themselves in output or quality has not been clearly addressed yet.

## **B lymphopoiesis in mouse bone marrow**

B lymphopoiesis is a stringent process that consists of different checkpoints and developmental stages to ensure the output cells have functional immunoglobulin



recombination and sufficient number to augment adaptive immune responses effectively (Figure 1) (Hardy and Hayakawa, 2001; Smith and Sigvardsson, 2004; Lebien and Tedder, 2008; Welner et al., 2008; Melchers, 2015). The generation of the B lineage cells in mouse bone marrow can be traced back to a subset of hematopoietic progenitor populations: common lymphoid progenitors (CLPs). CLPs are characterized by the expression of c-Kit and Il-7 receptor  $\alpha$  chain on their cell surface without the expression of lineage-associated cell surface markers such as CD11b for myeloid lineage, B220/CD45R for B lineage, and Ter119 for erythroid lineage. CLPs still retain the potential of differentiate into B, T, NK, and plasmacytoid dendritic cell(pDC) progeny (Welner et al., 2008).

The stage right downstream of CLP begins to express only cell surface lineage marker CD45R/B220 while express HSA/CD24 in low level is defined as Fraction A or pre-pro B cells. The next stage of development, Fraction B or pro-B cell, is characterized by the expression surface CD19 and increased expression of CD24 marker. Notably, transcription factor Pax5 also begin to be expressed in Fraction B, which has been shown to be associate

with the B lineage commitment at this stage. Commitment to B lineage will also trigger the immunoglobulin heavy chain (IgH) D to J region rearrangement (Melchers, 2015).

The subsequent developmental stage Fraction C or pre-BI cells is characterized by increased surface BP-1 protein expression and the induction of immunoglobulin V to DJ rearrangement on one IgH allele. Once IgH locus is successfully recombined and transcribed, the recombination machinery, including the recombinase RAG, would be shut down to avoid the rearrangement on additional IgH allele (Hardy and Hayakawa, 2001; Melchers, 2015). The expression of the IgH protein on cell surface and the autonomous activation of pre-B cell receptor(preBCR) signaling by the interaction of IgH and surrogate light chain proteins result in the passing of the preBCR checkpoint and the transition into the next stage: Fraction C' or large pre-BII cells. Fraction C' is characterized by a slight increase in CD24 surface protein expression per cell, generally larger cell size, and rapid proliferation. The initiation of the proliferation phase is shown to be associated with the activation of Il-7 receptor signaling and pre-BCR signaling, while the latter also involves in the termination of the proliferative phase and initiation of differentiation to the next stage: Fraction D or small pre-BII cells (Clark et al., 2013).

Fraction D is characterized by the decreased surface CD43 protein expression, smaller cell size compared to Fraction C', and the rearrangement of immunoglobulin light chain V to J region. Once the IgL allele is productively rearranged and expressed, the recombination machinery will be turned off by decreasing RAG expression and proceed to the next stage: Fraction E or immature B cells. Fraction E is characterized by the expression of complete B cell receptor on cell surface and the readiness to enter circulation for further maturation in the peripheral lymph organs (Melchers, 2015).

## Checkpoints in early B lymphopoiesis

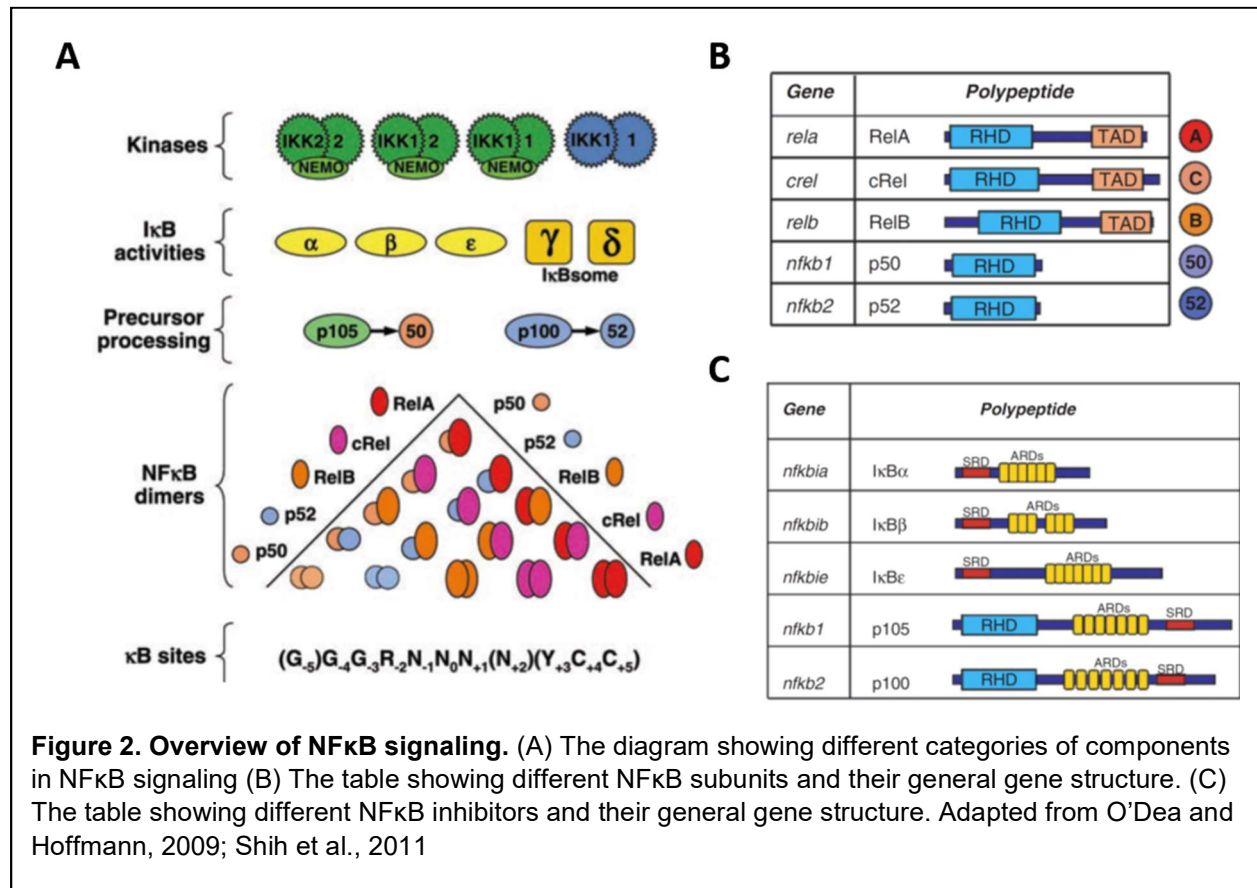
One crucial quality control step in early B lymphopoiesis is the pre-BCR checkpoint, where expressed immunoglobulin heavy chain is tested for compatibility with surrogate light chain to ensure the heavy chain recombination process is properly completed and prevent progenitors with certain self-reactive recombination from proceeding further into developmental pathway (Geier and Schlissel, 2006; Keenan et al., 2008). Once the recombined immunoglobulin heavy chain is confirmed to be good fit to the surrogate light chain, the assembled pre-BCR would trigger its downstream signaling cascade which allows the entry to proliferative phase followed by differentiation phase with the initiation of immunoglobulin  $\kappa$  light chain recombination (Mårtensson and Ceredig, 2000; Hendriks et al., 2004; Geier and Schlissel, 2006; Clark et al., 2013).

After the activation of the recombination machinery for the rearrangement of IgL V to J regions, there is another checkpoint to ensure the final IgL allele is productive and not self-reactive. If the IgL arrangement is not productive in the first attempt, the recombination machinery would stay active and enable additional recombination or even induce VH replacement on rearranged IgH chain loci. However, if the resulting IgL chain loci is still non-productive or self-reactive after additional attempts, the immature B cell would be directed toward apoptosis. As a result, this checkpoint can prevent the immature B cells carrying defective or self-reactive BCR egressing from bone marrow entering circulation (Melchers, 2015).

Since these checkpoints are critical for the control of precursor cell number and quality in early B lymphopoiesis, it would be interesting to understand how inflammation or aging affect the robustness of the checkpoint and the subsequent developmental programs.

## NFκB signaling systems

NFκB signaling systems consist of its upstream kinase such as IKK2, the inhibitors such as IκBα, and the NFκB dimers which can potentially activate transcriptional activities (Figure 2A). Upon the receive of the stimulation that activate the upstream kinase activity, the upstream kinase would phosphorylate the inhibitor protein and render the inhibitor susceptible to proteasomal degradation. With the degradation of the inhibitor, the inhibitor bound NFκB dimers are released. Some of these NFκB can then enter the nucleus and bound to specific motif and augment transcriptional activities. There are five different members of NFκB subunit: RelA, RelB, cRel, p50, and p52. Among them, RelA, RelB, and cRel contain the rel-homology domain (RHD) which enable the binding to DNA and function as transcription factors (Figure 2B). The inhibitors include IκBα, IκBβ, IκBε, p100, and

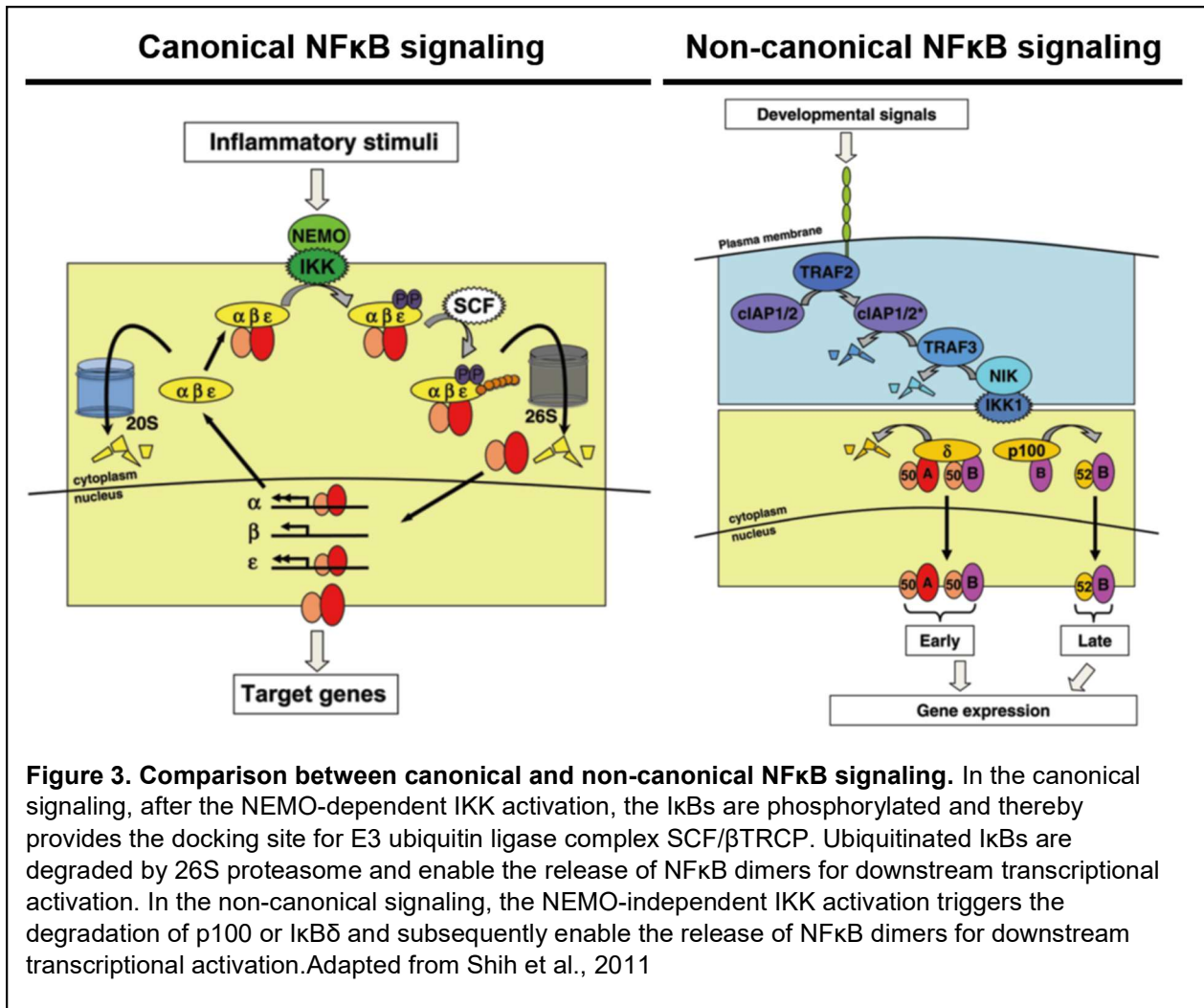


p105, which all have ankyrin repeat domains (ARDs) capable of binding to NF $\kappa$ B dimers (Figure 2C).

Based on how the stimulus signal is mediated, the signaling pathways can be further categorized into canonical signaling pathway and non-canonical signaling pathway.

Canonical NF $\kappa$ B signaling pathway is defined as the upstream signal being mediated by NEMO-dependent IKK while non-canonical NF $\kappa$ B signaling pathway is defined as NEMO-independent. The primary effectors of canonical pathway are RelA and cRel in homodimer or heterodimer with p50, which is known to activate inflammatory responses or promote cell survival. The stimuli that activate canonical signaling pathway are shown to be associated with pathogen defense or inflammation, while the non-canonical signaling stimuli are related to the development of dendritic cells and lymphoid organ (O'Dea and Hoffmann, 2009; Shih et al., 2011).

In summary, NF $\kappa$ B signaling controls and mediates cellular responses to inflammatory signals (Lawrence et al., 2009; Shih et al., 2011; Zhang et al., 2017), and recent studies also suggest potential involvement of canonical NF $\kappa$ B signaling in inflammation-associated aging and cellular senescence (Salminen et al., 2008; Franceschi and Campisi, 2008; Chien et al., 2011; Balistreri et al., 2013). Therefore, the involvement of canonical NF $\kappa$ B signaling systems in hematopoietic under aging, infection, or inflammation may worth further investigation.



## NFκB and early B lymphopoiesis

The absence of NFκB by genetic ablation has been shown to reduce fetal B lineage hematopoietic outputs and severely impact secondary lymphoid organ generation (Horwitz et al., 1997; Grossmann et al., 2002; Alcamo et al., 2002; Claudio et al., 2009). Reduction of NFκB activation by a deficiency in upstream kinase functionality or a trans-dominant inhibitor mutant has also been shown to decrease B lymphopoietic outputs and pre-B and immature B cell subsets respectively (Feng et al., 2004; Jimi et al., 2005; Balkhi et al., 2012). On the other hand, partial loss of NFκB inhibitors also lead to decreased B

lymphopoiesis in fetal liver and bone marrow (Goudeau et al., 2003; Guo et al., 2012). All these previous studies have demonstrated the importance of precise dosage requirement on NF $\kappa$ B in general B cell development, nonetheless, how NF $\kappa$ B is regulated throughout the early B lymphopoietic stages and the consequences of dysregulation remain unknown.

## **Focus of study**

Here, we have uncovered dramatic dynamic regulation in RelA during early B lymphopoiesis while the dysregulation of RelA dynamics correlates with diminished bone marrow B cell output in aging. Through the genetic perturbation with specific I $\kappa$ B mutants that alter RelA dynamics, we found that dysregulation on RelA dynamics leads to severe B lymphopenia in a cell-intrinsic manner. By using mathematical modeling of the differentiation pathway, we described the seemingly paradoxical phenomenon that a differentiation hypermorph leads to developmental deficiency of diminished population of mature cells. Transcriptomic analysis on single-cell resolution suggested that the RelA dynamic dysregulation resulted in an upregulation in NF $\kappa$ B target genes and accelerated transcriptomic states that are not in synch with the classically defined progenitor cell type. Dysregulated RelA dynamics also override the preBCR checkpoint, trigger premature  $\kappa$ -light chain recombination, and consequently result in B-cells with nonfunctional immunoglobulin. Our findings establish a new paradigm for how aging and inflammation impact humoral immunity via dysregulation of RelA dynamics: accelerated differentiation diminishes the B-cell pool and the BCR repertoire.

**Chapter 2: NF $\kappa$ B RelA dynamic control in early B  
lymphopoiesis and aging**

## **Abstract**

B lymphopoiesis is stringently regulated by checkpoints controlling the progression through developmental stages to ensure both the quantity and the diversity of the output B cells, which are critical for adaptive immune responses. Aging and inflammation have been shown to reduce both, leading to reduced responsiveness to vaccination, a diminished antibody repertoire, vulnerability to infection, and higher mortality. The prevailing explanation for the reduced lymphoid output is a skewing in cell differentiation decisions by multipotent progenitors, leading to myeloid-biased hematopoiesis. However, the molecular mechanisms underlying remain unclear.

The NF $\kappa$ B signaling system mediates cellular responses to inflammatory signals and may thus mediate the detrimental effects of inflammation. However, it is the absence of NF $\kappa$ B by genetic ablation or trans-dominant inhibition that reduces fetal B lineage hematopoietic output, severely impacts secondary lymphoid organ generation, and decreases mature B cell survival. Interestingly, the converse partial loss of NF $\kappa$ B inhibitors also leads to decreased B lymphopoiesis in fetal liver and bone marrow. These previous studies suggest that the precise control of NF $\kappa$ B is required for proper B cell development. However, how NF $\kappa$ B is regulated throughout the early B lymphopoietic stages and the consequences of dysregulation remain unknown.

In order to study how NF $\kappa$ B regulation affect early B lymphopoiesis, we have established a new knock-in mVenus-RelA fluorescent reporter mouse line to assess the RelA expression levels quantitatively and at single-cell resolution. By observing mVenus-RelA fluorescence intensity across different stages of early B lymphopoiesis with multicolor flow cytometry analysis, we have uncovered dramatic dynamics in RelA control during early B

lymphopoiesis that the downregulation of RelA protein expression coincide with major checkpoints in early B lymphopoiesis. Moreover, we found dysregulation of RelA dynamics in aged mice correlates with even further diminished bone marrow B cell output in addition to the reduction observed in normal aging.

To address whether there is a the causal relationship between RelA dynamic regulation and B lymphopoiesis, we perturbed the RelA dynamics genetically with specific I $\kappa$ B mutations and observed severe B lymphopenia in the peripheral blood and spleen, which we then traced back to the abnormal phenotypes in bone marrow progenitor and precursor B cell populations. By transplanting the bone marrow of I $\kappa$ B mutants to wild-type recipient mice and vice versa, we found that dysregulation on RelA dynamics leads to severe B lymphopenia in a cell-intrinsic manner. However, the analysis on apoptotic cell percentages and quantified cell progenitor and precursor cell counts was not compatible with the notion that the decreased B cell output from the bone marrow is caused by a survival defect or a differentiation block. As these commonly held mechanistic hypotheses did not explain the developmental phenotype, we turned to an unbiased approach by mathematically modeling the B-cell developmental pathway to interpret progenitor population data.

Quantitative fitting the data to the model revealed the seemingly paradoxical phenomenon that a differentiation hypermorph (in which developmental transitions are accelerated) leads to developmental deficiency of diminished downstream precursor population.

Simulations of the model illustrate that pauses in the differentiation pathway are essential for population expansion. As B lymphopoiesis is a continuous process, it is difficult to measure differentiation rate, timescales, or constants directly in vivo. To verify the interpretation of the modeling, we turned to an ex vivo differentiation experimental system, which has a defined differentiation starting point with purified common lymphoid

progenitors. The data indicated that the dysregulation in RelA dynamics resulted in an accelerated differentiation transition from Hardy Fraction B to D, confirming the model prediction.

To further investigate the mechanisms by which failure to downregulate NF $\kappa$ B RelA results in accelerated transitions during early B lymphopoiesis, we used single-cell RNA sequencing analysis on purified B cell progenitor/precursor populations. Transcriptomic profiling at singlecell resolution suggested that RelA dynamic dysregulation resulted in an upregulation of NF $\kappa$ B target genes and accelerated transcriptomic states that are not in sync with the classically defined progenitor cell type. Dysregulated RelA dynamics also override the pre-BCR checkpoint, a major quality control step to ensure proper immunoglobulin heavy chain recombination, thereby allowing cells to progress without having proper production of functional immunoglobulin heavy chains. Cells may sporadically undergo  $\kappa$ -light chain recombination, but these result in B-cells with nonfunctional immunoglobulin.

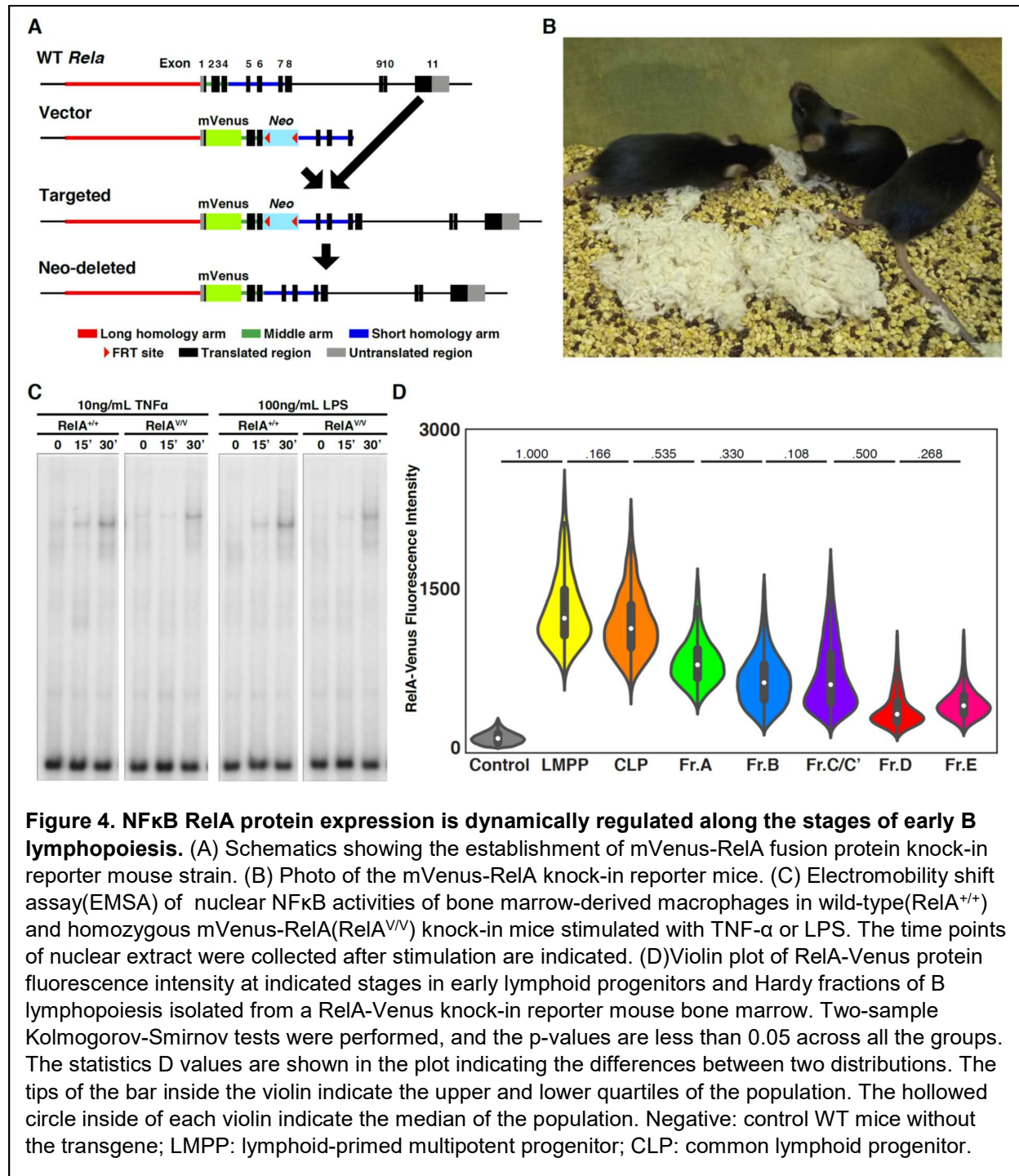
Our findings establish a new paradigm for how aging and inflammation impact humoral immunity via dysregulation of RelA dynamics: accelerated differentiation diminishes the B-cell pool and the immunoglobulin repertoire.

## **Results**

### **RelA protein expression is dynamically regulated during the early stages of healthy B lymphopoiesis**

In order to characterize the expression of the primary NF $\kappa$ B protein RelA during early B lymphopoiesis, a mouse strain with knock-in mVenus-RelA fusion protein was generated (Figure 4A). Homozygous mice were overtly healthy (Figure 4B) and derived cells showed

normal levels of stimulus-induced NFκB DNA binding activity (Figure 4C). Bone marrow cells were subjected to immunostaining of the surface markers that define the Hardy fractions (Hardy et al., 1991; Van Epps 2006) that identify specific B cell developmental



progenitors (Figure 5A, Material and Methods). The mVenus fluorescent protein indicated relatively high RelA expression at the common lymphoid progenitor (CLP) stage, marked downregulation to Fraction B, an increased expression in some Fraction C/C' cells before diminishing again in Fraction D, and a second increase in Fraction E (Figure 4D). Within this apparently highly dynamic regulation, we noted that the initial reduction of RelA protein expression during Fraction A and B coincides with B lineage commitment steps, and the subsequent downregulation from Fraction C/C' to Fraction D coincides with checkpoints between pro-B cell and pre-B cell stages (Hardy and Hayakawa, 2001; Smith and Sigvardsson, 2004; Welner et al., 2008; Melchers, 2015).

As the NF $\kappa$ B signaling system may mediate aging-associated inflammation (Salminen et al., 2008; Franceschi and Campisi, 2008; Chien et al., 2011; Balistreri et al., 2013), we compared the dynamic regulation of RelA protein levels in young (12 weeks old) and old (116 weeks old) mVenus-RelA knock-in reporter mice. For a rigorous quantitative analysis, we used the statistic D value from the two-sample Kolmogorov-Smirnov test, which quantifies the difference in the distributions of cellular RelA protein expression derived from aged and young mice. As the long-term process of aging results in heterogeneous outcomes, we sought to identify individuals in which RelA expression was particularly dysregulated and individuals in which it was closer to young mice. To this end we repeatedly divided aged individuals randomly into two groups and identified the grouping that minimized the p-value of two-way ANOVA results (Figure 5A). Based on this data-driven unbiased classification, we found that some aged mice showed RelA regulation along early B lymphopoiesis similar to young individuals (Figure 5B), while the other group showed abnormal RelA protein expression patterns (Figure 5C), which indicated a

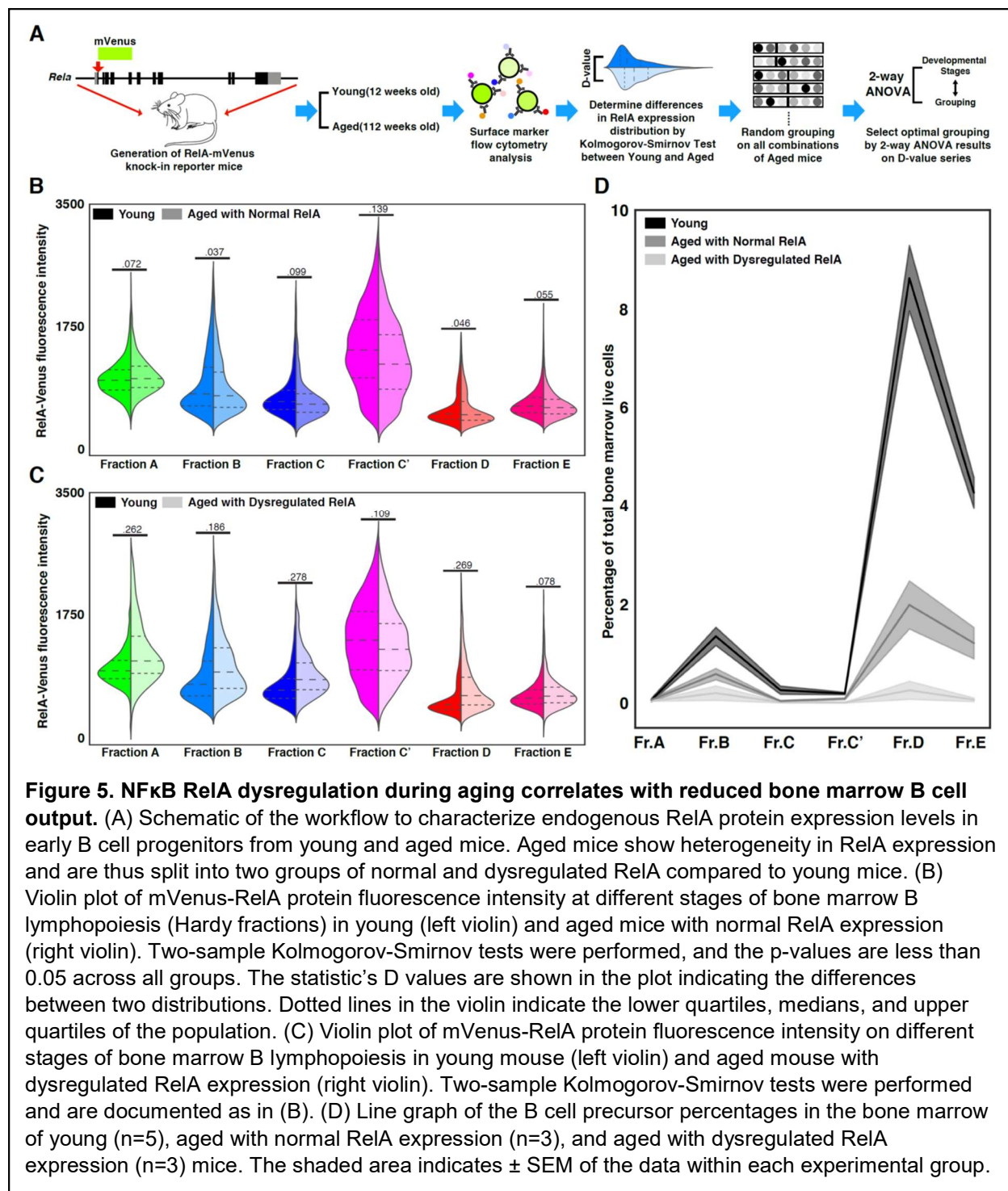
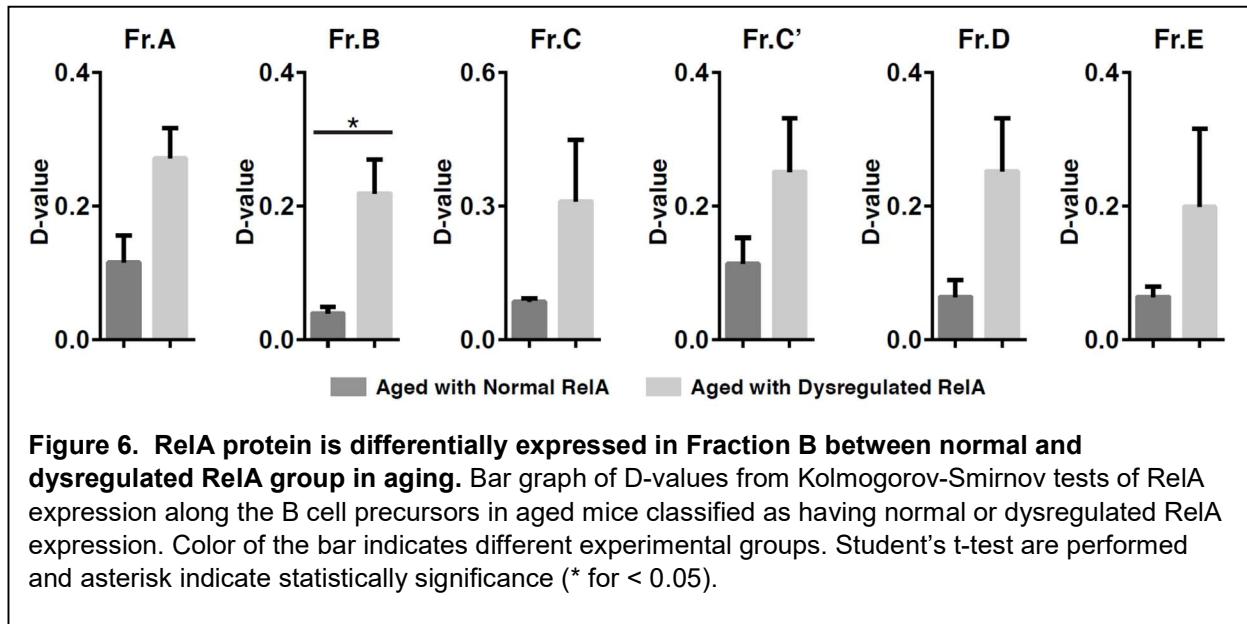


**Figure 5. NFκB RelA dysregulation during aging correlates with reduced bone marrow B cell output.** (A) Schematic of the workflow to characterize endogenous RelA protein expression levels in early B cell progenitors from young and aged mice. Aged mice show heterogeneity in RelA expression and are thus split into two groups of normal and dysregulated RelA compared to young mice. (B) Violin plot of mVenus-RelA protein fluorescence intensity at different stages of bone marrow B lymphopoiesis (Hardy fractions) in young (left violin) and aged mice with normal RelA expression (right violin). Two-sample Kolmogorov-Smirnov tests were performed, and the p-values are less than 0.05 across all groups. The statistic's D values are shown in the plot indicating the differences between two distributions. Dotted lines in the violin indicate the lower quartiles, medians, and upper quartiles of the population. (C) Violin plot of mVenus-RelA protein fluorescence intensity on different stages of bone marrow B lymphopoiesis in young mouse (left violin) and aged mouse with dysregulated RelA expression (right violin). Two-sample Kolmogorov-Smirnov tests were performed and are documented as in (B). (D) Line graph of the B cell precursor percentages in the bone marrow of young (n=5), aged with normal RelA expression (n=3), and aged with dysregulated RelA expression (n=3) mice. The shaded area indicates  $\pm$  SEM of the data within each experimental group.

dysregulated dynamic control of RelA. Notably, the statistical D values in Fraction B, the stage of substantial RelA downregulation in young mice, was significantly higher in the

aged group showing dysregulated RelA dynamics ( $D=0.22\pm 0.05$ ) than the aged group with normal RelA dynamics ( $D=0.04\pm 0.01$ ) when compared to healthy young mice (Figure 6).

We then examined the hematopoietic B-cell output of young mice and the two groups of aged mice. We found that aged mice showed lower percentages of Fraction D (small pre-BII cells,  $1.98\pm 0.48\%$ ) and Fraction E (immature B cell,  $1.21\pm 0.32\%$ ) cells compared to young mice ( $8.62\pm 0.66\%$  and  $4.26\pm 0.31\%$ , respectively), as previously reported (Van der Put et al., 2003; Guerrettaz et al., 2008), even when RelA dynamics were close to normal. However, in aged mice with dysregulated RelA, these cell populations were substantially further diminished (Fraction D:  $0.26\pm 0.18\%$ ; Fraction E:  $0.07\pm 0.04\%$ ) (Figure 5D). These results suggest that dysregulated RelA expression dynamics during aging are associated with diminished early B lymphopoiesis.



## Genetic dysregulation of RelA dynamics leads to severe B lymphopenia

In order to address the causal relationship between dynamic regulation of RelA to the functionality of early B lymphopoiesis, we sought to establish an experimental system in which RelA dynamics are perturbed genetically. Three I $\kappa$ B proteins control the dynamics of NF $\kappa$ B activity and hence the expression of RelA via an autoregulatory loop (Sung et al., 2014); while a homozygous I $\kappa$ B $\beta$  knockout is perinatal lethal, we found that a I $\kappa$ B heterozygosity even in conjunction with homozygosity of I $\kappa$ B $\alpha$  and I $\kappa$ B $\gamma$  alleles results in viable, overtly healthy mice. To determine whether the dynamics of RelA expression were compromised in this compound I $\kappa$ B mutant, we interbred it with the mVenus-RelA reporter mouse to produce a mouse model that lacked both alleles of *Nfkbie*, *Nfkbib*, one allele of *Nfkbia* and contained one knock-in allele of mVenus-RelA. We then used immunostaining to identify the Hardy fractions of B cell progenitors and determine the RelA expression dynamics during early B lymphopoiesis. We found that RelA protein expression was particularly elevated in Fraction B (Figure 7A), thus diminishing the downregulation of RelA expression characteristic of wild-type controls. Further, mutants did not show the upregulation of RelA characteristic of fraction C', nor the downregulation in fraction D, indicating a loss of RelA expression dynamics regulation associated with early B-cell development. We sought to restore aspects of this dysregulation by removing one allele of the *RELA* gene thus weakening the autoregulatory loop. The resulting *I $\kappa$ B $\epsilon$ <sup>-/-</sup>I $\kappa$ B $\delta$ <sup>-/-</sup>I $\kappa$ B $\alpha$ <sup>+/-</sup>RelA<sup>V/-</sup>* mouse strain indeed restored the downregulation at fraction B and partially the upregulation at fraction C' (Figure 7A).

To characterize the physiological outcome of NF $\kappa$ B RelA dysregulation in early B lymphopoiesis, we first analyzed the composition of mature B-cell populations in the spleens of *WT*, *I $\kappa$ B $\epsilon$ <sup>-/-</sup>I $\kappa$ B $\delta$ <sup>-/-</sup>I $\kappa$ B $\alpha$ <sup>+/-</sup>RelA<sup>V/+</sup>* (RelA dynamics mutant) and *I $\kappa$ B $\epsilon$ <sup>-/-</sup>I $\kappa$ B $\delta$ <sup>-/-</sup>I $\kappa$ B $\alpha$ <sup>+/-</sup>*

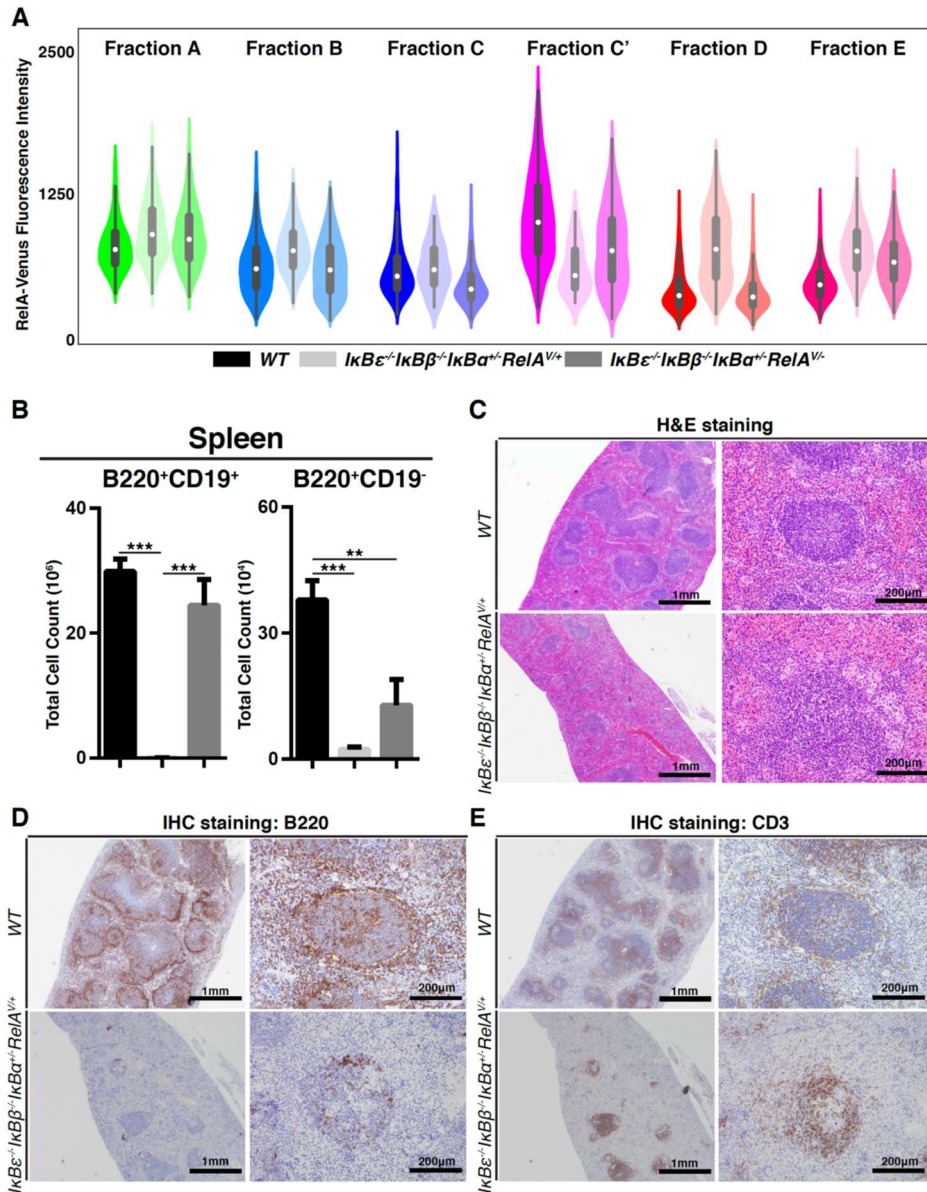
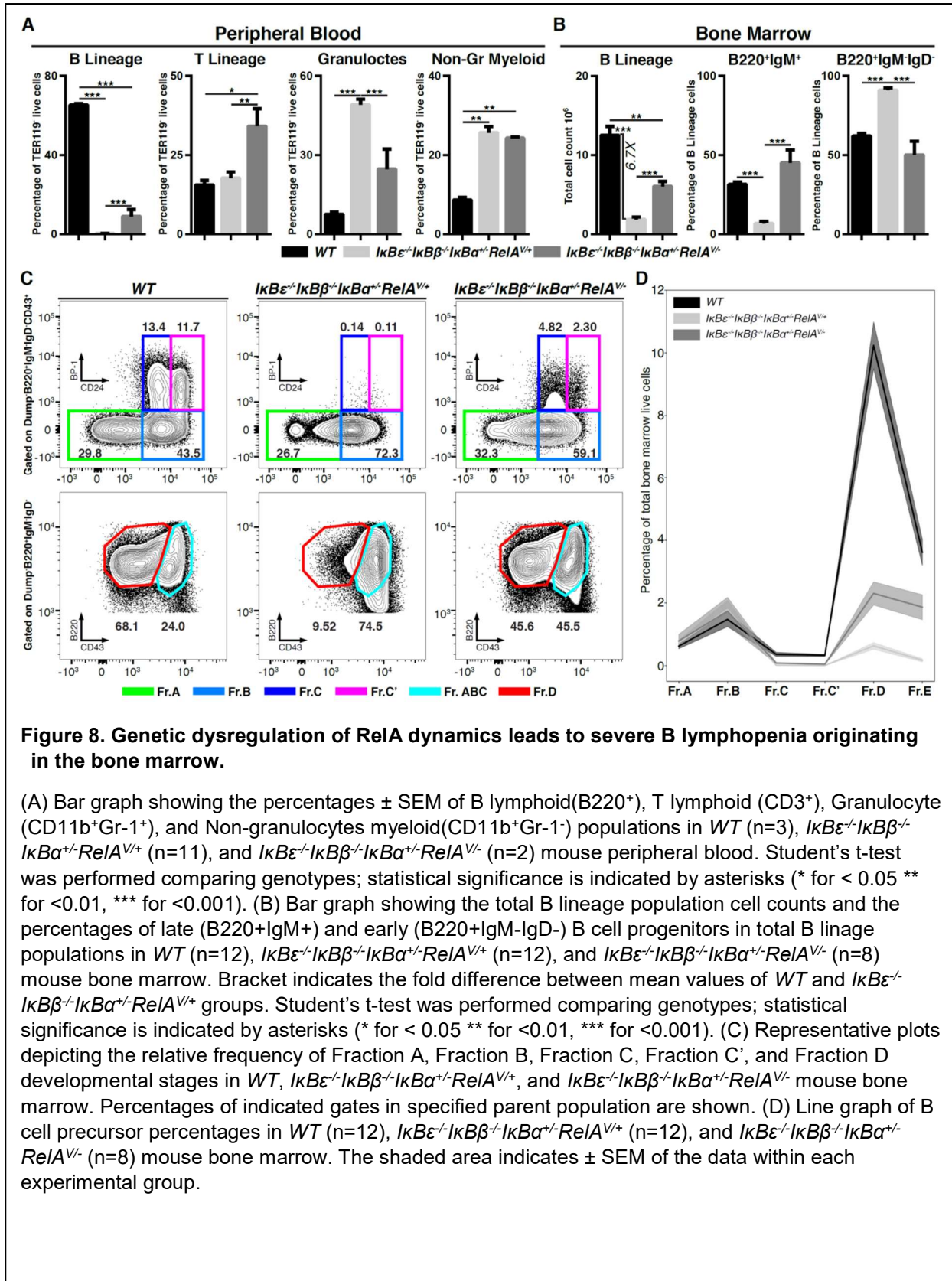


**Figure 7. Genetic dysregulation of RelA dynamics leads to severe B lymphopenia in the spleen.** (A) Violin plot of mVenus-RelA fluorescence in cells within indicated Hardy Fraction A to Fraction E derived from WT,  $IkB\epsilon^{-/-}IkB\beta^{-/-}IkB\alpha^{+/-}$ , and  $IkB\epsilon^{-/-}IkB\beta^{-/-}IkB\alpha^{+/-}RelA^{+/-}$  mouse bone marrow. Two-sample Kolmogorov-Smirnov tests were performed, and the p-values are lower than 0.05 across all the groups. The tips of the bar inside the violin indicate the upper and lower quartiles of the population. The hollowed circle inside of each violin indicate the median of the population. (B) Bar graph showing the cell numbers  $\pm$  SEM of B220<sup>+</sup>CD19<sup>-</sup> and B220<sup>+</sup>CD19<sup>+</sup> populations in  $RelA^{+/-}$  (n=13),  $IkB\epsilon^{-/-}IkB\beta^{-/-}IkB\alpha^{+/-}RelA^{+/-}$  (n=8), and  $IkB\epsilon^{-/-}IkB\beta^{-/-}IkB\alpha^{+/-}RelA^{-/-}$  (n=9) mouse spleens. (C-E) Histological section of WT (top) and  $IkB\epsilon^{-/-}IkB\beta^{-/-}IkB\alpha^{+/-}RelA^{+/-}$  (bottom) mouse spleen with (C) H&E staining, (D) Immunohistochemistry staining on surface B220, (E) Immunohistochemistry staining on surface CD3. Left panels are the lower power view, right panels are higher power view, as indicated on scale bars.

*RelA*<sup>V/-</sup> (partial revertant) mice by cell surface marker flow cytometry analysis. The analysis showed B220<sup>+</sup>CD19<sup>+</sup> population consists of 44.3±1.3% of total splenocytes in *WT* control mice, 0.51±0.24% in *IkBε*<sup>-/-</sup>*IkBβ*<sup>-/-</sup>*IkBα*<sup>+/-</sup>*RelA*<sup>V/+</sup> mice, and 37.2±5.0% in *IkBε*<sup>-/-</sup>*IkBβ*<sup>-/-</sup>*IkBα*<sup>+/-</sup>*RelA*<sup>V/-</sup> mice, indicating that the B220<sup>+</sup>CD19<sup>+</sup> population was severely impaired in *IkBε*<sup>-/-</sup>*IkBβ*<sup>-/-</sup>*IkBα*<sup>+/-</sup>*RelA*<sup>V/+</sup> mouse spleens and that *Rela* heterozygosity could significantly rescue this phenotype (Figure 7B). We then used histological sectioning and immunohistochemistry staining in *WT* and *IkBε*<sup>-/-</sup>*IkBβ*<sup>-/-</sup>*IkBα*<sup>+/-</sup>*RelA*<sup>V/+</sup> to reveal well-formed follicles interspersed with red pulp composed of red blood cell precursors, megakaryocytes, and other cells in *WT* mouse spleen, while *IkBε*<sup>-/-</sup>*IkBβ*<sup>-/-</sup>*IkBα*<sup>+/-</sup>*RelA*<sup>V/+</sup> mouse spleen showed diminished follicle structures, and more intervening red pulp (Figure 7C, left panels). The individual follicles in *WT* spleens showed proper zoning, with bigger cells towards the germinal center and smaller cells around the edges, whereas such organization was absent in *IkBε*<sup>-/-</sup>*IkBβ*<sup>-/-</sup>*IkBα*<sup>+/-</sup>*RelA*<sup>V/+</sup> spleens (Figure 7C, right panels). In *WT* splenic structure, B-cells were distributed around the periphery of the follicle around the T-cell periarteriolar sheath where germinal centers normally bud off (Figure 7D, 7E, upper panels). However, such distribution was impaired in *IkBε*<sup>-/-</sup>*IkBβ*<sup>-/-</sup>*IkBα*<sup>+/-</sup>*RelA*<sup>V/+</sup> mouse spleens due to the severe reduction in the B cell population; the reduced follicular structures were composed primarily of T cells (Figure 7D, 7E, lower panels). Quantification of the percentages of different hematopoietic cell types in peripheral blood showed the B lineage population (B220<sup>+</sup>CD19<sup>+</sup>) consisted of 64.4±0.7% of purified peripheral blood leukocytes in *WT* control mice, 0.11±0.05% in *IkBε*<sup>-/-</sup>*IkBβ*<sup>-/-</sup>*IkBα*<sup>+/-</sup>*RelA*<sup>V/+</sup> mice, and 8.04±3.32% in *IkBε*<sup>-/-</sup>*IkBβ*<sup>-/-</sup>*IkBα*<sup>+/-</sup>*RelA*<sup>V/-</sup> mice. These data indicated severely diminished B lineage populations in *IkBε*<sup>-/-</sup>*IkBβ*<sup>-/-</sup>*IkBα*<sup>+/-</sup>*RelA*<sup>V/+</sup> mouse circulation, while *Rela* heterozygosity provided a partial rescue (Figure 8A). Although the percentages of granulocytes (49.1±2.1%) and non-



granulocyte myeloid lineages ( $25.7 \pm 1.6\%$ ) were also increased in *IkBε<sup>-/-</sup>IkBβ<sup>-/-</sup>IkBα<sup>+/-</sup>RelA<sup>V/+</sup>* mouse peripheral blood compared to *WT* ( $7.59 \pm 0.76\%$  and  $8.65 \pm 0.69\%$ , respectively), this may be the result of the substantial reduction in B cells. Together, these results suggest that precise dynamic regulation of RelA expression during B lymphopoiesis is essential for normal B cell output from the bone marrow.

In order to identify the origin of the reduced B lymphopoietic output in *IkBε<sup>-/-</sup>IkBβ<sup>-/-</sup>IkBα<sup>+/-</sup>RelA<sup>V/+</sup>* mice, we characterized B cell development in the bone marrow using cell surface marker flow cytometry (Figure 8B, 8C). By excluding all the non-B lineage cells, the overall B lineage population percentages was  $22.6 \pm 1.8\%$  in *WT* mice and  $4.12 \pm 0.61\%$  in *IkBε<sup>-/-</sup>IkBβ<sup>-/-</sup>IkBα<sup>+/-</sup>RelA<sup>V/+</sup>* mice. Compared to wild type controls, in *IkBε<sup>-/-</sup>IkBβ<sup>-/-</sup>IkBα<sup>+/-</sup>RelA<sup>V/+</sup>* mice the overall B lineage cell number diminished significantly. In *IkBε<sup>-/-</sup>IkBβ<sup>-/-</sup>IkBα<sup>+/-</sup>RelA<sup>V/+</sup>* mice, the reduction was more pronounced at the late B cell progenitor stage (B220<sup>+</sup>IgM<sup>+</sup>,  $6.82 \pm 1.33\%$  compared to  $31.5 \pm 1.6\%$  in *WT*), while the early B cell progenitor proportion (B220<sup>+</sup>IgM<sup>-</sup>IgD<sup>-</sup>,  $91.1 \pm 1.5\%$ ) increased in comparison to *WT* mice ( $62.0 \pm 1.8\%$ ), suggesting that the origin of the reduced B-cell output is in early B cell progenitor populations (Figure 8B). Removing one allele of the *Rela* gene partially rescued B lineage numbers ( $11.1 \pm 1.1\%$ ) and the percentages of late or early B cell progenitors ( $45.2 \pm 8.0\%$  and  $50.2 \pm 8.5\%$ , respectively) (Figure 8B). By further investigating the early B cell progenitor populations, we found B cell development was severely disrupted in the mutant, not only in the distribution of Fraction A to Fraction C' (within the Dump-IgM<sup>-</sup>B220<sup>+</sup>CD43<sup>+</sup> population) but also in the relative proportion of Fraction ABC to Fraction D cells (Figure 8C, left and middle panel). In particular, Fraction C and Fraction C' populations were severely diminished and the subsequent Fraction D population was also substantially decreased, while additional genetic deletion of one *Rela* allele provided a partial rescue of these

phenotypes (Figure 8C, right panels). To quantitatively assess how dysregulation in RelA expression dynamics affect each progenitor or precursor populations, we graphed the cell number percentages of these progenitor populations in the total bone marrow and found significant reductions in Fraction C ( $0.014 \pm 0.002\%$ ), Fraction C' ( $0.004 \pm 0.001\%$ ), Fraction D ( $0.63 \pm 0.11\%$ ), and Fraction E ( $0.17 \pm 0.05\%$ ) in *I $\kappa$ B $\epsilon$ <sup>-/-</sup>I $\kappa$ B $\beta$ <sup>-/-</sup>I $\kappa$ B $\alpha$ <sup>+/-</sup>RelA<sup>V/+</sup>* mice compared to the Fraction C ( $0.36 \pm 0.06\%$ ), Fraction C' ( $0.33 \pm 0.03\%$ ), Fraction D ( $10.2 \pm 0.7\%$ ), and Fraction E ( $3.6 \pm 0.4\%$ ) in *WT* control mice, while Fraction A and Fraction B populations were insignificantly affected (Figure 8D). In this context *Rela* heterozygosity provided partial rescue of these phenotypes (Fraction C:  $0.08 \pm 0.02\%$ , Fraction C':  $0.05 \pm 0.01\%$ , Fraction D:  $2.3 \pm 0.4\%$ , and Fraction E:  $1.9 \pm 0.4\%$ ; Figure 8D), suggesting that RelA dysregulation is indeed responsible for defects in the B cell progenitors of Fraction C and on, resulting in a severe reduction in the overall bone marrow B cell output.

## RelA dynamics control early B lymphopoiesis in a cell lineage-intrinsic manner

To further investigate how the dysregulation of RelA expression dynamics leads to the developmental defects in early B lymphopoiesis, we first determined whether the phenotypes are caused by bone marrow cell-intrinsic or bone marrow cell-extrinsic factors using bone marrow chimera experiments. To this end we transplanted donor bone marrow cells with dysregulated RelA ( $I\kappa B\epsilon^{-}/I\kappa B\beta^{-}/I\kappa B\alpha^{+/}$ ) into control recipient mice ( $WT$ ) and *vice versa*, and monitored the lineage percentages in peripheral blood at 6, 8, 12, and 15 weeks post transplantation. We found that the “bone marrow cell-intrinsic” experimental group ( $I\kappa B\epsilon^{-}/I\kappa B\beta^{-}/I\kappa B\alpha^{+/}$  into  $WT$ ) showed diminished B lymphoid lineage percentages across all time points ( $1.44\pm 0.30\%$ ,  $0.76\pm 0.17\%$ ,  $1.40\pm 0.14\%$ ,  $0.63\pm 0.09\%$ ), when compared to the control group ( $WT$  into  $WT$ ,  $65.1\pm 3.7\%$ ,  $62.1\pm 1.8\%$ ,  $56.8\pm 9.7\%$ ,  $49.4\pm 3.0\%$ ) (Figure 9A). We also observed increased percentages in granulocytes ( $42.7\pm 6.1\%$ ,  $46.7\pm 1.5\%$ ,  $26.7\pm 2.7\%$ ,  $38.0\pm 2.5\%$  compared to  $13.5\pm 3.4\%$ ,  $16.8\pm 1.8\%$ ,  $15.3\pm 7.7\%$ ,  $14.2\pm 3.6\%$ ) and non-granulocyte myeloid cells ( $26.2\pm 1.4\%$ ,  $30.6\pm 2.7\%$ ,  $40.5\pm 4.3\%$ ,  $33.7\pm 1.6\%$  compared to  $5.3\pm 0.3\%$ ,  $7.1\pm 0.5\%$ ,  $7.6\pm 1.2\%$ ,  $9.3\pm 1.0\%$ ) but no significant differences in T lymphoid lineage cells. Thus, the peripheral blood phenotype in the “bone marrow cell-intrinsic” experimental group ( $I\kappa B\epsilon^{-}/I\kappa B\beta^{-}/I\kappa B\alpha^{+/}$  into  $WT$ ) resembled that in native of  $I\kappa B\epsilon^{-}/I\kappa B\beta^{-}/I\kappa B\alpha^{+/}RelA^{V/+}$  mice (Figure 8C). In contrast, peripheral blood lineage percentages in the “bone marrow cell-extrinsic” experimental group ( $WT$  to  $I\kappa B\epsilon^{-}/I\kappa B\beta^{-}/I\kappa B\alpha^{+/}$ ) showed only minor changes over controls, and did not resemble the native peripheral blood phenotypes (Figure 9B, 8A). We next investigated B cell progenitor populations in the bone marrow of recipient mice to determine whether the origin of the phenotypes was also similar. In the  $WT$  recipient mice bone marrow, we found reduced overall B lymphoid lineage cell numbers ( $1.5\pm 0.4$  million cells) compared to the control group ( $4.3\pm 0.3$  million cells) (Figure 9E), the disrupted

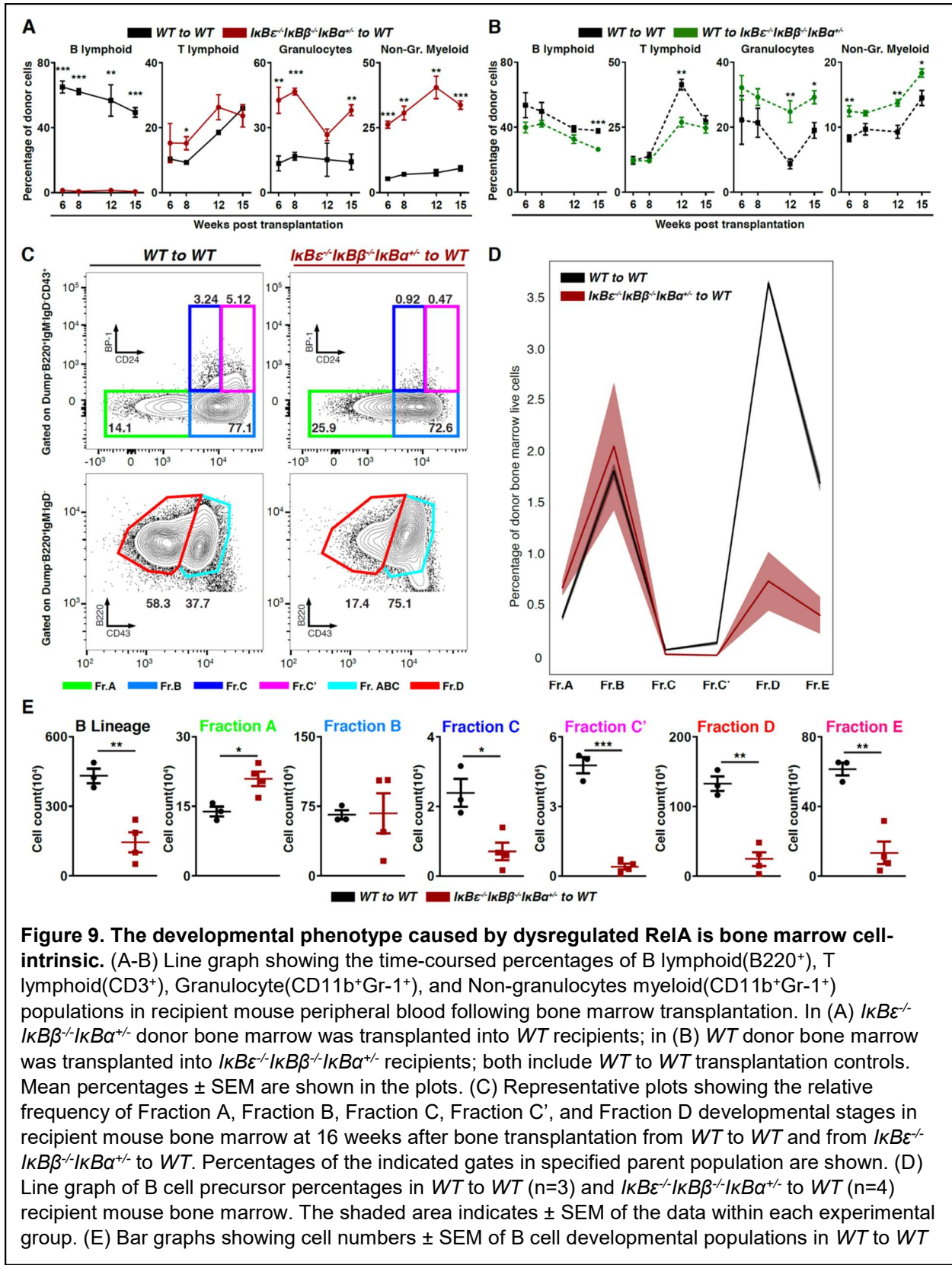


**Figure 9 continued.** (n=3) and *IκBε<sup>-/-</sup>IκBβ<sup>-/-</sup>IκBα<sup>+/-</sup>* to *WT* (n=4) recipient mouse bone marrow. Student's t-test was performed comparing different experimental groups and statistical significance is indicated by asterisks (\* for < 0.05 \*\* for <0.01, \*\*\* for <0.001).

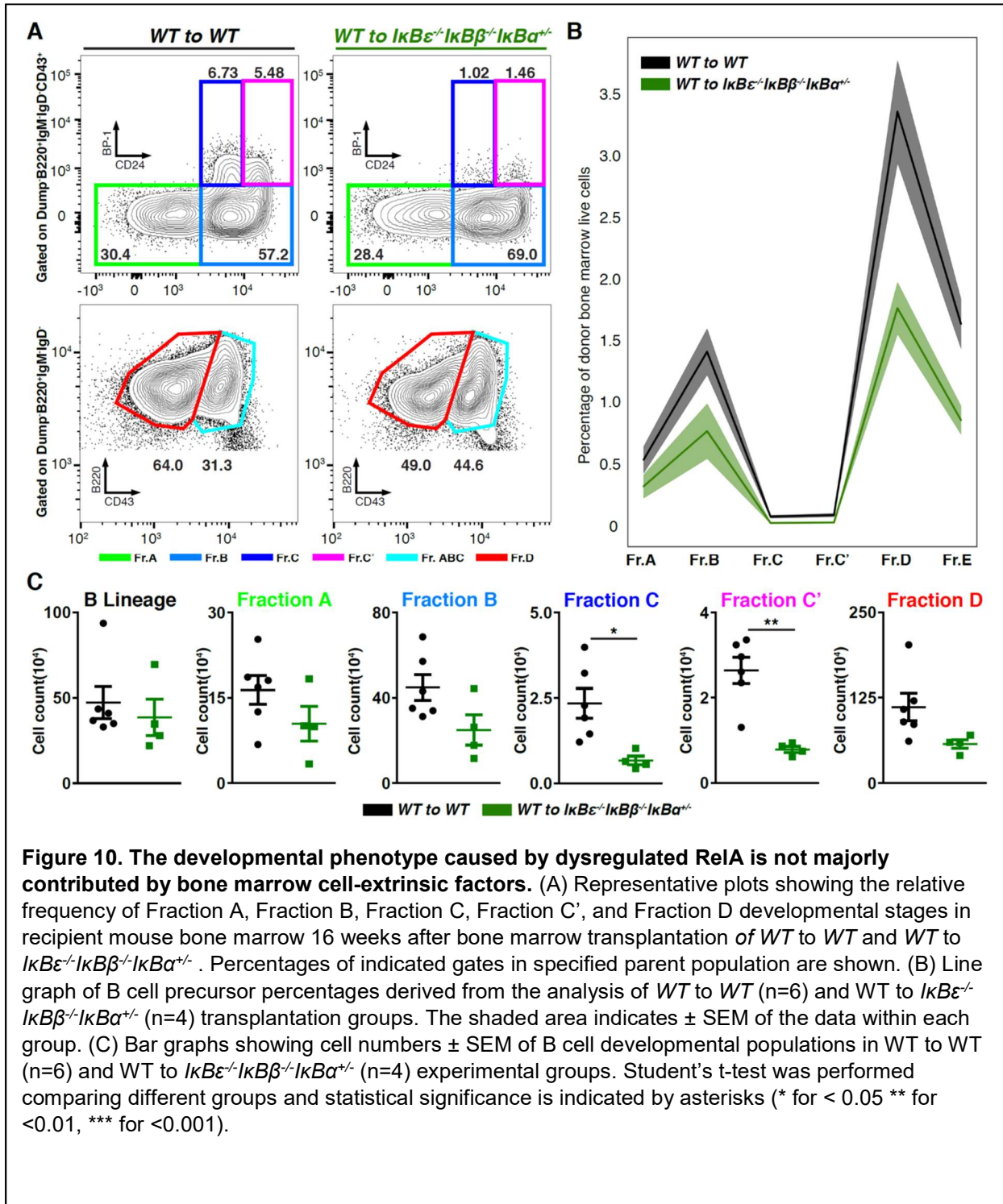
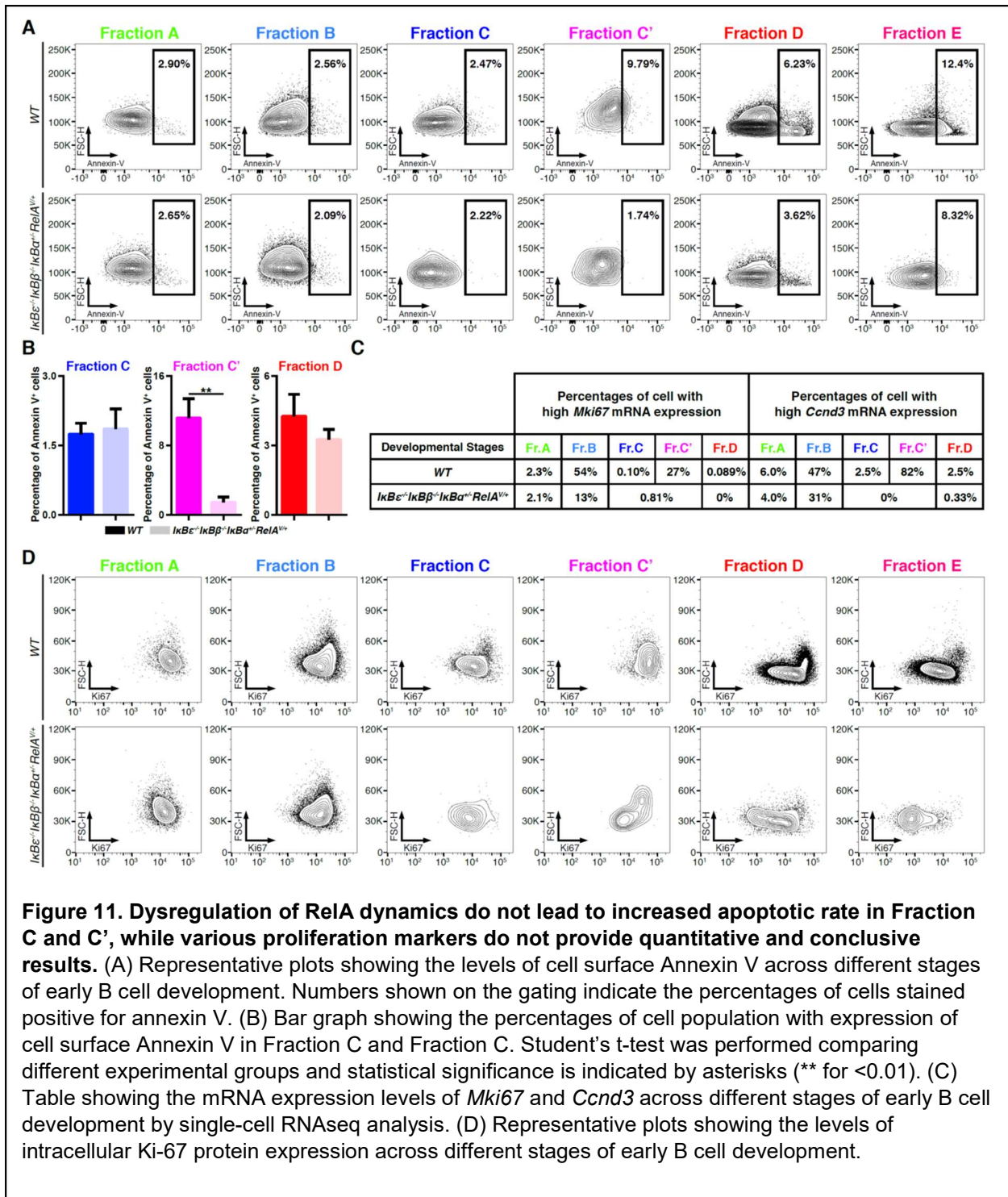


**Figure 10. The developmental phenotype caused by dysregulated RelA is not majorly contributed by bone marrow cell-extrinsic factors.** (A) Representative plots showing the relative frequency of Fraction A, Fraction B, Fraction C, Fraction C', and Fraction D developmental stages in recipient mouse bone marrow 16 weeks after bone marrow transplantation of *WT* to *WT* and *WT* to *IκBε<sup>-/-</sup>IκBβ<sup>-/-</sup>IκBα<sup>+/-</sup>*. Percentages of indicated gates in specified parent population are shown. (B) Line graph of B cell precursor percentages derived from the analysis of *WT* to *WT* (n=6) and *WT* to *IκBε<sup>-/-</sup>IκBβ<sup>-/-</sup>IκBα<sup>+/-</sup>* (n=4) transplantation groups. The shaded area indicates ± SEM of the data within each group. (C) Bar graphs showing cell numbers ± SEM of B cell developmental populations in *WT* to *WT* (n=6) and *WT* to *IκBε<sup>-/-</sup>IκBβ<sup>-/-</sup>IκBα<sup>+/-</sup>* (n=4) experimental groups. Student's t-test was performed comparing different groups and statistical significance is indicated by asterisks (\* for < 0.05 \*\* for <0.01, \*\*\* for <0.001).

proportions of Fractions A to D (Figure 9C) and the diminished populations of Fraction C to Fraction E by percentages (0.021±0.007%, 0.012±0.004%, 0.73±0.28%, 0.40±0.18% compared to 0.064±0.007%, 0.13±0.02%, 3.63±0.03%, 1.69±0.08%) or cell numbers (0.7±0.3 10<sup>4</sup> cells, 0.4±0.1 10<sup>4</sup> cells, 24.5±9.9 10<sup>4</sup> cells, 13.4±6.3 10<sup>4</sup> cells, compared to 2.4±0.4 10<sup>4</sup> cells, 4.8±0.3 10<sup>4</sup> cells, 132.9±10.5 10<sup>4</sup> cells, 61.5±3.7 10<sup>4</sup> cells) are all similar to the native bone marrow phenotype in *IκBε*<sup>-/-</sup>*IκBβ*<sup>-/-</sup>*IκBa*<sup>+/+</sup>*RelA*<sup>V/+</sup> mice (Figure 9D, 9E). On the other hand, the bone marrow B cell progenitor proportions (Figure 10A), percentages (Figure 10B), and cell number (Figure 10C) in the “bone marrow cell-extrinsic” experimental group (*WT* to *IκBε*<sup>-/-</sup>*IκBβ*<sup>-/-</sup>*IκBa*<sup>+/+</sup>) did not recapitulate the native phenotype of *IκBε*<sup>-/-</sup>*IκBβ*<sup>-/-</sup>*IκBa*<sup>+/+</sup>*RelA*<sup>V/+</sup> mice. Therefore, we concluded that dysregulation of RelA expression dynamics impact early B lymphopoiesis in a bone marrow cell-intrinsic manner.

### **Unbiased, quantitative phenotyping with a mathematical model of early lymphopoiesis**

Two causes for deficiencies in mature cell populations are commonly identified: a differentiation block, or a loss of progenitor survival (Prendes et al., 2003; Claudio et al., 2009; Liu et al., 2014, Almaden et al., 2016). In the case of *IκBε*<sup>-/-</sup>*IκBβ*<sup>-/-</sup>*IκBa*<sup>+/+</sup>*RelA*<sup>V/+</sup> bone marrow, we did not observe an accumulation of cells in Fraction B progenitor cell percentages in the bone marrow (Figure 8D), which suggested that the reduction in Fraction C and Fraction C' populations is not due to a differentiation block (Figure 8D). Further, Annexin V staining indicated that apoptotic cell percentages are not increased in Fraction C (1.2±0.3% compared to 1.6±0.2% in *WT* mice) while in Fraction C' the apoptotic cell proportion actually decreased (1.1±0.4% compared to 4.6±0.6% in *WT* mice) (Figure 11A, 11B). These results indicated that neither of the commonly observed cell biological explanations apply to the B lymphoid developmental phenotype in *IκBε*<sup>-/-</sup>*IκBβ*<sup>-/-</sup>*IκBa*<sup>+/+</sup>*RelA*<sup>V/+</sup> bone marrow.



We therefore turned to an unbiased approach to explain the phenotype by mathematically modeling the B-cell developmental pathway to interpret progenitor population data by quantitative fitting. To this end we formulated a simple linear compartment model that

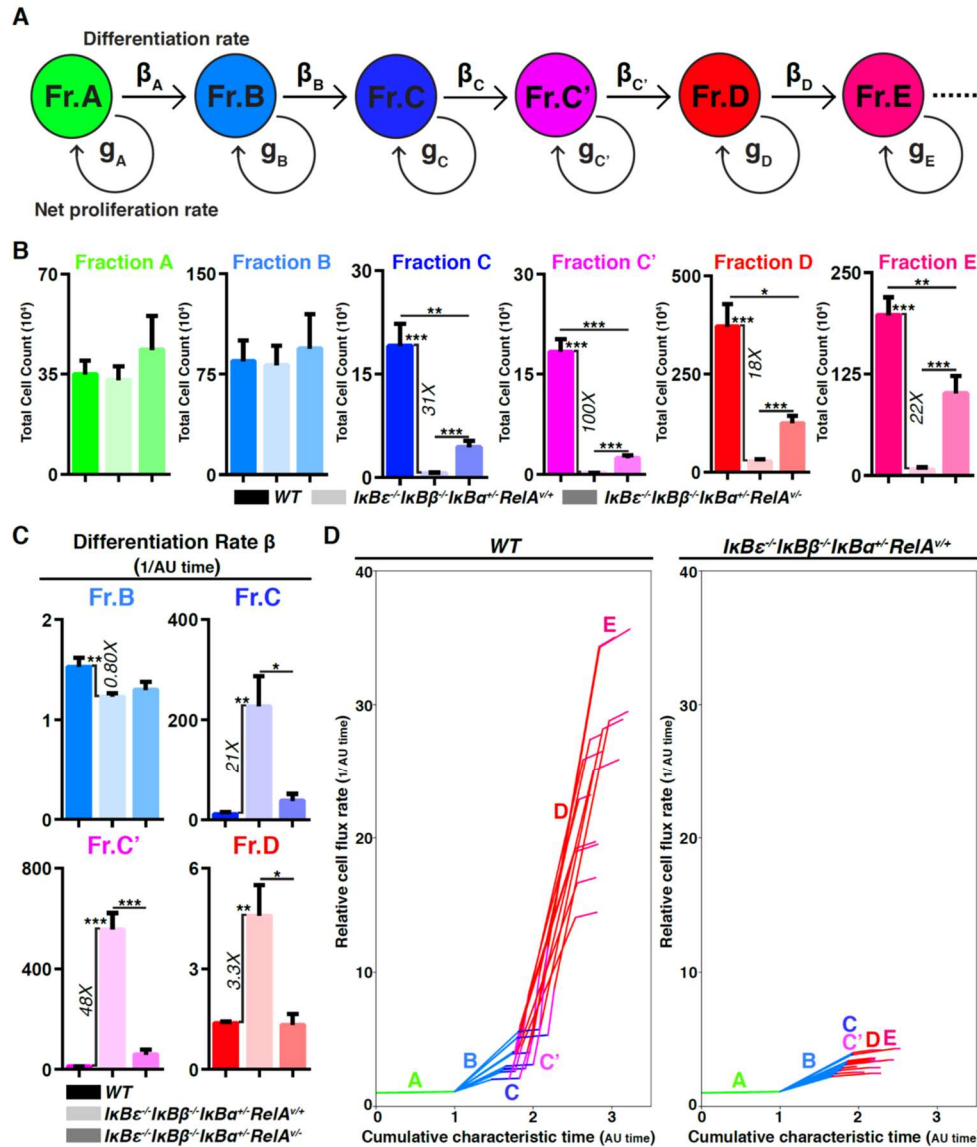


**Figure 12. Mathematical modeling suggests increased differentiation rates in Fraction C and Fraction C' could lead to diminished B cell outputs in mouse bone marrow with dysregulated RelA dynamics.** (A) Schematics showing the mathematical modeling framework of using B cell progenitor population numbers to understand the transition between developmental stages in steady states. (B) Bar graphs showing cell number  $\pm$  SEM of B cell developmental populations in WT (n=12),  $IkB\epsilon^{-/-}IkB\beta^{-/-}IkB\alpha^{+/-}RelA^{+/+}$  (n=12), and  $IkB\epsilon^{-/-}IkB\beta^{-/-}IkB\alpha^{+/-}RelA^{-/-}$  (n=8) mouse bone marrow. Brackets demonstrate the fold differences between mean value of WT and  $IkB\epsilon^{-/-}IkB\beta^{-/-}IkB\alpha^{+/-}RelA^{+/+}$  groups. Student's t-test was performed comparing genotypes; statistical significance is indicated by asterisks (\* for  $< 0.05$ , \*\* for  $< 0.01$ , \*\*\* for  $< 0.001$ ). (C) Bar graph showing the B cell progenitor differentiation rate  $\pm$  SEM from the results of mathematical modeling fitting on experimental data. Brackets demonstrate the fold differences between mean value of WT and  $IkB\epsilon^{-/-}IkB\beta^{-/-}IkB\alpha^{+/-}RelA^{+/+}$  groups. Student's t-test was performed comparing genotypes; statistical significance is indicated by asterisks (\* for  $< 0.05$ , \*\* for  $< 0.01$ , \*\*\* for  $< 0.001$ ). (D) Line graph showing the progression of relative cell flux rate over cumulative characteristic time in WT and  $IkB\epsilon^{-/-}IkB\beta^{-/-}IkB\alpha^{+/-}RelA^{+/+}$  mouse bone marrow from the mathematical modeling.

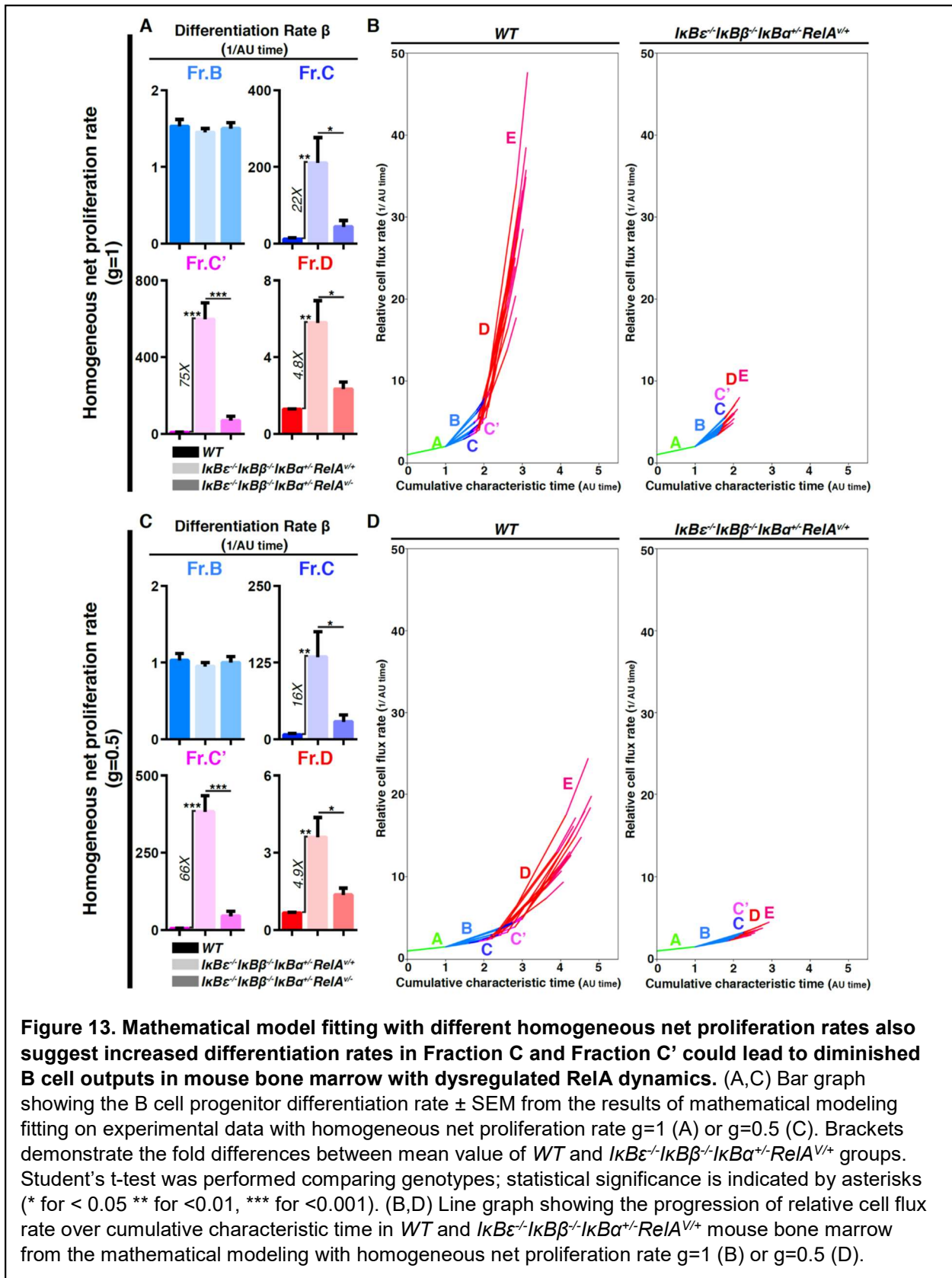


**Figure 13. Mathematical model fitting with different homogeneous net proliferation rates also suggest increased differentiation rates in Fraction C and Fraction C' could lead to diminished B cell outputs in mouse bone marrow with dysregulated RelA dynamics.** (A,C) Bar graph showing the B cell progenitor differentiation rate  $\pm$  SEM from the results of mathematical modeling fitting on experimental data with homogeneous net proliferation rate  $g=1$  (A) or  $g=0.5$  (C). Brackets demonstrate the fold differences between mean value of WT and  $IkB\epsilon^{-/-}IkB\beta^{-/-}IkBa^{+/+}RelA^{+/+}$  groups. Student's t-test was performed comparing genotypes; statistical significance is indicated by asterisks (\* for  $<0.05$ , \*\* for  $<0.01$ , \*\*\* for  $<0.001$ ). (B,D) Line graph showing the progression of relative cell flux rate over cumulative characteristic time in WT and  $IkB\epsilon^{-/-}IkB\beta^{-/-}IkBa^{+/+}RelA^{+/+}$  mouse bone marrow from the mathematical modeling with homogeneous net proliferation rate  $g=1$  (B) or  $g=0.5$  (D).

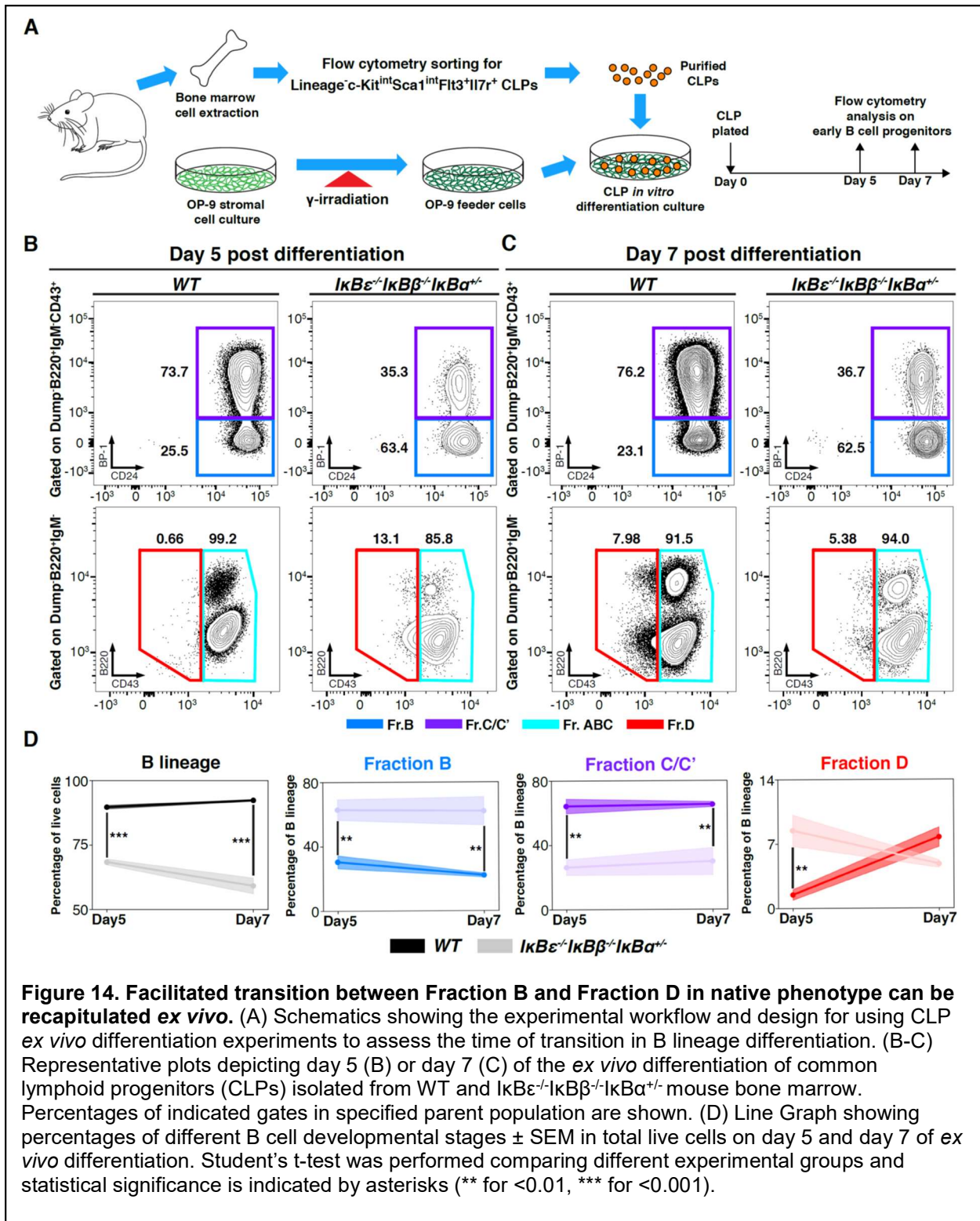
describes the developmental progression of early B lymphoid progenitors through Fraction E cells, which migrate toward circulation eventually, via five differentiation transitions (Figure A). To fit the model, we measured absolute numbers of progenitor cells in each defined population in the bone marrow of *WT* and *IκBε<sup>-/-</sup>IκBβ<sup>-/-</sup>IκBα<sup>+/-</sup>RelA<sup>V/+</sup>* mice assumed to be in steady state (Figure 12A, 12B). Notably, absolute cell counts revealed that *WT* and *IκBε<sup>-/-</sup>IκBβ<sup>-/-</sup>IκBα<sup>+/-</sup>RelA<sup>V/+</sup>* mice differed by 31-fold in Fraction C, 100-fold in Fraction C' and 18-fold in Fraction D, which confirmed the idea that these developmental phenotypes were not due to differentiation block.

We fit the differentiation transition rates of the model to these data and constrained fitting of the net proliferation rate based on relative measurements of the proliferation marker Ki-67, proliferation-associated gene expression (*Ccnd3* and *Mki67*) and the cell death marker annexin V (Figure 11C, Supplementary spreadsheet). Remarkably, model fitting suggested that the differentiation rates from Fraction C to C' to D are  $11.0 \pm 3.9$ ,  $11.6 \pm 0.8$ , and  $1.38 \pm 0.04$  in *WT*, while  $227.5 \pm 59.5$ ,  $556.6 \pm 64.8$ , and  $4.59 \pm 0.91$  in *IκBε<sup>-/-</sup>IκBβ<sup>-/-</sup>IκBα<sup>+/-</sup>RelA<sup>V/+</sup>*. These data suggested a dramatically accelerated transition from Fraction C to Fraction D in *IκBε<sup>-/-</sup>IκBβ<sup>-/-</sup>IκBα<sup>+/-</sup>RelA<sup>V/+</sup>* mice compared to *WT* (Figure 12C), while *Rela* heterozygosity could partially restore them. Using the derived parameters for control and mutant data, we calculated the relative cell flux rate of each progenitor population, and found that *IκBε<sup>-/-</sup>IκBβ<sup>-/-</sup>IκBα<sup>+/-</sup>RelA<sup>V/+</sup>* mice were predicted to have substantially decreased cell flux in the end of Fraction D and E (Figure 12D). We examined whether this result was dependent on the net proliferation rates which could only be roughly estimated (Figure 11), but found that fixing this rate at different levels had quantitative effects but consistently resulted in a model fit with higher Fraction C to C' to D transition rates causing diminished hematopoietic output (Figure 13). These results indicate that a differentiation hypermorph

(*IκBε*<sup>-/-</sup>*IκBβ*<sup>-/-</sup>*IκBα*<sup>+/-</sup>*RelA*<sup>V/+</sup> mice) leads to severe developmental defects in producing mature B cells for secondary lymphoid organs.

### ***Ex vivo* differentiation system confirms model predictions of accelerated differentiation**

As B lymphopoiesis is a continuous process (Orkin and Zon, 2008; Dorshkind and Montecino-Rodriguez, 2007), it is difficult to measure differentiation rate, timescales, or constants directly *in vivo*. We turned to an *ex vivo* differentiation experimental system (Holmes et al., 2006), which has a defined differentiation starting point with purified CLPs (Figure 14A). After five days of culture we observed fraction C/C' cells composing 64.2±4.4% of B lineage cells in *WT* and 26.2±4.8% in *IκBε*<sup>-/-</sup>*IκBβ*<sup>-/-</sup>*IκBα*<sup>+/-</sup> cultures, akin to the reduction in the fraction C/C' population in native *IκBε*<sup>-/-</sup>*IκBβ*<sup>-/-</sup>*IκBα*<sup>+/-</sup>*RelA*<sup>V/+</sup> bone marrow (Figure 14B, 14D, 8C). However, we found the percentages of Fraction D cells significantly higher in *IκBε*<sup>-/-</sup>*IκBβ*<sup>-/-</sup>*IκBα*<sup>+/-</sup> than in *WT* cultures (8.5±1.7% vs. 1.5±0.6%) (Figure 14B, 14D). Interestingly, by day 7 of culture the *IκBε*<sup>-/-</sup>*IκBβ*<sup>-/-</sup>*IκBα*<sup>+/-</sup> contained a smaller percentage fraction D cells than the *WT* counterpart (4.8±0.4% vs. 7.7±1.1%) (Figure 14C, 14D). These data indicated that the mutant culture was able to generate fraction D cells more rapidly than the control. The results suggest that dysregulation in RelA dynamics resulted in an accelerated differentiation transition from Fraction B to D, confirming the mathematical model-aided interpretation of quantitative *in vivo* cell population datasets. Overall then, these results argue that a failure in proper dynamic regulation of RelA may result in a “rushed-through” transition through Fraction C/C', thereby causing reduced bone marrow B cell output.



### Single-cell RNAseq analysis reveals uncoordinated progression of transcriptomic states

To further investigate the underlying cause of accelerated differentiation, we performed single cell RNA sequencing analysis on B-cell progenitors isolated by sorting out the CD11b<sup>+</sup>CD3<sup>+</sup>CD49b<sup>+</sup>Ter119<sup>-</sup>CD3<sup>+</sup>F4/80<sup>-</sup>Gr-1<sup>-</sup>B220<sup>+</sup>IgD<sup>-</sup>IgM<sup>-</sup> population from WT and *IkBε*<sup>-/-</sup>*IkBβ*<sup>-/-</sup>*IkBα*<sup>+/-</sup> bone marrow. With the exclusion of potential doublets by Scrublet and DoubletDetection (Gayyoso and Shor, 2018; Wolock et al., 2019), we used Cellranger pipelines and analyzed the data with lowest number of principal components as possible. After plotting the cell clusters in t-SNE space by transcriptomic profiles, we found the distribution of clusters in *IkBε*<sup>-/-</sup>*IkBβ*<sup>-/-</sup>*IkBα*<sup>+/-</sup> mice showed distinct patterns compared to *WT* mice, especially in Cluster C (Figure 15A). To understand what causes the spatial discrepancy between *WT* and *IkBε*<sup>-/-</sup>*IkBβ*<sup>-/-</sup>*IkBα*<sup>+/-</sup> in t-SNE space, we performed differential gene expression analysis in each cluster and found that Cluster B, C, and C' showed a large number of upregulated genes (Figure 15B, Figure 16A), which contained NFκB/RelA binding motifs in their regulatory region (Figure 15C, Figure 16B), unlike downregulated genes (Figure 16C). These results suggested that the spatial differences in t-SNE space between *WT* and *IkBε*<sup>-/-</sup>*IkBβ*<sup>-/-</sup>*IkBα*<sup>+/-</sup> mice are due to elevated NFκB/RelA transcriptional activity, particularly in cluster C and C'.

We then used the progenitor frequency based on the surface marker profiles (Hardy fractionation scheme) and key marker genes identified by bulk mRNA-sequencing (Material and methods). These analyses allowed us to identify progenitor populations in the *IkBε*<sup>-/-</sup>*IkBβ*<sup>-/-</sup>*IkBα*<sup>+/-</sup> sample. Remarkably, we found that the Fraction B population in *IkBε*<sup>-/-</sup>*IkBβ*<sup>-/-</sup>*IkBα*<sup>+/-</sup> contains multiple types of transcriptomic profiles (Figure 15D). Notably, the majority of transcriptomic cluster C and C' in the *IkBε*<sup>-/-</sup>*IkBβ*<sup>-/-</sup>*IkBα*<sup>+/-</sup> sample, which showed

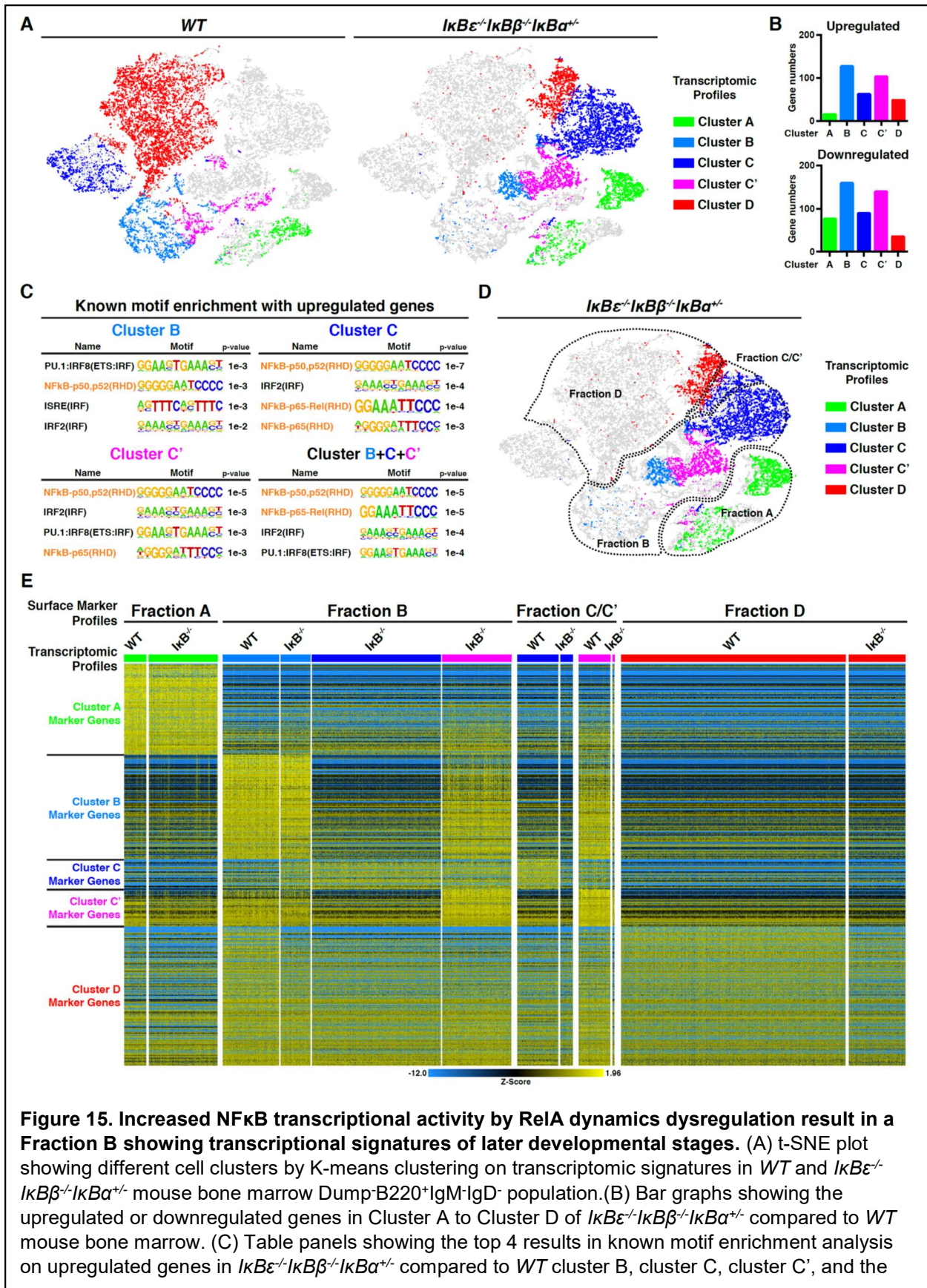


**Figure 15 continued.** combination of the clusters mentioned. Motifs related to NFκB/RelA were highlighted with orange-colored font. (D) t-SNE plot showing the comparison between transcriptomic profiles and surface marker profiles in cell clusters of *IκBε<sup>-/-</sup>IκBβ<sup>-/-</sup>IκBα<sup>+/-</sup>* mouse bone marrow Dump<sup>+</sup>B220<sup>+</sup>IgM<sup>-</sup>IgD<sup>-</sup> population. Approximate area of the cell surface marker profiles is indicated by dotted lines with the developmental stages labeled respectively. (E) Heatmap showing the Z-score of developmental stage marker gene expression in *WT* and *IκBε<sup>-/-</sup>IκBβ<sup>-/-</sup>IκBα<sup>+/-</sup>* mouse bone marrow Dump<sup>+</sup>B220<sup>+</sup>IgM<sup>-</sup>IgD<sup>-</sup> population based on their cell surface marker and transcriptomic profiles. Surface marker profiles are indicated on the top panel labels while transcriptomic profiles based on K-means clustering are shown in color-coded blocks. *IκBε<sup>-/-</sup>IκBβ<sup>-/-</sup>IκBα<sup>+/-</sup>* is abbreviated as *IκB<sup>-/-</sup>*.

increased NFκB/RelA transcriptional activity, were in fact included in the Fraction B population progenitor identity defined by surface marker profiles in *WT* and *IκBε<sup>-/-</sup>IκBβ<sup>-/-</sup>IκBα<sup>+/-</sup>* mice, we found that Fraction B in *IκBε<sup>-/-</sup>IκBβ<sup>-/-</sup>IκBα<sup>+/-</sup>* mice includes multiple transcriptomic signatures that resembled Cluster C and Cluster C' in *WT*. These results suggested that progenitors defined as Fraction B by cell surface marker profiles, contained transcriptomic states that had moved on to subsequent developmental stages (Figure 15E). Combined with previous results on facilitated transition in Fraction C/C' of *IκBε<sup>-/-</sup>IκBβ<sup>-/-</sup>IκBα<sup>+/-</sup>* mice, we concluded that dysregulated RelA dynamics may facilitate the transition from Fraction B to Fraction D, while cell surface markers used for traditional identification lag behind.

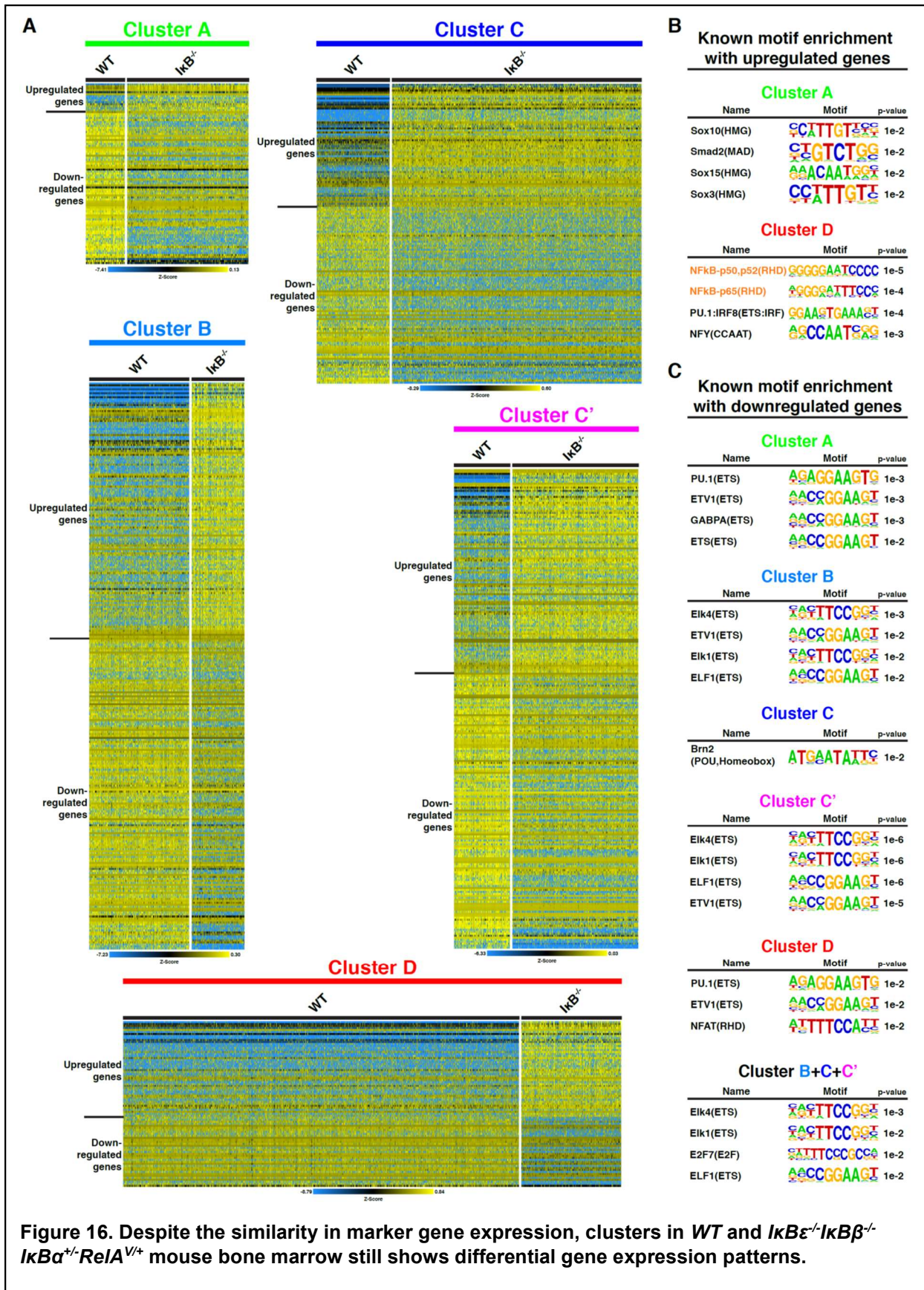
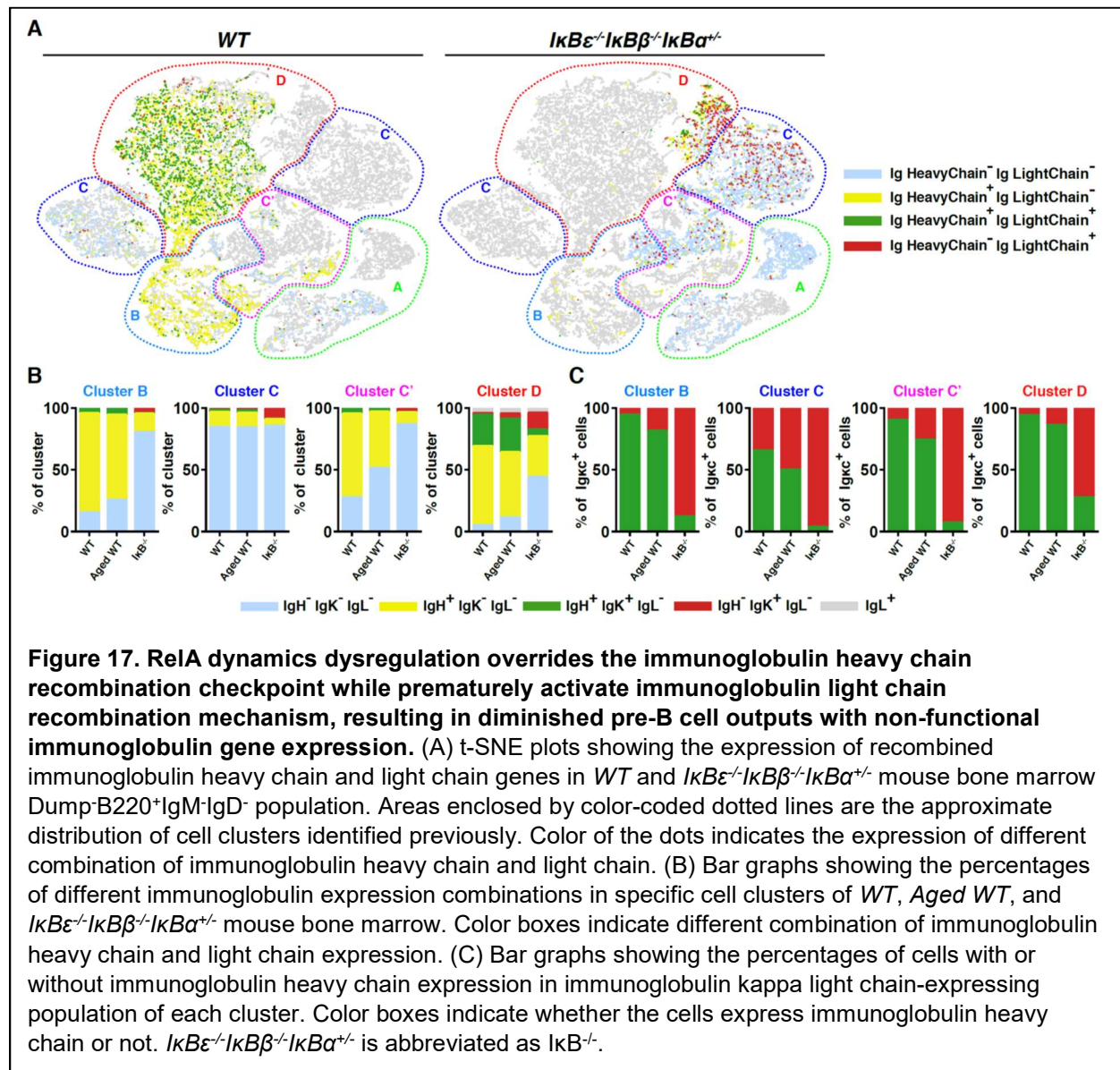


**Figure 16 continued.** (A) Heatmaps showing the differentially expressed genes in each cell cluster in *WT* and *IkBε<sup>-/-</sup>IkBβ<sup>-/-</sup>IkBα<sup>+/-</sup>RelA<sup>V/+</sup>* mouse bone marrow Dump-B220<sup>+</sup>IgM<sup>-</sup>IgD<sup>-</sup> population. Colored box indicates the specific cluster demonstrated in the heatmap, and the black bars indicate the cells from different genotypes. Colormaps of the respective heatmaps are shown. *IkB<sup>-/-</sup>* is abbreviated for *IkBε<sup>-/-</sup>IkBβ<sup>-/-</sup>IkBα<sup>+/-</sup>*. (B) Table panels showing the top 4 results in known motif enrichment analysis on upregulated genes in *IkBε<sup>-/-</sup>IkBβ<sup>-/-</sup>IkBα<sup>+/-</sup>* compared to *WT* cluster A and cluster D. Motifs related to NFκB/RelA were highlighted with orange-colored font. (C) Table panels showing the top 4 results in known motif enrichment analysis on downregulated genes in *IkBε<sup>-/-</sup>IkBβ<sup>-/-</sup>IkBα<sup>+/-</sup>* compared to *WT* clusters. *IkBε<sup>-/-</sup>IkBβ<sup>-/-</sup>IkBα<sup>+/-</sup>* is abbreviated as *IkB<sup>-/-</sup>*. Motifs related to NFκB/RelA were highlighted with orange-colored font. (D) t-SNE plot showing the comparison between transcriptomic profiles and surface marker profiles in cell clusters of *IkBε<sup>-/-</sup>IkBβ<sup>-/-</sup>IkBα<sup>+/-</sup>* mouse bone marrow Dump-B220<sup>+</sup>IgM<sup>-</sup>IgD<sup>-</sup> populations. Populations associated with the cell surface marker profiles are indicated by dotted lines and developmental stage labels. (E) Heatmap showing the Z-scores of developmental stage marker gene expression in *WT* and *IkBε<sup>-/-</sup>IkBβ<sup>-/-</sup>IkBα<sup>+/-</sup>* mouse bone marrow Dump-B220<sup>+</sup>IgM<sup>-</sup>IgD<sup>-</sup> populations based on their cell surface marker and transcriptomic profiles. Surface marker profiles are indicated on the top panel labels while transcriptomic profiles based on K-means clustering are shown in color-coded blocks. *IkBε<sup>-/-</sup>IkBβ<sup>-/-</sup>IkBα<sup>+/-</sup>* is abbreviated as *IkB<sup>-/-</sup>*. Colormaps of the respective heatmaps are shown.

### **Immunoglobulin expression profiling reveals that RelA dysregulation overrides the pre-BCR developmental checkpoint**

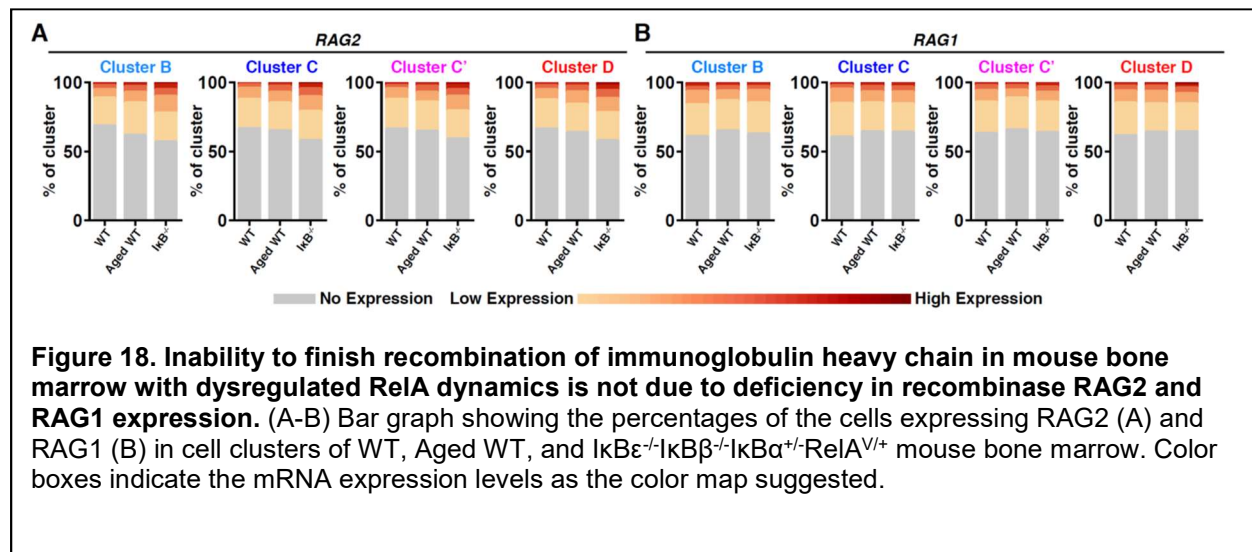
Previous studies have shown that the immunoglobulin heavy chain (IgH) recombination checkpoint is essential to ensure the generation of a functional BCR by requiring signaling activity from the pre-BCR (Geier and Schlissel, 2006; Keenan et al., 2008; Clark et al., 2013). This recombination checkpoint occurs between Fraction C and Fraction C', coinciding with where we found a discrepancy between cell surface markers and transcriptomic states when RelA dynamics are dysregulated. In order to assess the immunoglobulin recombination, we employed immune-profiling by scRNA-seq analysis. In the *WT* sample, we found that 84.0% of the cells expressing recombined IgH as early as cluster B with 89.4% of the cells in cluster D expressing IgH and immunoglobulin κ-light chain as suggested by previous literature (Hardy and Hayakawa, 2001; Melchers, 2015) (Figure 17A). However, in *IkBε<sup>-/-</sup>IkBβ<sup>-/-</sup>IkBα<sup>+/-</sup>* mice we found that merely 14.7% of the B-cell precursors expressing IgH in cluster B, while 5.2% of the cells expressing both IgH and

immunoglobulin  $\kappa$ -light chain in Cluster D (Figure 17A, 17B). Strikingly, some of the cells that did not express IgH showed immunoglobulin light chain expression as early as Cluster B (Figure 17A). To quantitatively assess the differences, we plotted the percentages of cells showing heavy or light chain expression in each cluster, and found that in  $I\kappa B\epsilon^{-/-}I\kappa B\beta^{-/-}I\kappa B\alpha^{+/+}$  mice a considerably number of cells failed to express a recombined IgH chain (Figure 17B). Since the successful recombination is required for the expression of functional pre-BCR



(Jung and Alt, 2004), these results indicate that dysregulation of RelA dynamics negatively affect immunoglobulin recombination despite the fact that mRNA expression levels of *RAG1* and *RAG2* were unaltered (Figure 18A, 18B).

Strikingly, there were also substantially more cells expressing immunoglobulin kappa light chain (Igx) only without the expression of IgH across all clusters in *IκBε<sup>-/-</sup>IκBβ<sup>-/-</sup>IκBα<sup>+/+</sup>* mice (Cluster B: 3.92%, Cluster C: 8.41%, Cluster C':2.95%, Cluster D: 13.6%) compared to *WT* mice (Cluster B: 0.21%, Cluster C: 0.88%, Cluster C':0.38%, Cluster D: 1.53%) (Figure 17B). Within all the cell population expressing Igk, there fewer cells also expressed IgH in *IκBε<sup>-/-</sup>IκBβ<sup>-/-</sup>IκBα<sup>+/+</sup>* mice (Cluster B: 12.1%, Cluster C: 3.61%, Cluster C':7.14%, Cluster D: 27.7%) than *WT* mice (Cluster B: 94.3%, Cluster C: 65.4%, Cluster C':90.3%, Cluster D: 94.3%) (Figure 17C). As pre-BCR signaling activation after the pre-BCR checkpoint was shown to be required for Igk recombination in most cases (Geier and Schlissel, 2006; Keenan et al., 2008; Clark et al., 2013), the data suggested that dysregulation in RelA dynamics enable the B cell progenitors to move on to Igk recombination and differentiation without the requirement of pre-BCR assembly.



Given that dysregulation of RelA dynamics was associated with diminished B cell output in aged mice (Figure 5C, 5D), we examined the immunoglobulin repertoire in this context. We found that the percentages of cells with no immunoglobulin expression, the cells with only IgH expression, and the Igk-expressing cells without IgH expression in *Aged WT* mice (100 weeks old) all seem to follow the trend toward *IkBε<sup>-/-</sup>IkBβ<sup>-/-</sup>IkBα<sup>+/-</sup>* mice (Figure 17B, 17C). These results suggest that dysregulated RelA dynamics tend to elevate NFκB RelA transcriptional activity during Fraction B to Fraction D transition, thus overriding the IgH recombination checkpoint and allowing progenitors to proceed with Igk recombination and differentiation without checkpoint control.

## Discussion

Prompted by previous reports that both absence and elevation of NFκB impacts B cell development (Horwitz et al., 1997; Grossmann et al., 2002; Alcamo et al., 2002; Feng et al., 2004; Jimi et al., 2005; Gerondakis et al., 2006; Claudio et al., 2009; Balkhi et al., 2012; Almaden et al., 2016), our analysis has uncovered the dynamic nature of RelA protein regulation in early B lymphopoiesis. In fact, we found that RelA dynamic regulation plays a crucial role in the proper pacing and coordination of diverse molecular events associated with key developmental stages during early B lymphopoiesis. Perturbed RelA dynamics were found in inflammation-associated aging and cause a reduction in the quantity and quality of the hematopoietic B-cell output.

Previous studies have established that aging is associated with myeloid-biased hematopoiesis that may diminish B-cell production (Beerman et al., 2010b; Chung and Park, 2017; Pietras, 2017). Other studies have suggested that aging-associated B cells in peripheral lymph organ may impact the pro-B cell to pre-B cell transition by altering

selection to favor low surrogate light-chain expressing cells and reducing pre-B cell outputs *in vitro* (Ratliff et al., 2015; Riley et al., 2018). Our results suggest that the dynamic control of RelA is essential to coordinate developmental pacing and maintain the stringency and effectiveness of preBCR checkpoint. Without the proper regulation on RelA dynamics, the differentiation transitions are rushed not allowing sufficient time in proliferative phases and the preBCR checkpoint may be overridden; together, the consequence is a vastly diminished Fraction D (pre-B cell) population with less immunoglobulin diversity and more non-functional immunoglobulin expression. While acute inflammation may transiently accelerate B-cell production via RelA control of precursors, chronic inflammatory conditions is detrimental. This newly described mechanism provides insights in how aging diminishes vaccination efficacy and increases the risk of infection-associated morbidity.

In addition to the the preBCR checkpoint reducing auto-reactive immunoglobulin recombination in adults (Keenan et al., 2008), a recent study of fetal B-cell development suggested that when the pre-BCR checkpoint is bypassed by premature immunoglobulin kappa light chain recombination self-reactive and specificity-biased mature B cell receptors may result in native B-1a cell populations (Wong et al., 2019). While the majority of Fraction D cells in mice with dysregulated RelA dynamics expressed only immunoglobulin kappa light chain, we found a minor population of Fraction D cells expressing both immunoglobulin heavy and kappa light chains. The similarity in premature immunoglobulin kappa light chain recombination during normal fetal B-cell development and in adult mice with dysregulated RelA suggests that establishing the dynamic regulation of RelA may play a role in the transition between fetal B lymphopoiesis and adult B lymphopoiesis; failure to establish it because of chronic inflammatory conditions

may thus play a role in the generation of auto-reactive antibody in the onset of autoimmunity disease.

B acute lymphoblastic leukemia (B-ALL) is one of the most common leukemias in adults and in children (Terwilliger and Abdul-Hay, 2017). In the patient population suffering B-ALL, Ras pathway mutations are prevalent in relapsed cases and these mutations can potentially activate Elk transcription factors (Irving et al., 2014; Knight and Irving, 2014). Interestingly, dysregulated RelA dynamics mice cause the downregulation of genes Clusters B to C' that are associated with Elk binding motifs (Figure 16C), while NFκB binding motifs are enriched in the regulatory regions of upregulated genes (Figure 15C). Fractions B to C' are the key developmental stages for the onset of B-ALL. The reciprocal relationship between NFκB and Elk family transcription factors in our motif enrichment analysis, suggest some caution in pursuing NFκB inhibition for the treatment of leukemias and chemotherapy (Lopez-Guerra et al., 2010; Zhou et al., 2015; Carrà et al., 2016).

Our study has demonstrated the importance of NFκB RelA dynamic regulation in the pacing of developmental transitions along successive progenitor cell fates and the integrity of preBCR checkpoint. Our findings have also established a new paradigm for how aging and inflammation impact humoral immunity via dysregulation of RelA dynamics: accelerated and uncoordinated differentiation diminishes the B-cell pool and the immunoglobulin repertoire.

## Supplementary tables

Table 1. Input Progenitor Cell Number

Genotype	Fraction A	Fraction B	Fraction C	Fraction C'	Fraction D	Fraction E
WT	349547	1411533	111828	215463	5099111	1184414
WT	265060	745111	229279	306153	4664895	1072940
WT	188948	309888	145169	85478	5517324	2555195
WT	346877	596898	109041	174457	7106660	2118315
WT	553699	1591397	55789	227683	7132488	3225101
WT	650884	1921365	66204	190662	8905639	3168169
WT	600068	875140	268829	235308	5695333	2314813
WT	204142	817433	414673	140704	4088034	1411466
WT	180033	805391	268752	225120	4025187	1233932
WT	310158	590413	323325	187821	6832669	2243060
WT	240791	220038	166852	96959	5041104	1986579
WT	305789	276948	131572	116019	3876650	1200358
IκBε <sup>-/-</sup> -IκBβ <sup>-/-</sup> -IκBα <sup>+/-</sup> -RelAV/+	144485	358293	3886	934	261630	28328
IκBε <sup>-/-</sup> -IκBβ <sup>-/-</sup> -IκBα <sup>+/-</sup> -RelAV/+	574784	806682	5559	2297	656646	167446
IκBε <sup>-/-</sup> -IκBβ <sup>-/-</sup> -IκBα <sup>+/-</sup> -RelAV/+	496527	1344805	2682	1979	237616	24498
IκBε <sup>-/-</sup> -IκBβ <sup>-/-</sup> -IκBα <sup>+/-</sup> -RelAV/+	555808	2007291	7087	3412	515356	271036
IκBε <sup>-/-</sup> -IκBβ <sup>-/-</sup> -IκBα <sup>+/-</sup> -RelAV/+	434720	1245308	2140	1823	411475	96681
IκBε <sup>-/-</sup> -IκBβ <sup>-/-</sup> -IκBα <sup>+/-</sup> -RelAV/+	80530	276245	6023	557	175705	21461
IκBε <sup>-/-</sup> -IκBβ <sup>-/-</sup> -IκBα <sup>+/-</sup> -RelAV/+	130773	257094	4244	1656	124631	52999
IκBε <sup>-/-</sup> -IκBβ <sup>-/-</sup> -IκBα <sup>+/-</sup> -RelAV/+	291647	484650	10849	2243	144250	92081
IκBε <sup>-/-</sup> -IκBβ <sup>-/-</sup> -IκBα <sup>+/-</sup> -RelAV/+	261115	570024	6622	2823	55878	616
IκBε <sup>-/-</sup> -IκBβ <sup>-/-</sup> -IκBα <sup>+/-</sup> -RelAV/+	341919	875993	16192	1856	328529	132118
IκBε <sup>-/-</sup> -IκBβ <sup>-/-</sup> -IκBα <sup>+/-</sup> -RelAV/+	279248	760570	3259	957	283375	35403
IκBε <sup>-/-</sup> -IκBβ <sup>-/-</sup> -IκBα <sup>+/-</sup> -RelAV/+	365723	807592	5042	1521	158053	16326
IκBε <sup>-/-</sup> -IκBβ <sup>-/-</sup> -IκBα <sup>+/-</sup> -RelAV/-	84619	149180	29454	12109	1546479	1633234
IκBε <sup>-/-</sup> -IκBβ <sup>-/-</sup> -IκBα <sup>+/-</sup> -RelAV/-	563368	1029765	83970	40081	1747227	1520893
IκBε <sup>-/-</sup> -IκBβ <sup>-/-</sup> -IκBα <sup>+/-</sup> -RelAV/-	524655	2323657	32019	20181	1999099	485527
IκBε <sup>-/-</sup> -IκBβ <sup>-/-</sup> -IκBα <sup>+/-</sup> -RelAV/-	476017	741524	52909	24205	984754	1297975
IκBε <sup>-/-</sup> -IκBβ <sup>-/-</sup> -IκBα <sup>+/-</sup> -RelAV/-	1118092	1639652	20044	14312	770671	232726
IκBε <sup>-/-</sup> -IκBβ <sup>-/-</sup> -IκBα <sup>+/-</sup> -RelAV/-	52469	471519	13227	17307	349492	236096
IκBε <sup>-/-</sup> -IκBβ <sup>-/-</sup> -IκBα <sup>+/-</sup> -RelAV/-	266560	354672	43198	18826	1358998	1533069
IκBε <sup>-/-</sup> -IκBβ <sup>-/-</sup> -IκBα <sup>+/-</sup> -RelAV/-	392985	825537	78290	45055	1243276	1185249

Table 2. Inferred Input Net Proliferation Rate(g)

Name	Description	Value
$g_{w1}$	Net proiferation rate in fraction A in wild-type	0.1
$g_{w2}$	Net proiferation rate in fraction B in wild-type	1
$g_{w3}$	Net proiferation rate in fraction C in wild-type	0.1
$g_{w4}$	Net proiferation rate in fraction C' in wild-type	5
$g_{w5}$	Net proiferation rate in fraction D in wild-type	1
$g_{w6}$	Net proiferation rate in fraction E in wild-type	0.1
$g_{m1}$	Net proiferation rate in fraction A in $I\kappa B\epsilon^{-}/-I\kappa B\beta^{-}/-I\kappa B\alpha^{+}/-RelAV/+$ mice	0.1
$g_{m2}$	Net proiferation rate in fraction B in $I\kappa B\epsilon^{-}/-I\kappa B\beta^{-}/-I\kappa B\alpha^{+}/-RelAV/+$ mice	0.8
$g_{m3}$	Net proiferation rate in fraction C in $I\kappa B\epsilon^{-}/-I\kappa B\beta^{-}/-I\kappa B\alpha^{+}/-RelAV/+$ mice	0.1
$g_{m4}$	Net proiferation rate in fraction C' in $I\kappa B\epsilon^{-}/-I\kappa B\beta^{-}/-I\kappa B\alpha^{+}/-RelAV/+$ mice	1
$g_{m5}$	Net proiferation rate in fraction D in $I\kappa B\epsilon^{-}/-I\kappa B\beta^{-}/-I\kappa B\alpha^{+}/-RelAV/+$ mice	0.02
$g_{m6}$	Net proiferation rate in fraction E in $I\kappa B\epsilon^{-}/-I\kappa B\beta^{-}/-I\kappa B\alpha^{+}/-RelAV/+$ mice	0.01

Table 3. Differentiation Rate from model fitting with progenitor cell number with inferred input net proliferation rate

Genotype	Fraction A	Fraction B	Fraction C	Fraction C'	Fraction D	Fraction E
WT	1	1.2476	15.848	13.225	1.5588	6.8111
WT	1	1.3557	4.5059	8.3745	1.5496	6.8373
WT	1	1.6097	3.5362	11.006	1.1705	2.6274
WT	1	1.5811	8.7553	10.472	1.2571	4.3173
WT	1	1.3479	38.55	14.446	1.4611	3.3314
WT	1	1.3388	38.953	18.526	1.3966	4.0259
WT	1	1.6857	5.5875	11.384	1.4703	3.7176
WT	1	1.2497	2.5636	12.555	1.4321	4.2479
WT	1	1.2235	3.7667	9.4967	1.5311	5.0947
WT	1	1.5253	2.8853	9.967	1.274	3.9807
WT	1	2.0943	2.8619	9.9249	1.1909	3.122
WT	1	2.1041	4.529	10.136	1.3034	4.3093
IκBε <sup>-/-</sup> -IκBβ <sup>-/-</sup> -IκBα <sup>+/-</sup> -RelAV <sup>+/+</sup>	1	1.2033	111.05	463.05	1.8529	17.123
IκBε <sup>-/-</sup> -IκBβ <sup>-/-</sup> -IκBα <sup>+/-</sup> -RelAV <sup>+/+</sup>	1	1.5125	219.6	532.44	2.0625	8.098
IκBε <sup>-/-</sup> -IκBβ <sup>-/-</sup> -IκBα <sup>+/-</sup> -RelAV <sup>+/+</sup>	1	1.1692	586.47	795.82	6.8267	66.224
IκBε <sup>-/-</sup> -IκBβ <sup>-/-</sup> -IκBα <sup>+/-</sup> -RelAV <sup>+/+</sup>	1	1.0769	305.1	634.68	4.4025	8.381
IκBε <sup>-/-</sup> -IκBβ <sup>-/-</sup> -IκBα <sup>+/-</sup> -RelAV <sup>+/+</sup>	1	1.1491	668.88	786.21	3.6826	15.683
IκBε <sup>-/-</sup> -IκBβ <sup>-/-</sup> -IκBα <sup>+/-</sup> -RelAV <sup>+/+</sup>	1	1.0915	50.16	543.64	1.9227	15.751
IκBε <sup>-/-</sup> -IκBβ <sup>-/-</sup> -IκBα <sup>+/-</sup> -RelAV <sup>+/+</sup>	1	1.3087	79.375	204.4	2.9163	6.8677
IκBε <sup>-/-</sup> -IκBβ <sup>-/-</sup> -IκBα <sup>+/-</sup> -RelAV <sup>+/+</sup>	1	1.4018	62.721	304.31	4.9327	7.7373
IκBε <sup>-/-</sup> -IκBβ <sup>-/-</sup> -IκBα <sup>+/-</sup> -RelAV <sup>+/+</sup>	1	1.2581	108.39	255.23	13.096	1188
IκBε <sup>-/-</sup> -IκBβ <sup>-/-</sup> -IκBα <sup>+/-</sup> -RelAV <sup>+/+</sup>	1	1.1903	64.498	563.77	3.3845	8.4259
IκBε <sup>-/-</sup> -IκBβ <sup>-/-</sup> -IκBα <sup>+/-</sup> -RelAV <sup>+/+</sup>	1	1.1672	272.47	929.08	3.3371	26.721
IκBε <sup>-/-</sup> -IκBβ <sup>-/-</sup> -IκBα <sup>+/-</sup> -RelAV <sup>+/+</sup>	1	1.2529	200.79	666.76	6.6144	64.047
IκBε <sup>-/-</sup> -IκBβ <sup>-/-</sup> -IκBα <sup>+/-</sup> -RelAV <sup>-/-</sup>	1	1.3672	7.0249	18.087	0.3416	0.3335
IκBε <sup>-/-</sup> -IκBβ <sup>-/-</sup> -IκBα <sup>+/-</sup> -RelAV <sup>-/-</sup>	1	1.3471	16.62	35.819	1.0217	1.1837
IκBε <sup>-/-</sup> -IκBβ <sup>-/-</sup> -IκBα <sup>+/-</sup> -RelAV <sup>-/-</sup>	1	1.0258	74.543	119.27	1.404	5.7909
IκBε <sup>-/-</sup> -IκBβ <sup>-/-</sup> -IκBα <sup>+/-</sup> -RelAV <sup>-/-</sup>	1	1.4419	20.309	45.392	1.3157	1.0082
IκBε <sup>-/-</sup> -IκBβ <sup>-/-</sup> -IκBα <sup>+/-</sup> -RelAV <sup>-/-</sup>	1	1.4819	121.32	170.92	3.374	11.183
IκBε <sup>-/-</sup> -IκBβ <sup>-/-</sup> -IκBα <sup>+/-</sup> -RelAV <sup>-/-</sup>	1	0.9113	32.586	25.903	1.4828	2.2049
IκBε <sup>-/-</sup> -IκBβ <sup>-/-</sup> -IκBα <sup>+/-</sup> -RelAV <sup>-/-</sup>	1	1.5516	12.839	30.46	0.622	0.5613
IκBε <sup>-/-</sup> -IκBβ <sup>-/-</sup> -IκBα <sup>+/-</sup> -RelAV <sup>-/-</sup>	1	1.276	13.555	24.554	1.0898	1.1532

IκBε<sup>-/-</sup>-IκBβ<sup>-/-</sup>-IκBα<sup>+/-</sup>-RelAV<sup>-/-</sup> cell numbers were fitted with assumed net proliferation rate of IκBε<sup>-/-</sup>-IκBβ<sup>-/-</sup>-IκBα<sup>+/-</sup>-RelAV<sup>+/+</sup>

Table 4. Differentiation Rate from model fitting with progenitor cell number with homogeneous net proliferation rate = 0.5

Genotype	Fraction A	Fraction B	Fraction C	Fraction C'	Fraction D	Fraction E
WT	1	0.7476	9.9369	5.6574	0.7391	3.6818
WT	1	0.8557	3.281	2.9571	0.6941	3.5177
WT	1	1.1097	2.8689	5.3723	0.5832	1.7593
WT	1	1.0811	6.4182	4.5116	0.6108	2.549
WT	1	0.8479	24.687	6.5492	0.7091	2.0681
WT	1	0.8388	24.842	9.1261	0.6954	2.4547
WT	1	1.1857	4.3598	5.4809	0.7264	2.2873
WT	1	0.7497	1.9779	6.3292	0.7178	2.5791
WT	1	0.7235	2.6683	3.6854	0.7061	2.8034
WT	1	1.0253	2.3723	4.5838	0.626	2.4069
WT	1	1.5943	2.6025	4.9786	0.5958	2.0118
WT	1	1.6041	3.8766	4.8963	0.6465	2.588
IkBε-/-IkBβ-/-IkBα+/-RelAV/+	1	0.9033	83.785	349.12	1.7462	16.627
IkBε-/-IkBβ-/-IkBα+/-RelAV/+	1	1.2125	176.47	427.55	1.9956	8.3257
IkBε-/-IkBβ-/-IkBα+/-RelAV/+	1	0.8692	436.42	591.96	5.4292	53.159
IkBε-/-IkBβ-/-IkBα+/-RelAV/+	1	0.7769	220.54	458.54	3.5362	7.2238
IkBε-/-IkBβ-/-IkBα+/-RelAV/+	1	0.8491	494.68	581.21	3.0745	13.585
IkBε-/-IkBβ-/-IkBα+/-RelAV/+	1	0.7915	36.801	398.62	1.7632	14.935
IkBε-/-IkBβ-/-IkBα+/-RelAV/+	1	1.0087	61.602	158.35	2.6044	6.6243
IkBε-/-IkBβ-/-IkBα+/-RelAV/+	1	1.1018	49.719	240.93	4.2471	7.1533
IkBε-/-IkBβ-/-IkBα+/-RelAV/+	1	0.9581	82.969	195.1	10.358	940.06
IkBε-/-IkBβ-/-IkBα+/-RelAV/+	1	0.8903	48.667	425.15	2.9014	7.7148
IkBε-/-IkBβ-/-IkBα+/-RelAV/+	1	0.8672	202.86	691.48	2.8349	23.191
IkBε-/-IkBβ-/-IkBα+/-RelAV/+	1	0.9529	153.13	508.25	5.3895	52.678
IkBε-/-IkBβ-/-IkBα+/-RelAV/-	1	1.0672	5.9054	14.864	0.6164	1.0836
IkBε-/-IkBβ-/-IkBα+/-RelAV/-	1	1.0471	13.341	28.449	1.1526	1.8241
IkBε-/-IkBβ-/-IkBα+/-RelAV/-	1	0.7258	53.171	84.86	1.3567	6.086
IkBε-/-IkBβ-/-IkBα+/-RelAV/-	1	1.1419	16.505	36.576	1.399	1.5614
IkBε-/-IkBβ-/-IkBα+/-RelAV/-	1	1.1819	97.182	136.61	3.0369	10.557
IkBε-/-IkBβ-/-IkBα+/-RelAV/-	1	0.6113	22.291	17.536	1.3684	2.5256
IkBε-/-IkBβ-/-IkBα+/-RelAV/-	1	1.2516	10.776	25.226	0.8495	1.253
IkBε-/-IkBβ-/-IkBα+/-RelAV/-	1	0.976	10.792	19.253	1.1977	1.7563

Table 5. Differentiation Rate from model fitting with progenitor cell number with homogeneous net proliferation rate = 1

Genotype	Fraction A	Fraction B	Fraction C	Fraction C'	Fraction D	Fraction E
WT	1	1.2476	16.748	9.6925	1.4096	7.0684
WT	1	1.3557	5.4059	5.0485	1.3313	6.7883
WT	1	1.6097	4.4362	8.5342	1.1322	3.4447
WT	1	1.5811	9.6553	7.0348	1.1727	4.9342
WT	1	1.3479	39.45	10.666	1.3405	3.9646
WT	1	1.3388	39.853	14.838	1.3177	4.704
WT	1	1.6857	6.4875	8.4117	1.3475	4.3155
WT	1	1.2497	3.4636	11.208	1.3857	5.0135
WT	1	1.2235	4.6667	6.5712	1.3675	5.4609
WT	1	1.5253	3.7853	7.5163	1.2066	4.6755
WT	1	2.0943	3.7619	7.4737	1.1437	3.9023
WT	1	2.1041	5.429	7.1569	1.2142	4.9213
IκBε-/-IκBβ-/-IκBα+/-RelAV/+	1	1.4033	130.39	543.53	2.9401	28.154
IκBε-/-IκBβ-/-IκBα+/-RelAV/+	1	1.7125	249.53	604.86	3.1158	13.219
IκBε-/-IκBβ-/-IκBα+/-RelAV/+	1	1.3692	687.67	932.97	8.7688	86.051
IκBε-/-IκBβ-/-IκBα+/-RelAV/+	1	1.2769	362.65	754.2	5.9938	12.397
IκBε-/-IκBβ-/-IκBα+/-RelAV/+	1	1.3491	786.19	923.91	5.0926	22.674
IκBε-/-IκBβ-/-IκBα+/-RelAV/+	1	1.2915	60.232	652.61	3.068	26.118
IκBε-/-IκBβ-/-IκBα+/-RelAV/+	1	1.5087	92.39	237.75	4.1595	10.781
IκBε-/-IκBβ-/-IκBα+/-RelAV/+	1	1.6018	72.556	351.87	6.4724	11.139
IκBε-/-IκBβ-/-IκBα+/-RelAV/+	1	1.4581	126.51	297.72	16.043	1456.3
IκBε-/-IκBβ-/-IκBα+/-RelAV/+	1	1.3903	76.218	666.04	4.7621	12.842
IκBε-/-IκBβ-/-IκBα+/-RelAV/+	1	1.3672	320.04	1091.1	4.6843	38.494
IκBε-/-IκBβ-/-IκBα+/-RelAV/+	1	1.4529	233.72	775.97	8.4651	82.953
IκBε-/-IκBβ-/-IκBα+/-RelAV/-	1	1.5672	8.9378	22.74	1.1781	2.1155
IκBε-/-IκBβ-/-IκBα+/-RelAV/-	1	1.5471	19.973	42.843	1.9828	3.2779
IκBε-/-IκBβ-/-IκBα+/-RelAV/-	1	1.2258	89.957	143.72	2.4509	11.091
IκBε-/-IκBβ-/-IκBα+/-RelAV/-	1	1.6419	24.012	53.487	2.3147	2.7561
IκBε-/-IκBβ-/-IκBα+/-RelAV/-	1	1.6819	138.58	195.09	4.6229	16.309
IκBε-/-IκBβ-/-IκBα+/-RelAV/-	1	1.1113	40.616	32.04	2.5867	4.829
IκBε-/-IκBβ-/-IκBα+/-RelAV/-	1	1.7516	15.381	36.293	1.5028	2.3321
IκBε-/-IκBβ-/-IκBα+/-RelAV/-	1	1.476	16.564	29.783	2.0793	3.1811

Table 6. Residence Time from model fitting with progenitor cell number with inferred input net proliferation rate

Genotype	Fraction A	Fraction B	Fraction C	Fraction C'	Fraction D	Fraction E
WT	1.1111	4.0382	0.0635	0.1216	1.7894	0.149
WT	1.1111	2.8111	0.227	0.2963	1.8195	0.1484
WT	1.1111	1.6401	0.291	0.1665	5.8649	0.3957
WT	1.1111	1.7208	0.1155	0.1827	3.8899	0.2371
WT	1.1111	2.8741	0.026	0.1059	2.1685	0.3095
WT	1.1111	2.9519	0.0257	0.0739	2.5213	0.2547
WT	1.1111	1.4584	0.1822	0.1567	2.1262	0.2764
WT	1.1111	4.0042	0.4059	0.1324	2.3141	0.2411
WT	1.1111	4.4736	0.2727	0.2224	1.8828	0.2002
WT	1.1111	1.9036	0.359	0.2013	3.6499	0.2577
WT	1.1111	0.9138	0.3621	0.203	5.2386	0.3309
WT	1.1111	0.9057	0.2258	0.1947	3.2965	0.2376
IκBε <sup>-/-</sup> IκBβ <sup>-/-</sup> IκBα <sup>+/-</sup> RelAV <sup>+/+</sup>	1.1111	2.4798	0.012	0.0029	0.8051	0.0751
IκBε <sup>-/-</sup> IκBβ <sup>-/-</sup> IκBα <sup>+/-</sup> RelAV <sup>+/+</sup>	1.1111	1.4035	0.0057	0.0023	0.6694	0.1505
IκBε <sup>-/-</sup> IκBβ <sup>-/-</sup> IκBα <sup>+/-</sup> RelAV <sup>+/+</sup>	1.1111	2.7084	0.0023	0.0017	0.2029	0.0201
IκBε <sup>-/-</sup> IκBβ <sup>-/-</sup> IκBα <sup>+/-</sup> RelAV <sup>+/+</sup>	1.1111	3.6115	0.0045	0.0022	0.3296	0.1626
IκBε <sup>-/-</sup> IκBβ <sup>-/-</sup> IκBα <sup>+/-</sup> RelAV <sup>+/+</sup>	1.1111	2.8646	0.002	0.0017	0.3884	0.0847
IκBε <sup>-/-</sup> IκBβ <sup>-/-</sup> IκBα <sup>+/-</sup> RelAV <sup>+/+</sup>	1.1111	3.4303	0.0275	0.0025	0.7993	0.0842
IκBε <sup>-/-</sup> IκBβ <sup>-/-</sup> IκBα <sup>+/-</sup> RelAV <sup>+/+</sup>	1.1111	1.966	0.0164	0.0064	0.4768	0.1851
IκBε <sup>-/-</sup> IκBβ <sup>-/-</sup> IκBα <sup>+/-</sup> RelAV <sup>+/+</sup>	1.1111	1.6618	0.0203	0.0042	0.2685	0.1626
IκBε <sup>-/-</sup> IκBβ <sup>-/-</sup> IκBα <sup>+/-</sup> RelAV <sup>+/+</sup>	1.1111	2.183	0.0121	0.0052	0.1017	0.0011
IκBε <sup>-/-</sup> IκBβ <sup>-/-</sup> IκBα <sup>+/-</sup> RelAV <sup>+/+</sup>	1.1111	2.562	0.0208	0.0024	0.4194	0.1556
IκBε <sup>-/-</sup> IκBβ <sup>-/-</sup> IκBα <sup>+/-</sup> RelAV <sup>+/+</sup>	1.1111	2.7236	0.0049	0.0015	0.4288	0.0493
IκBε <sup>-/-</sup> IκBβ <sup>-/-</sup> IκBα <sup>+/-</sup> RelAV <sup>+/+</sup>	1.1111	2.2082	0.0066	0.002	0.2049	0.0203
IκBε <sup>-/-</sup> IκBβ <sup>-/-</sup> IκBα <sup>+/-</sup> RelAV <sup>-/-</sup>	1.1111	1.763	0.185	0.0747	8.8744	3.3775
IκBε <sup>-/-</sup> IκBβ <sup>-/-</sup> IκBα <sup>+/-</sup> RelAV <sup>-/-</sup>	1.1111	1.8279	0.0779	0.0369	1.5507	1.0303
IκBε <sup>-/-</sup> IκBβ <sup>-/-</sup> IκBα <sup>+/-</sup> RelAV <sup>-/-</sup>	1.1111	4.4289	0.019	0.0119	1.1692	0.2301
IκBε <sup>-/-</sup> IκBβ <sup>-/-</sup> IκBα <sup>+/-</sup> RelAV <sup>-/-</sup>	1.1111	1.5578	0.0625	0.0284	1.1238	1.2094
IκBε <sup>-/-</sup> IκBβ <sup>-/-</sup> IκBα <sup>+/-</sup> RelAV <sup>-/-</sup>	1.1111	1.4665	0.0103	0.0074	0.3944	0.1104
IκBε <sup>-/-</sup> IκBβ <sup>-/-</sup> IκBα <sup>+/-</sup> RelAV <sup>-/-</sup>	1.1111	8.9866	0.0459	0.0598	1.1389	0.6267
IκBε <sup>-/-</sup> IκBβ <sup>-/-</sup> IκBα <sup>+/-</sup> RelAV <sup>-/-</sup>	1.1111	1.3306	0.0973	0.042	2.9098	2.075
IκBε <sup>-/-</sup> IκBβ <sup>-/-</sup> IκBα <sup>+/-</sup> RelAV <sup>-/-</sup>	1.1111	2.1007	0.0972	0.0554	1.448	1.0704

IκBε<sup>-/-</sup>IκBβ<sup>-/-</sup>IκBα<sup>+/-</sup>RelAV<sup>-/-</sup> cell numbers were fitted with assumed net proliferation rate of IκBε<sup>-/-</sup>IκBβ<sup>-/-</sup>IκBα<sup>+/-</sup>RelAV<sup>+/+</sup>

Table 7. Residence Time from model fitting with progenitor cell number with homogeneous net proliferation rate = 0.5

Genotype	Fraction A	Fraction B	Fraction C	Fraction C'	Fraction D	Fraction E
WT	Infinity	4.0382	0.0635	0.115	2.4417	0.1648
WT	Infinity	2.8111	0.227	0.247	3.0182	0.1728
WT	Infinity	1.6401	0.291	0.1327	7.5633	0.409
WT	Infinity	1.7208	0.1155	0.1657	5.7906	0.2542
WT	Infinity	2.8741	0.026	0.1035	2.9369	0.3373
WT	Infinity	2.9519	0.0257	0.0723	3.1479	0.27
WT	Infinity	1.4584	0.1822	0.1349	2.8774	0.3016
WT	Infinity	4.0042	0.4059	0.098	2.5924	0.2492
WT	Infinity	4.4736	0.2727	0.1795	2.721	0.2242
WT	Infinity	1.9036	0.359	0.1535	4.84	0.2721
WT	Infinity	0.9138	0.3621	0.1545	6.9567	0.3445
WT	Infinity	0.9057	0.2258	0.1624	4.6688	0.255
IκBε-/-IκBβ-/-IκBα+/-RelAV/+	Infinity	2.4798	0.0077	0.0018	0.5154	0.0368
IκBε-/-IκBβ-/-IκBα+/-RelAV/+	Infinity	1.4035	0.004	0.0017	0.4726	0.0818
IκBε-/-IκBβ-/-IκBα+/-RelAV/+	Infinity	2.7084	0.0015	0.0011	0.1287	0.0118
IκBε-/-IκBβ-/-IκBα+/-RelAV/+	Infinity	3.6115	0.0028	0.0013	0.2002	0.0877
IκBε-/-IκBβ-/-IκBα+/-RelAV/+	Infinity	2.8646	0.0013	0.0011	0.2443	0.0461
IκBε-/-IκBβ-/-IκBα+/-RelAV/+	Infinity	3.4303	0.0169	0.0015	0.4836	0.0398
IκBε-/-IκBβ-/-IκBα+/-RelAV/+	Infinity	1.966	0.0109	0.0042	0.3165	0.1022
IκBε-/-IκBβ-/-IκBα+/-RelAV/+	Infinity	1.6618	0.014	0.0029	0.1827	0.0986
IκBε-/-IκBβ-/-IκBα+/-RelAV/+	Infinity	2.183	0.008	0.0034	0.0665	0.0007
IκBε-/-IκBβ-/-IκBα+/-RelAV/+	Infinity	2.562	0.0133	0.0015	0.2658	0.0844
IκBε-/-IκBβ-/-IκBα+/-RelAV/+	Infinity	2.7236	0.0031	0.0009	0.2714	0.0267
IκBε-/-IκBβ-/-IκBα+/-RelAV/+	Infinity	2.2082	0.0043	0.0013	0.134	0.0122
IκBε-/-IκBβ-/-IκBα+/-RelAV/-	Infinity	1.763	0.126	0.046	5.6162	0.8965
IκBε-/-IκBβ-/-IκBα+/-RelAV/-	Infinity	1.8279	0.0527	0.0239	1.0175	0.439
IκBε-/-IκBβ-/-IκBα+/-RelAV/-	Infinity	4.4289	0.0112	0.007	0.6892	0.0991
IκBε-/-IκBβ-/-IκBα+/-RelAV/-	Infinity	1.5578	0.0435	0.0191	0.7606	0.5694
IκBε-/-IκBβ-/-IκBα+/-RelAV/-	Infinity	1.4665	0.0073	0.0052	0.276	0.0653
IκBε-/-IκBβ-/-IκBα+/-RelAV/-	Infinity	8.9866	0.0252	0.0322	0.6303	0.2612
IκBε-/-IκBβ-/-IκBα+/-RelAV/-	Infinity	1.3306	0.0695	0.0283	1.989	0.7507
IκBε-/-IκBβ-/-IκBα+/-RelAV/-	Infinity	2.1007	0.0642	0.0347	0.9265	0.4585

Table 8. Residence Time from model fitting with progenitor cell number with homogeneous net proliferation rate = 1

Genotype	Fraction A	Fraction B	Fraction C	Fraction C'	Fraction D	Fraction E
WT	2	4.0382	0.106	0.1939	4.1832	0.3143
WT	2	2.8111	0.3596	0.407	5.1527	0.3314
WT	2	1.6401	0.4221	0.2052	12.015	0.7941
WT	2	1.7208	0.169	0.2493	9.0292	0.488
WT	2	2.8741	0.0413	0.1653	4.7833	0.6377
WT	2	2.9519	0.0411	0.1159	5.1182	0.5116
WT	2	1.4584	0.2591	0.2008	4.416	0.5595
WT	2	4.0042	0.6766	0.1715	4.5905	0.481
WT	2	4.4736	0.4612	0.3139	4.8516	0.4341
WT	2	1.9036	0.5341	0.2449	7.9363	0.5244
WT	2	0.9138	0.4756	0.2233	10.443	0.6615
WT	2	0.9057	0.2962	0.2275	6.8244	0.4789
IκBε <sup>-/-</sup> -IκBβ <sup>-/-</sup> -IκBα <sup>+/-</sup> -RelAV <sup>+/+</sup>	2	2.4798	0.012	0.0029	0.8024	0.062
IκBε <sup>-/-</sup> -IκBβ <sup>-/-</sup> -IκBα <sup>+/-</sup> -RelAV <sup>+/+</sup>	2	1.4035	0.0057	0.0023	0.6686	0.1278
IκBε <sup>-/-</sup> -IκBβ <sup>-/-</sup> -IκBα <sup>+/-</sup> -RelAV <sup>+/+</sup>	2	2.7084	0.0023	0.0017	0.2029	0.019
IκBε <sup>-/-</sup> -IκBβ <sup>-/-</sup> -IκBα <sup>+/-</sup> -RelAV <sup>+/+</sup>	2	3.6115	0.0045	0.0022	0.3294	0.1487
IκBε <sup>-/-</sup> -IκBβ <sup>-/-</sup> -IκBα <sup>+/-</sup> -RelAV <sup>+/+</sup>	2	2.8646	0.002	0.0017	0.3884	0.0764
IκBε <sup>-/-</sup> -IκBβ <sup>-/-</sup> -IκBα <sup>+/-</sup> -RelAV <sup>+/+</sup>	2	3.4303	0.0275	0.0025	0.7917	0.0693
IκBε <sup>-/-</sup> -IκBβ <sup>-/-</sup> -IκBα <sup>+/-</sup> -RelAV <sup>+/+</sup>	2	1.966	0.0164	0.0063	0.4752	0.1633
IκBε <sup>-/-</sup> -IκBβ <sup>-/-</sup> -IκBα <sup>+/-</sup> -RelAV <sup>+/+</sup>	2	1.6618	0.0203	0.0042	0.2669	0.1503
IκBε <sup>-/-</sup> -IκBβ <sup>-/-</sup> -IκBα <sup>+/-</sup> -RelAV <sup>+/+</sup>	2	2.183	0.0121	0.0051	0.1014	0.0011
IκBε <sup>-/-</sup> -IκBβ <sup>-/-</sup> -IκBα <sup>+/-</sup> -RelAV <sup>+/+</sup>	2	2.562	0.0208	0.0024	0.4164	0.1386
IκBε <sup>-/-</sup> -IκBβ <sup>-/-</sup> -IκBα <sup>+/-</sup> -RelAV <sup>+/+</sup>	2	2.7236	0.0049	0.0014	0.4283	0.0441
IκBε <sup>-/-</sup> -IκBβ <sup>-/-</sup> -IκBα <sup>+/-</sup> -RelAV <sup>+/+</sup>	2	2.2082	0.0066	0.002	0.2045	0.0192
IκBε <sup>-/-</sup> -IκBβ <sup>-/-</sup> -IκBα <sup>+/-</sup> -RelAV <sup>-/-</sup>	2	1.763	0.185	0.0696	8.592	1.7134
IκBε <sup>-/-</sup> -IκBβ <sup>-/-</sup> -IκBα <sup>+/-</sup> -RelAV <sup>-/-</sup>	2	1.8279	0.0779	0.0358	1.5323	0.7552
IκBε <sup>-/-</sup> -IκBβ <sup>-/-</sup> -IκBα <sup>+/-</sup> -RelAV <sup>-/-</sup>	2	4.4289	0.019	0.0119	1.1673	0.179
IκBε <sup>-/-</sup> -IκBβ <sup>-/-</sup> -IκBα <sup>+/-</sup> -RelAV <sup>-/-</sup>	2	1.5578	0.0625	0.0277	1.1123	0.9421
IκBε <sup>-/-</sup> -IκBβ <sup>-/-</sup> -IκBα <sup>+/-</sup> -RelAV <sup>-/-</sup>	2	1.4665	0.0103	0.0073	0.3942	0.0994
IκBε <sup>-/-</sup> -IκBβ <sup>-/-</sup> -IκBα <sup>+/-</sup> -RelAV <sup>-/-</sup>	2	8.9866	0.0459	0.0587	1.1516	0.4937
IκBε <sup>-/-</sup> -IκBβ <sup>-/-</sup> -IκBα <sup>+/-</sup> -RelAV <sup>-/-</sup>	2	1.3306	0.0973	0.0404	2.8616	1.328
IκBε <sup>-/-</sup> -IκBβ <sup>-/-</sup> -IκBα <sup>+/-</sup> -RelAV <sup>-/-</sup>	2	2.1007	0.0972	0.0533	1.4333	0.796

Table 9. Cumulative characteristic time(AU time) of Cell Flux from model fitting with progenitor cell number with inferred input net proliferation rate

Genotype-serial	CLP-FrA	FrA-FrB	FrB-FrC	FrC-FrC'	FrC'-FrD	FrD-FrE	FrE-
WT-1	0	1	1.8015	1.8646	1.9402	2.5817	2.7285
WT-2	0	1	1.7376	1.9595	2.079	2.7243	2.8705
WT-3	0	1	1.6212	1.904	1.9949	2.8492	3.2298
WT-4	0	1	1.6325	1.7467	1.8422	2.6377	2.8693
WT-5	0	1	1.7419	1.7678	1.837	2.5214	2.8216
WT-6	0	1	1.747	1.7726	1.8266	2.5426	2.791
WT-7	0	1	1.5932	1.7722	1.86	2.5402	2.8092
WT-8	0	1	1.8002	2.1903	2.2699	2.9682	3.2036
WT-9	0	1	1.8173	2.0828	2.1881	2.8412	3.0375
WT-10	0	1	1.6556	2.0022	2.1025	2.8875	3.1387
WT-11	0	1	1.4775	1.8269	1.9277	2.7674	3.0877
WT-12	0	1	1.4753	1.6961	1.7947	2.562	2.794
KO-1	0	1	1.8311	1.8401	1.8422	2.3819	2.4403
KO-2	0	1	1.6611	1.6657	1.6676	2.1524	2.2759
KO-3	0	1	1.8553	1.857	1.8582	2.0047	2.0198
KO-4	0	1	1.9286	1.9319	1.9334	2.1606	2.2799
KO-5	0	1	1.8703	1.8718	1.873	2.1446	2.2083
KO-6	0	1	1.9162	1.9361	1.9379	2.458	2.5215
KO-7	0	1	1.7641	1.7767	1.7816	2.1245	2.2701
KO-8	0	1	1.7134	1.7293	1.7326	1.9353	2.0646
KO-9	0	1	1.7949	1.8041	1.808	1.8844	1.8852
KO-10	0	1	1.8401	1.8556	1.8574	2.1529	2.2715
KO-11	0	1	1.8568	1.8605	1.8615	2.1612	2.1986
KO-12	0	1	1.7982	1.8032	1.8047	1.9558	1.9715

WT: Control, KO:  $I\kappa B\epsilon^{-/-}I\kappa B\beta^{-/-}I\kappa B\alpha^{+/-}RelA^{+/-}$

Table 10. Relative cell flux rate(1/AU time) of Cell Flux from model fitting with progenitor cell number with inferred input net proliferation rate

Genotype-serial	CLP-FrA	FrA-FrB	FrB-FrC	FrC-FrC'	FrC'-FrD	FrD-FrE	FrE-
WT-1	1	1.1	5.1382	5.1702	8.2522	22.84	23.179
WT-2	1	1.1	3.9111	3.9976	9.7728	27.372	27.777
WT-3	1	1.1	2.7401	2.8169	5.0788	34.279	35.631
WT-4	1	1.1	2.8208	2.8522	5.3669	25.854	26.465
WT-5	1	1.1	3.9741	3.9842	6.0402	18.922	19.504
WT-6	1	1.1	4.0519	4.0621	5.5267	19.209	19.696
WT-7	1	1.1	2.5584	2.6032	4.5639	14.055	14.441
WT-8	1	1.1	5.1042	5.3074	8.7536	28.779	29.471
WT-9	1	1.1	5.5736	5.7229	11.975	34.333	35.019
WT-10	1	1.1	3.0036	3.1078	6.1357	28.165	28.889
WT-11	1	1.1	2.0138	2.0831	4.0965	25.032	25.857
WT-12	1	1.1	2.0057	2.0487	3.9457	16.623	17.016
KO-1	1	1.1	3.0838	3.0865	3.093	3.4551	3.4571
KO-2	1	1.1	2.2228	2.2237	2.2277	2.4562	2.4591
KO-3	1	1.1	3.2667	3.2673	3.2713	3.367	3.3675
KO-4	1	1.1	3.9892	3.9905	3.9966	4.182	4.1869
KO-5	1	1.1	3.3917	3.3922	3.3964	3.5857	3.5879
KO-6	1	1.1	3.8443	3.8517	3.8587	4.295	4.2977
KO-7	1	1.1	2.6728	2.676	2.6887	2.8793	2.8833
KO-8	1	1.1	2.4294	2.4331	2.4408	2.5397	2.5429
KO-9	1	1.1	2.8464	2.849	2.8598	2.9026	2.9026
KO-10	1	1.1	3.1496	3.1543	3.1598	3.3519	3.3558
KO-11	1	1.1	3.2789	3.2801	3.2835	3.4865	3.4877
KO-12	1	1.1	2.8666	2.8679	2.8721	2.9585	2.959

WT: Control, KO:  $I\kappa B\epsilon^{-/-}I\kappa B\beta^{-/-}I\kappa B\alpha^{+/-}RelA^{V/+}$

Table 11 Cumulative characteristic time(AU time) of Cell Flux from model fitting with progenitor cell number with homogenous net proliferation rate = 0.5

Genotype-serial	CLP-FrA	FrA-FrB	FrB-FrC	FrC-FrC'	FrC'-FrD	FrD-FrE	FrE-
WT-1	0	1	2.3375	2.4382	2.6149	3.968	4.2396
WT-2	0	1	2.1686	2.4734	2.8115	4.2523	4.5366
WT-3	0	1	1.9011	2.2497	2.4358	4.1504	4.7188
WT-4	0	1	1.925	2.0808	2.3024	3.9397	4.3321
WT-5	0	1	2.1793	2.2198	2.3725	3.7828	4.2664
WT-6	0	1	2.1922	2.2325	2.3421	3.7801	4.1875
WT-7	0	1	1.8434	2.0728	2.2552	3.6318	4.069
WT-8	0	1	2.3338	2.8394	2.9974	4.3904	4.7782
WT-9	0	1	2.3821	2.7569	3.0282	4.4444	4.8011
WT-10	0	1	1.9753	2.3968	2.615	4.2124	4.6279
WT-11	0	1	1.6272	2.0115	2.2123	3.8909	4.3879
WT-12	0	1	1.6234	1.8813	2.0856	3.6323	4.0187
KO-1	0	1	2.1071	2.119	2.1219	2.6946	2.7547
KO-2	0	1	1.8247	1.8304	1.8327	2.3338	2.454
KO-3	0	1	2.1505	2.1527	2.1544	2.3386	2.3574
KO-4	0	1	2.2872	2.2917	2.2939	2.5767	2.7151
KO-5	0	1	2.1777	2.1798	2.1815	2.5067	2.5803
KO-6	0	1	2.2634	2.2906	2.2931	2.8602	2.9272
KO-7	0	1	1.9914	2.0077	2.014	2.3979	2.5489
KO-8	0	1	1.9076	1.9277	1.9319	2.1673	2.3071
KO-9	0	1	2.0438	2.0558	2.0609	2.1575	2.1585
KO-10	0	1	2.1232	2.1437	2.1461	2.4907	2.6204
KO-11	0	1	2.1532	2.1581	2.1596	2.5123	2.5554
KO-12	0	1	2.0495	2.056	2.058	2.2435	2.2625

WT: Control, KO:  $I\kappa B\epsilon^{-/-}I\kappa B\beta^{-/-}I\kappa B\alpha^{+/-}RelA^{+/-}$

Table 12 Relative cell flux rate(1/AU time) of Cell Flux from model fitting with progenitor cell number with homogenous net proliferation rate = 0.5

Genotype-serial	CLP-FrA	FrA-FrB	FrB-FrC	FrC-FrC'	FrC'-FrD	FrD-FrE	FrE-
WT-1	1	1.5	3.5191	3.6791	3.9873	11.281	12.975
WT-2	1	1.5	2.9056	3.3381	3.9156	12.715	14.739
WT-3	1	1.5	2.32	2.7042	2.9304	17.53	24.292
WT-4	1	1.5	2.3604	2.5176	2.769	13.013	16.066
WT-5	1	1.5	2.9371	2.9874	3.193	9.6338	12.546
WT-6	1	1.5	2.976	3.0268	3.1733	10.014	12.448
WT-7	1	1.5	2.2292	2.4532	2.6493	7.3948	9.3236
WT-8	1	1.5	3.5021	4.5178	4.8624	14.875	18.332
WT-9	1	1.5	3.7368	4.4832	5.1084	16.287	19.714
WT-10	1	1.5	2.4518	2.973	3.2758	14.291	17.907
WT-11	1	1.5	1.9569	2.3034	2.5047	12.973	17.098
WT-12	1	1.5	1.9528	2.168	2.3577	8.6964	10.659
KO-1	1	1.5	2.7399	2.7533	2.7566	3.662	3.76
KO-2	1	1.5	2.2017	2.2066	2.2086	2.7798	2.9254
KO-3	1	1.5	2.8542	2.8569	2.8589	3.0982	3.1229
KO-4	1	1.5	3.3057	3.3121	3.3152	3.7788	4.0226
KO-5	1	1.5	2.9323	2.9348	2.9369	3.4101	3.5213
KO-6	1	1.5	3.2152	3.2526	3.256	4.347	4.4802
KO-7	1	1.5	2.483	2.4992	2.5055	2.9821	3.1847
KO-8	1	1.5	2.3309	2.3495	2.3533	2.6006	2.7585
KO-9	1	1.5	2.5915	2.6042	2.6096	2.7166	2.7178
KO-10	1	1.5	2.781	2.8047	2.8074	3.2878	3.481
KO-11	1	1.5	2.8618	2.8677	2.8694	3.3768	3.4401
KO-12	1	1.5	2.6041	2.611	2.6131	2.8292	2.8515

WT: Control, KO:  $I\kappa B\epsilon^{-/-}I\kappa B\beta^{-/-}I\kappa B\alpha^{+/-}RelA^{+/-}$

Table 13 Cumulative characteristic time(AU time) of Cell Flux from model fitting with progenitor cell number with homogenous net proliferation rate = 1

Genotype-serial	CLP-FrA	FrA-FrB	FrB-FrC	FrC-FrC'	FrC'-FrD	FrD-FrE	FrE-
WT-1	0	1	1.8015	1.8612	1.9644	2.6738	2.8153
WT-2	0	1	1.7376	1.9226	2.1207	2.8718	3.0191
WT-3	0	1	1.6212	1.8466	1.9638	2.847	3.1373
WT-4	0	1	1.6325	1.736	1.8782	2.7309	2.9336
WT-5	0	1	1.7419	1.7672	1.861	2.607	2.8592
WT-6	0	1	1.747	1.7721	1.8394	2.5984	2.8109
WT-7	0	1	1.5932	1.7474	1.8663	2.6083	2.8401
WT-8	0	1	1.8002	2.0889	2.1781	2.8997	3.0992
WT-9	0	1	1.8173	2.0316	2.1838	2.915	3.0981
WT-10	0	1	1.6556	1.9198	2.0528	2.8816	3.0955
WT-11	0	1	1.4775	1.7433	1.8771	2.7514	3.0077
WT-12	0	1	1.4753	1.6594	1.7992	2.6228	2.826
KO-1	0	1	1.7126	1.7203	1.7221	2.0623	2.0978
KO-2	0	1	1.5839	1.5879	1.5896	1.9105	1.9862
KO-3	0	1	1.7303	1.7318	1.7329	1.8469	1.8585
KO-4	0	1	1.7831	1.7859	1.7872	1.9541	2.0347
KO-5	0	1	1.7412	1.7425	1.7436	1.94	1.9841
KO-6	0	1	1.7743	1.7909	1.7924	2.1184	2.1567
KO-7	0	1	1.6628	1.6737	1.6779	1.9183	2.011
KO-8	0	1	1.6243	1.6381	1.6409	1.7954	1.8852
KO-9	0	1	1.6858	1.6937	1.6971	1.7594	1.7601
KO-10	0	1	1.7193	1.7324	1.7339	1.9439	2.0217
KO-11	0	1	1.7314	1.7346	1.7355	1.949	1.9749
KO-12	0	1	1.6883	1.6926	1.6939	1.812	1.8241

WT: Control, KO:  $I\kappa B\epsilon^{-/-}I\kappa B\beta^{-/-}I\kappa B\alpha^{+/-}RelA^{+/-}$

Table 14 Relative cell flux rate(1/AU time) of Cell Flux from model fitting with progenitor cell number with homogenous net proliferation rate = 1

Genotype-serial	CLP-FrA	FrA-FrB	FrB-FrC	FrC-FrC'	FrC'-FrD	FrD-FrE	FrE-
WT-1	1	2	6.0382	6.3581	6.9745	21.562	24.951
WT-2	1	2	4.8111	5.6761	6.8311	24.431	28.478
WT-3	1	2	3.6401	4.4084	4.8608	34.061	47.584
WT-4	1	2	3.7208	4.0351	4.5381	25.026	31.132
WT-5	1	2	4.8741	4.9749	5.3861	18.268	24.092
WT-6	1	2	4.9519	5.0536	5.3466	19.029	23.896
WT-7	1	2	3.4584	3.9064	4.2985	13.79	17.647
WT-8	1	2	6.0042	8.0355	8.7248	28.75	35.664
WT-9	1	2	6.4736	7.9664	9.2168	31.575	38.429
WT-10	1	2	3.9036	4.946	5.5516	27.581	34.813
WT-11	1	2	2.9138	3.6068	4.0094	24.945	33.195
WT-12	1	2	2.9057	3.336	3.7154	16.393	20.318
KO-1	1	2	4.4798	4.5067	4.5132	6.3239	6.52
KO-2	1	2	3.4035	3.4131	3.4171	4.5595	4.8509
KO-3	1	2	4.7084	4.7138	4.7178	5.1964	5.2457
KO-4	1	2	5.6115	5.6242	5.6304	6.5576	7.0452
KO-5	1	2	4.8646	4.8695	4.8737	5.8203	6.0427
KO-6	1	2	5.4303	5.5051	5.512	7.6939	7.9604
KO-7	1	2	3.966	3.9984	4.0111	4.9641	5.3694
KO-8	1	2	3.6618	3.699	3.7067	4.2013	4.517
KO-9	1	2	4.183	4.2084	4.2192	4.4332	4.4356
KO-10	1	2	4.562	4.6093	4.6148	5.5756	5.962
KO-11	1	2	4.7236	4.7353	4.7387	5.7535	5.8803
KO-12	1	2	4.2082	4.222	4.2261	4.6583	4.703

WT: Control, KO:  $I\kappa B\epsilon^{-/-}I\kappa B\beta^{-/-}I\kappa B\alpha^{+/-}RelA^{+/-}$

## Material and methods

### Material details

#### *Mice*

All the experimental mice are maintained in the environmental-controlled facilities at the University of California, Los Angeles Division of Laboratory Animal Medicine. All the mice with both sexes were 12-16 weeks old unless otherwise indicated. The wild-type control mice are in C57BL/6J background ordered from The Jackson Lab. Littermates of the different sex were randomly pooled to experimental groups. The  $\text{I}\kappa\text{B}\epsilon^{-/-}\text{I}\kappa\text{B}\beta^{-/-}\text{I}\kappa\text{B}\alpha^{+/+}$  and  $\text{I}\kappa\text{B}\epsilon^{-/-}\text{I}\kappa\text{B}\beta^{-/-}\text{I}\kappa\text{B}\alpha^{+/+}\text{RelA}^{+/+}$  mice were generated by interbreeding  $\text{I}\kappa\text{B}\epsilon^{-/-}$  (Genetic symbol: *Nfkbie<sup>-/-</sup>*),  $\text{I}\kappa\text{B}\beta^{-/-}$  (Genetic symbol: *Nfkbig<sup>-/-</sup>*),  $\text{I}\kappa\text{B}\alpha^{+/+}$  (Genetic symbol: *Nfkbia<sup>+/+</sup>*), with or without *RelA<sup>+/+</sup>* (Genetic symbol: *Rela<sup>+/+</sup>*) mice from the strains described in previous studies (Beg et al., 1995; Hoffmann et al., 2002). The mVenus-RelA knockin mouse line was generated by Ingenious Targeting Laboratory. A donor sequence encoding the monomeric variant of the Venus fluorescent protein (Koushik et al., 2006) joined by a short flexible linker sequence directly upstream of the start codon of the murine *Rela* locus was used to generate, via homologous recombination, a tagged embryonic stem cell line, that was implanted into blastocysts to yield chimeric and then heterozygous mice. These mice were then bred with a mouse line constitutively expressing the *Flp* recombinase to remove the *Neo* resistance marker included in the homologous donor sequence. We then back-crossed the resultant mice with wild-type C57BL/6J mice to remove the *Flp* background and generate homozygously-tagged mice. The mVenus-RelA mice are then interbred with  $\text{I}\kappa\text{B}\epsilon^{-/-}\text{I}\kappa\text{B}\beta^{-/-}\text{I}\kappa\text{B}\alpha^{+/+}$  and  $\text{I}\kappa\text{B}\epsilon^{-/-}\text{I}\kappa\text{B}\beta^{-/-}\text{I}\kappa\text{B}\alpha^{+/+}\text{RelA}^{+/+}$  mice to generate  $\text{I}\kappa\text{B}\epsilon^{-/-}\text{I}\kappa\text{B}\beta^{-/-}\text{I}\kappa\text{B}\alpha^{+/+}\text{RelA}^{+/+}$  and  $\text{I}\kappa\text{B}\epsilon^{-/-}\text{I}\kappa\text{B}\beta^{-/-}\text{I}\kappa\text{B}\alpha^{+/+}\text{RelA}^{V/-}$  mice. B6.SJL-*Ptpca<sup>a</sup> Pepc<sup>b</sup>*/BoyJ mice were ordered from the Jackson laboratory serving as the donor or recipient of the bone marrow chimera

experiments. All animal was maintained and experiments were conducted in compliance with the guidelines under animal protocols approved by UCLA Institutional Animal Care and Use Committee.

### ***Cell Lines***

OP9-M2 cell lines were acquired from Mikkola lab in UCLA. The cells were cultured in OP9 media[MEM $\alpha$  with no nucleosides(Gibco Cat#12561056) with 20% of fetal bovine serum(FBS), 1% 200mM L-glutamine solution(Corning Cat# 25-005-CI), 1% Penicillin-Streptomycin Solution(Corning Cat# 30-002-CI) and 1% MEM Non-Essential Amino Acids Solution(Corning Cat# 25-005-CI)]. The cells were maintained at up to 80% confluency in 37°C with 5% carbon dioxide air-jacketed incubators.

### **Method details**

#### ***Electrophoretic mobility shift assay (EMSA)***

Nuclear extract from L929-differentiated bone marrow-derived macrophages were prepared as described, and EMSA was carried out with standard methods as previous literatures (Hoffmann et al, 2002; Werner et al, 2005; Mitchell et al., 2019). In brief, 2.5 $\mu$ L total normalized nuclear extracts were incubated for 15-min with 0.01pmol of P<sup>32</sup>-labeled 38bp double-stranded oligonucleotide containing two consensus  $\kappa$ B sites, as described in KEY RESOURCES TABLE,

with binding buffer [10mM Tris-Cl (pH 7.5), 50mM NaCl, 10% glycerol, 1% NP-40, 1mM EDTA, 0.1mg/mL Poly(deoxyinosinic-deoxycytidylic)] in a final reaction of 6 $\mu$ L. The reaction mixtures were run on a non-denaturing 5% acrylamide (30:0.8) gel containing 5% glycerol and 1X TGE buffer [24.8mM Tris, 190 mM glycine, 1mM EDTA] at 200 volts for 2 hours. The

gel was visualized by Amersham Typhoon Scanner (GE Healthcare Life Sciences) and analyzed in ImageQuant TL software.

### ***Surface marker flow cytometry analysis***

Primary cells from mouse bone marrow, spleen, and peripheral blood were extracted and purified with methods from previous literature (Montecino-Rodriguez et al., 1997; Pietras et al., 2015; Almaden et al., 2016). The surface marker flow cytometry protocol was revised based on the public protocol “BestProtocols: Staining Cell Surface Targets for Flow Cytometry” provided by Invitrogen. Once the purified cells were prepared as described, the live cell percentages were analyzed by staining and the aliquoted cells with 7-AAD Viability Staining Solution and acquired the cell samples with CytoFlex flow cytometer. The live cell concentration can then be determined by the live cell count from gated non-debris FSC-SSC 7AAD<sup>-</sup> population and dilution factor of the aliquots. 2-3 million of cells from each sample could be aliquoted into individual 1.5ml Eppendorf tubes. The cells were then pelleted by centrifugation at 400g for 5 minutes in 4°C. After removing the supernatant, the cell pellet was resuspended with 50µl of flow cytometry buffer(FACS buffer, 3% FBS in calcium and magnesium-free DPBS, Gibco Cat#14200075) with the addition of 1µl Purified anti-mouse CD16/32 Antibody and incubated for 15 minutes on ice in order to block the unspecific Fc receptor binding. The staining master mix should be prepared in 50µl of FACS buffer for each sample with extra volume to accommodate pipetting error. The combination of antibodies should be referred to the staining panels in KEY RESOURCES TABLE and manufacturer’s specification of individual antibodies. After aliquoting 50µl of the master staining mix to the respective samples, the cells are incubated for 45 minutes on ice in dark. After the primary antibody staining incubation, the cells are washed twice with FACS buffer before proceeding to the different procedures according to the staining panel. For all

the sample stained with panel 2B, 3, and 6, the cell pellets were resuspended in 100µl of FACS buffer with respective fluorophore-conjugated streptavidin, incubated for 30 minutes on ice in dark, and washed twice with FACS buffer before proceeding to the further steps. For the sample stained by panel 2B, 3, 4, 5, 6, 9, and 11, the cell pellets were then resuspended to 300 to 500µl FACS buffer with 0.5µg/ml of DAPI for viability staining, strained through 40µm cell strainer(Fisherbrand, Cat#22-363-547), and subjected to flow cytometry sample acquisition. For sample stained with panel 1, 2A, 7, 8, and 10, Fixable Viability Dye eFluor™ 506 staining was applied prior to the surface antibody staining according to the manufacturer's protocol. All flow cytometry sample data were acquired on BD LSRFortessa X-20 Special Order Product in UCLA Janis V. Flow Cytometry Core Laboratory with adequate compensation setup by using UltraComp eBeads™ Compensation Beads and live cells with staining antibodies and isotype controls prior to actual sample acquisition. The definitions of the B cell developmental population are as follows:

Lineage<sup>-</sup> : B220<sup>-</sup> CD3e<sup>-</sup> CD8a<sup>-</sup> F4/80<sup>-</sup> Gr-1<sup>-</sup> CD11b<sup>-</sup> CD49b<sup>-</sup> TER-119<sup>-</sup>

Dump<sup>-</sup> : CD3e<sup>-</sup> CD8a<sup>-</sup> F4/80<sup>-</sup> Gr-1<sup>-</sup> CD11b<sup>-</sup> CD49b<sup>-</sup> TER-119<sup>-</sup>

LMPP (lymphoid-primed multi-potent progenitor) : Lineage<sup>-</sup> c-Kit<sup>+</sup> Sca1<sup>+</sup> Flt3<sup>+</sup>

CLP (common lymphoid progenitor) : Lineage<sup>-</sup> c-Kit<sup>int</sup> Sca1<sup>int</sup> Flt3<sup>+</sup> Il7r<sup>+</sup>

Fraction A (pre-pro B cell) : Dump<sup>-</sup> B220<sup>+</sup> IgM<sup>-</sup> IgD<sup>-</sup> CD43<sup>+</sup> CD24<sup>-</sup> BP-1<sup>-</sup>

Fraction B (pro-B cell) : Dump<sup>+</sup> B220<sup>+</sup> IgM<sup>-</sup> IgD<sup>+</sup> CD43<sup>+</sup> CD24<sup>+</sup> BP-1<sup>-</sup>

Fraction C (pre-BI cell) : Dump<sup>-</sup> B220<sup>+</sup> IgM<sup>-</sup> IgD<sup>-</sup> CD43<sup>+</sup> CD24<sup>+</sup> BP-1<sup>+</sup>

Fraction C' (large pre-BII cell) : Dump<sup>-</sup> B220<sup>+</sup> IgM<sup>-</sup> IgD<sup>-</sup> CD43<sup>+</sup> CD24<sup>++</sup> BP-1<sup>+</sup>

Fraction D (small pre-BII cell) : Dump<sup>-</sup> B220<sup>+</sup> IgM<sup>-</sup> IgD<sup>-</sup> CD43<sup>-</sup>

Fraction E (immature B cell) : Dump<sup>-</sup> B220<sup>+</sup> IgM<sup>+</sup> IgD<sup>-</sup>

Fraction F (mature B cell) : Dump<sup>-</sup> B220<sup>+</sup> IgM<sup>+</sup> IgD<sup>+</sup>

### ***Immunohistochemistry analysis***

Extracted tissues from mice were immediately fixed with 4% paraformaldehyde (Electron Microscopy Sciences, Cat#RT-15710) diluted in DPBS. All the subsequent tissue procurement, section, H&E staining, and immunohistochemical staining were done by UCLA Translational Pathology Core Laboratory. Paraffin-embedded sections were cut at 4µm thickness and paraffin removed with xylene and rehydrated through graded ethanol. Endogenous peroxidase activity was blocked with 3% hydrogen peroxide in methanol for 10 min. Heat-induced antigen retrieval (HIER) or proteolytic induced epitope retrieval (PIER) was applied on all sample except antigen retrieval was not done for CD45R/B220 staining samples. The slides were then stained with anti-mouse CD3, CD45R, CD11b and Ly-6G antibodies (KEY RESOURCE TABLE). Rabbit anti-rat secondary antibodies were used for all except for CD3 staining samples. The signal was detected using the Dakocytomation Envision+ System Labelled Polymer HRP anti-rabbit (Agilent). All sections were visualized with the diaminobenzidine reaction and counterstained with hematoxylin.

### ***Analysis on apoptotic cell population***

Cell surface Annexing V levels were used to determine apoptotic cell population by following the Annexin V Apoptosis Detection Kit eFluor™ 450 manufacturer's instruction. After the surface marker staining on staining panel 7, the cells were being washed twice with Annexing V staining buffer prior to actual Annexing V staining. After the staining

incubation and two washes followed, the cells were resuspended to 300-500µl of Annexing V staining buffer with 0.5µg/ml of DAPI for viability staining, strained through 40µm cell strainer, and subjected to flow cytometry sample acquisition.

### ***Intracellular staining of Ki-67***

Intracellular Ki-67 protein expression levels were determined after finishing surface marker staining with the antibodies listed in panel 8 except for anti-mouse Ki-67 antibody. The cells were then fixed, permeablized, and stained with Brilliant Violet 421™ anti-mouse Ki-67 Antibody by following FIX & PERM™ Cell Permeabilization Kit manufacturer's instructions.

### ***Bone marrow chimera generation and analysis***

Donor bone marrow cells were isolated from femurs of C57BL/6J, B6.SJL-*Ptprca*<sup>a</sup> *Pepcb*<sup>b</sup>/BoyJ, or  $I\kappa B\epsilon^{-/-}I\kappa B\beta^{-/-}I\kappa B\alpha^{+/+}$  mice and retro-orbitally injected (3-5 million cells intravenously per mouse) into 2- to 3-month-old C57BL/6J, B6.SJL-*Ptprca*<sup>a</sup> *Pepcb*<sup>b</sup>/BoyJ, or  $I\kappa B\epsilon^{-/-}I\kappa B\beta^{-/-}I\kappa B\alpha^{+/+}$  mouse F1 recipients. Before injection, recipient mice were lethally irradiated (1000 rads). Chimeric mice were analyzed 6, 8, 12, and 15 weeks after bone marrow reconstitution. The composition of bone marrow B lymphoid progenitors and hematopoietic lineages in peripheral blood were identified using staining panel 5 and 6. Origin and composition of hematopoietic lineage cells was determined by Ly5.1 and Ly5.2 markers.

### ***Mathematical modeling: formulation***

The B cell lineage follows a hierarchical developmental trajectory as follows:

$$FrA \rightarrow FrB \rightarrow FrC \rightarrow FrC' \rightarrow FrD \rightarrow FrE$$

Let  $n_i$  be the number of cells in population  $i$ , with  $i = 1$  denoting *FrA*, and so on. To be compatible with the experimental data, we start from *FrA* in the current model.

Let  $g_i = \alpha_i - \delta_i$  be the net proliferation rate of population  $i$ , where  $\alpha_i$  is the replication rate and  $\delta_i$  is the death rate of population  $i$ . Besides, let  $\beta_i$  be the differentiation rate of population  $i$  to population  $i + 1$ .

It follows then that for any population,

$$\frac{dn_i}{dt} = \beta_{i-1}n_{i-1} + g_in_i - \beta_in_i. (1)$$

Normal hematopoiesis is a constant and continuous process in adult mouse bone marrow, therefore without further perturbation, the system should have reached steady state. From the flow cytometry results on the bone marrow B cell progenitors and precursors, we can acquire exact cell number of each respective stage in steady state (Figure 12B). At steady state,  $\frac{dn_i}{dt} = 0$  which gives the following expression,

$$n_i = n_{i-1} \frac{\beta_{i-1}}{\beta_i - g_i}. (2)$$

Eq.(2) gives a recursion relation on fitting the number  $n_i$  of population  $i$ . with When the net proliferation rates  $g_i$  are provided for each cell type, given an initial count of early progenitors (such as *FrA* cell), we can forwardly calculate the expected counts of subsequent cell types by fitting the differential rates  $\beta_i$ . The detailed fitting process is given below.

### ***Mathematical modeling: fitting process***

In detail, the model inputs are the measurements on the net proliferation rates  $g_i$  and cell number  $n_i$ . We start from taking the measured number  $n_1$  of *FrA*, choose a value for the free parameter  $\beta_1$ , take the net proliferation rates  $g_i$  from measurements, and then fit the

parameter  $\beta_2$  to match the number  $n_2$  of the experimental measurement by using Eq.(2).

We repeat this fitting procedure for the following populations 3, 4, ..., until the last fraction of cell population is fitted. All simulations were done using MATLAB version R2016b.

In the fitting protocol, we have used the quantified cell numbers from experiments and the inferred net proliferation rates. The cell numbers for each fraction are measured by flow cytometry, with multiple replicates. We have individually used each replicate of cell number measurement for the above fitting procedure and take the mean and the standard deviation of the inferred transition rates as the average and error bar in Figure 12B. For the net proliferation rates, we first analyze the experimental data on intracellular Ki67<sup>+</sup> population percentages and surface-Annexin<sup>+</sup> population percentages. The experimental conditions are detailed in the flow cytometry staining section. Based on these measurements, we set the inferred net proliferation rates for different cell fractions, as listed in Supplemental Tables. For example, both the percentage of cells with elevated *Mki67* mRNA expression (Figure 11C) as well as the Ki67 protein expression distribution in flow cytometry data (Figure 11D) in *WT*Fr.B is higher than that of *WT*Fr.A, the net-proliferation rates of *WT*Fr.B is assumed to be larger. As we focus on inferring the relative difference of the differential rates between cell fractions, only the relative ratio of net-proliferation rates would affect the inference.

We conduct the fitting for the replicates of data from *wt* control and  $\text{IkB}\epsilon^{-/-}\text{IkB}\beta^{-/-}\text{IkB}\alpha^{+/+}$   $\text{RelA}^{V/+}$  mice separately. For the data from  $\text{IkB}\epsilon^{-/-}\text{IkB}\beta^{-/-}\text{IkB}\alpha^{+/+}\text{RelA}^{V/-}$  mice, we have used the measurements on net proliferation rates of  $\text{IkB}\epsilon^{-/-}\text{IkB}\beta^{-/-}\text{IkB}\alpha^{+/+}$  mice, because their cell number are similar. The fitted cell numbers and predicted differentiation rates are plotted in Figure 12C.

The only free parameter in the fitting protocol is  $\beta_1$ , where we choose  $\beta_1 = 0.75$ , and its variation does not dramatically change the qualitative behavior of the predicted differentiation rates. Once  $\beta_1$  is fixed, the above fitting procedure gives an unbiased result of cell numbers matching the experimental data. Consequently, the differential rates for these cell populations are determined, without the necessity to do numerical parameter scans. The whole parameter sets are given in Supplemental Tables.

To further test the robustness of the inference under distinct net proliferation rates in our model, we have also considered the homogeneous net proliferation rates for each population. We take the average net proliferation rates of the cell populations from WT,  $\text{IkB}\epsilon^{-}/\text{IkB}\beta^{-}/\text{IkB}\alpha^{+}$ , and  $\text{IkB}\epsilon^{-}/\text{IkB}\beta^{-}/\text{IkB}\alpha^{+}/\text{RelA}^{+}$  mice separately, then repeat the above analysis. The predicted differential rates show similar trend, predicting higher rates for knockout  $\text{FrC}$  and  $\text{FrC}'$ , as illustrated in Figure 13.

### ***Mathematical modeling: implication***

From the modeling output, a few biological meaningful quantities can be extracted. The residence time is defined as  $1/(\beta_i - g_i)$  for each fraction. It corresponds to the time for the cells in a fraction to run out if the influx were switched off.

According to Eq.(1), the cell fluxes at steady state obey:

$$\beta_i n_i = \beta_{i-1} n_{i-1} + g_i n_i. \quad (3)$$

Therefore, when passing through the cell fraction  $i$ , the cell flux increases  $g_i n_i$ . By using Eq.(3) iteratively, the total cell outflux from  $\text{FrE}$  is:

$$\beta_6 n_6 = \beta_1 n_1 + \sum_{i=2}^6 g_i n_i,$$

where  $\beta_1 n_1$  denotes the cell influx from *FrA*. Note that the total cell outflux is fully determined by the influx, net proliferation rates and cell numbers of each fraction. It is not affected by the inferred transition rates  $\beta_i$  ( $2 < i < 6$ ). It tells that the flux increases are caused by the cell net proliferation flux after passing through each fraction.

### ***Enrichment and sorting of lymphoid progenitor***

Enrichment of the Lineage<sup>+</sup> or B lymphoid population was achieved by negative selection on all the non-B lineage cells with following protocols derived from Invitrogen MagniSort™ Mouse Hematopoietic Lineage Depletion Kit(Invitrogen, Cat#8804-6829-74). Total purified bone marrow cell number was determined by the live bone marrow cell counts from the 7AAD staining on aliquots. The cell pellets were transferred to sterile 5ml round bottom tube(Falcon, Cat#14-959A), resuspended in FACS buffer by the concentration of 10 million cells per 100 $\mu$ l, and incubated with all the biotin-conjugated antibody listed in panel 9 or 11 for 30 minutes on ice. After one wash with FACS buffer, the cell pellets were resuspended in FACS buffer by the concentration of 10 million cells per 100 $\mu$ l, followed by the addition of MagniSort™ Streptavidin Negative Selection Beads by the volume of 20 $\mu$ l per 10 million of cells, then incubated for 20 minutes on ice. After the incubation period, the cells were placed on a handmade magnetic stand with N52 neodymium block magnet attached and followed by the equivalent steps in Invitrogen MagniSort™ Mouse Hematopoietic Lineage Depletion Kit protocol. The cells were then washed and stained with the antibodies listed in surface marker staining panel 9 or 11. The enriched and surface marker-stained cells were then sorted with BD FACSAriaIII sorter in UCLA Janis V. Flow Cytometry Core Laboratory with adequate compensation setup by using UltraComp eBeads™ Compensation Beads and live cells with staining antibodies and isotype controls prior to actual sample sorting.

### ***OP9 feeder preparation***

80% confluent OP9-M2 cells were detached from culture dishes with 0.05% Trypsin-EDTA (Corning Cat# 25-052-Cl) incubated at 37°C for 5 minutes then neutralize the trypsin activity by adding two-fold volume of the trypsin solution. The cells were then pelleted with centrifugation at 400g for 5 minutes. After the centrifugation, the supernatant was removed and the pellet was resuspended with culture medium. The cell mixture was then irradiated at 4000 rads and further centrifugation followed to pellet the cells. The irradiated OP-9 feeder cells were then resuspend with 90% of FBS and 10% DMSO and aliquoted to cryopreservation vials followed by storing the cells in controlled rate freezing apparatus overnight and transferred to liquid nitrogen storage afterward. OP9 feeder cells were thawed, pelleted, resuspended to 0.25 million/ml in OP9 media, and plated at 0.5 million cells/well in the 6-well tissue culture plate (Corning, PN#3516) one day prior to the *ex vivo* differentiation experiments.

### ***CLP ex vivo differentiation assay***

Sorted common lymphoid progenitors from C57BL/6J and  $I\kappa B\epsilon^{-/-}I\kappa B\beta^{-/-}I\kappa B\alpha^{+/+}$  mice were pelleted, resuspended in OP9 media, and seeded at 500 cells per well in a 6-well plate with OP9 feeder cells without removing the existing conditioned OP9 media in the wells. Half volume of the media per well was removed and replenished with fresh OP9 media at 24 hours, 72 hours, 120 hours, and 168 hours after the initial seeding of the progenitor cells. At day 5 and day 7 post initial seeding, the cell mixture was detached by trypsinization and resuspended to single cell suspension by passing through 40 $\mu$ m cell strainer. The differentiated cell sample was then analyzed by flow cytometry analysis on surface marker staining panel 10.

### ***Single-cell RNA sequencing with Ig profiling***

Two of C57BL/6J(12 weeks old), C57BL/6J(100 weeks old), and  $I\kappa B\epsilon^{-/-}I\kappa B\beta^{-/-}I\kappa B\alpha^{+/+}$ (12 weeks old) mouse bone marrow were isolated, purified, and pooled according to their genotype and age respectively as independent samples. The pooled bone marrow cells were then enriched and stained for flow cytometry sorting based on panel 11 described. Notably, since we have also included surface marker staining for the detailed developmental population such as from Fraction A to Fraction D, we were able to acquire the developmental population frequency of each individual stages of the input for the single-cell RNA-sequencing. Sorted Dump<sup>-</sup> B220<sup>+</sup> IgM<sup>-</sup> IgD<sup>-</sup> B cell progenitor/precursors were first washed once and resuspended in PBS with 0.04% bovine serum albumin(BSA, Sigma, Cat#A3059) while the concentration was adjusted to 1200 cells/ $\mu$ l. The cells were then submitted to UCLA Technology Center for Genomics & Bioinformatics for 10X Genomics Chromium captures. Each independent sample was loaded into a separate GEM wells and Chromium Single Cell V(D)J Reagent Kit v1.0 protocol was applied. The cDNA and libraries were evaluated by Agilent TapeStation system to ensure the concentration and size distribution were up to standards. Enriched mouse B cell V(D)J profiling libraries across three samples were pooled and sequenced on one lane of NextSeq500 with 150bp paired-end reads setup, while the gene expression libraries were pooled and sequenced on half lane of Novaseq S2 with 50bp paired-end reads setup.

### ***Data analysis for scRNAseq with Ig profiling***

Cell ranger workflows from 10X genomics were applied in the data analysis. After fastq files were generated, data from Enriched mouse B cell V(D)J profiling libraries were processed by cell ranger vdj program to generate single-cell immunoglobulin sequences,

while the count from gene expression libraries were generated, aggregated, and normalized to the same sequencing depth by cell ranger count and aggr programs. Detection of potential doublets were applied by using DoubletDetection first to estimate the maximum number of potential doublets, then we used Scrublet by automatic setting to determine potential doublets. Then we altered the threshold value in Scrublet to yield the potential doublet number as close as possible to the predicted doublets number obtained from DoubletDetection. Finally, we took the mean of the threshold values obtained from Scrublet automatic setting and based on the DoubletDetection results as the final threshold value in Scrublet setting, and acquired the single-cell barcodes of the potential doublets. These doublets along with part of the immunoglobulin genes which can be detected in greater resolution from the data from B cell V(D)J profiling libraries and *Xist*, which can be differentially expressed based on pooling of mice with different genders, were then excluded by cell ranger reanalyze program. We then used the lowest number of principal component groups sufficient to separate clusters were used to reduce the dimensionality of the data by cellranger reanalyze program. Mapping of K-means clusters by gene expression profiles and their developmental stages in C57BL/6J(12 weeks old) and C57BL/6J(100 weeks old) samples were determined by the expression levels of *Pax5*, *Il7r*, *VpreB1*, *VpreB2*, *VpreB3*, *Igll1*, *Rag1*, *Ccnd3*, and *Mki67*. The mapping of the developmental stages of the  $\text{I}\kappa\text{B}\epsilon^{-}/\text{I}\kappa\text{B}\delta^{-}/\text{I}\kappa\text{B}\alpha^{+/}$  sample was done by using the frequency of the developmental stages which we acquired during the cell sorting along with the expression levels of *VpreB1*, *VpreB2*, *VpreB3*, *Igll1*, and *Ccnd3* in bulk RNA-sequencing data for Fraction B, Fraction C/C', and Fraction D. Data from gene expression libraries and B cell V(D)J profiling libraries were then combined and visualized in loupe cell browser. The marker gene list for developmental population were generated by running differential gene expression analysis on different K-

means clusters by cell ranger in C57BL/6J(12 weeks old) sample. The heatmap of these developmental marker genes was then generated by re-arranging the cells by its developmental stage information with pandas and plotted by seaborn in python platform. Differential gene expression between C57BL/6J(12 weeks old) and  $I\kappa B\epsilon^{-/-}I\kappa B\beta^{-/-}I\kappa B\alpha^{+/}$ (12 weeks old) sample between clusters was determined by cell ranger and known motif enrichment analysis was applied with HOMER. The expression of immunoglobulin heavy chain in single cell was determined by *Ighm* inclusion while the expression of immunoglobulin light chain was determined *Igkc* and *Iglc* inclusion in the immunoglobulin profiling data. The visualization of the single-cell immunoglobulin profiling data with the clustering based on gene expression were integrated by loupe cell browser.

### ***Quantification and statistical analysis***

Quantification of the total cell number in specific population was done by multiplying the specific cell population frequency in purified and live bone marrow cells, acquired from the respective flow-cytometry analysis, by the total live bone marrow or splenocyte cell count, determined by the 7AAD<sup>-</sup> population count under FSC-SSC gate right after primary cell extraction.

Details of the statistical tests applied to replicates of datasets shown in Figures can be found in the corresponding Figure legends. The value 'n' described in the figure legends indicated the number of the animals used in each group. All the numerical figures described in the context were displayed as mean value of the group  $\pm$  SEM. Unpaired Student's *t* tests and two-way analysis of variance (ANOVA) were applied using GraphPad Prism 6 software (\**p* < 0.05, \*\**p* < 0.01, and \*\*\**p* < 0.001). Two-sample Kolmogorov-Smirnov Test were applied using Scipy.stat.kstest package in python platform.

### *Data and code availability*

The sequencing data generated during this study are available Gene Expression Omnibus Series GSE137966. Original data for all the figures in the paper are available at <http://dx.doi.org/10.17632/s38w7jm49c.1>. Equations of the mathematical model of the differentiation pathway are provided in Supplemental Tables. MATLAB code for all models is available at <http://www.signalingystems.ucla.edu/models-and-code/>.

### **Key resource table**

REAGENT or RESOURCE	SOURCE	IDENTIFIER
Antibodies		
<i>Staining Panel 1: Bone marrow lymphoid progenitors</i>		
Pacific Blue™ anti-mouse Lineage Cocktail	BioLegend	Cat#133310 ; RRID: AB_11150779
PE anti-mouse CD117 (c-Kit) Antibody	BioLegend	Cat#105808 ; RRID: AB_313217
PE/Dazzle™ 594 anti-mouse CD127 (IL-7R $\alpha$ ) Antibody	BioLegend	Cat#135032 ; RRID: AB_2564217
CD135 (Flt3) Monoclonal Antibody (A2F10), PerCP-eFluor 710, eBioscience™	Invitrogen	Cat#46-1351-82 ; RRID: AB_10733393
PE/Cy7 anti-mouse Ly-6A/E (Sca-1) Antibody	BioLegend	Cat#108114 ; RRID: AB_493596
CD34 Monoclonal Antibody (RAM34), eFluor 660, eBioscience™	Invitrogen	Cat#50-0341-82 ; RRID: AB_10596826
APC/Cyanine7 anti-mouse CD16/32 Antibody	BioLegend	Cat#101328 ; RRID: AB_2104158
<i>Staining Panel 2: Bone marrow B lineage progenitors</i>		
Purified anti-mouse CD16/32 Antibody (Fc receptor blocker)	BioLegend	Cat#101302 ; RRID: AB_312801
PE anti-mouse CD3 $\epsilon$ Antibody	BioLegend	Cat#100308 ; RRID: AB_312673
CD8a Monoclonal Antibody (53-6.7), PE, eBioscience™	Invitrogen	Cat#12-0081-83 ; RRID: AB_465531
PE anti-mouse F4/80 Antibody	BioLegend	Cat#123110 ; RRID: AB_893486
CD11b Monoclonal Antibody (M1/70), PE, eBioscience™	Invitrogen	Cat#12-0112-83 ; RRID: AB_2734870
PE anti-mouse Ly-6G/Ly-6C (Gr-1) Antibody	BioLegend	Cat#108408 ; RRID: AB_313373
PE anti-mouse CD49b (pan-NK cells) Antibody	BioLegend	Cat#108908 ; RRID: AB_313415

PE anti-mouse TER-119/Erythroid Cells Antibody	BioLegend	Cat#116208 ; RRID: AB_313709
PE/Dazzle™ 594 anti-mouse IgM Antibody	BioLegend	Cat#406530 ; RRID: AB_2566586
CD249 (BP-1) Monoclonal Antibody (6C3), PerCP-eFluor 710, eBioscience™	Invitrogen	Cat#46-5891-82 ; RRID: AB_2573797
PE/Cy7 anti-mouse CD43 Antibody	BioLegend	Cat#143210 ; RRID: AB_2564349
APC anti-mouse/human CD45R/B220 Antibody	BioLegend	Cat#103212 ; RRID: AB_312997
APC/Fire™ 750 anti-mouse CD24 Antibody	BioLegend	Cat#101840 ; RRID: AB_2650876
IgD Monoclonal Antibody (11-26c (11-26)), eFluor 450, eBioscience™	Invitrogen	Cat#48-5993-82 ; RRID: AB_1272202
<i>Staining Panel 3: Lymphoid lineages in splenocyte</i>		
Purified anti-mouse CD16/32 Antibody (Fc receptor blocker)	BioLegend	Cat#101302 ; RRID: AB_312801
FITC anti-mouse CD3ε Antibody	BioLegend	Cat#100306 ; RRID: AB_312671
PE anti-mouse CD23 Antibody	BioLegend	Cat#101608 ; RRID: AB_312833
PerCP/Cy5.5 anti-mouse CD93 (AA4.1, early B lineage) Antibody	BioLegend	Cat#136512 ; RRID: AB_10642683
IgM Monoclonal Antibody (II/41), PE-Cyanine7, eBioscience™	Invitrogen	Cat#25-5790-82 ; RRID: AB_469655
APC anti-mouse CD19 Antibody	BioLegend	Cat#152410 ; RRID: AB_2629839
APC/Fire™ 750 anti-mouse/human CD45R/B220 Antibody	BioLegend	Cat#103260 ; RRID: AB_2572109
Biotin anti-mouse Ly-6G/Ly-6C (Gr-1) Antibody	BioLegend	Cat#108404 ; RRID: AB_313369
Biotin anti-mouse/human CD11b Antibody	BioLegend	Cat#101204 ; RRID: AB_312787
Biotin anti-mouse CD49b (pan-NK cells) Antibody	BioLegend	Cat#108904 ; RRID: AB_313411
Biotin anti-mouse TER-119/Erythroid Cells Antibody	BioLegend	Cat#116204 ; RRID: AB_313705
Streptavidin PE-eFluor™ 610 Conjugate	Invitrogen	Cat#61-4317-82 ; N/A
<i>Staining Panel 4: Lineages in peripheral blood</i>		
Purified anti-mouse CD16/32 Antibody (Fc receptor blocker)	BioLegend	Cat#101302 ; RRID: AB_312801
PE anti-mouse TER-119/Erythroid Cells Antibody	BioLegend	Cat#116208 ; RRID: AB_313709
PE/Dazzle™ 594 anti-mouse/human CD11b Antibody	BioLegend	Cat#101256 ; RRID: AB_2563648
CD3 Monoclonal Antibody (17A2), PerCP-eFluor 710, eBioscience™	Invitrogen	Cat#46-0032-82 ; RRID: AB_1834427
PE/Cy7 anti-mouse Ly-6G/Ly-6C (Gr-1) Antibody	BioLegend	Cat#108416 ; RRID: AB_313381

APC anti-mouse CD19 Antibody	BioLegend	Cat#152410 ; RRID: AB_2629839
APC/Fire™ 750 anti-mouse/human CD45R/B220 Antibody	BioLegend	Cat#103260 ; RRID: AB_2572109
<i>Staining Panel 5: Bone Marrow Chimera experiment: Lineages in peripheral blood</i>		
Purified anti-mouse CD16/32 Antibody (Fc receptor blocker)	BioLegend	Cat#101302 ; RRID: AB_312801
FITC anti-mouse CD45.2 Antibody	BioLegend	Cat#109806 ; RRID: AB_313443
PE anti-mouse TER-119/Erythroid Cells Antibody	BioLegend	Cat#116208 ; RRID: AB_313709
PE/Dazzle™ 594 anti-mouse/human CD11b Antibody	BioLegend	Cat#101256 ; RRID: AB_2563648
CD3 Monoclonal Antibody (17A2), PerCP-eFluor 710, eBioscience™	Invitrogen	Cat#46-0032-82 ; RRID: AB_1834427
PE/Cy7 anti-mouse Ly-6G/Ly-6C (Gr-1) Antibody	BioLegend	Cat#108416 ; RRID: AB_313381
APC anti-mouse/human CD45R/B220 Antibody	BioLegend	Cat#103212 ; RRID: AB_312997
APC/Fire™ 750 anti-mouse CD45.1 Antibody	BioLegend	Cat#110752 ; RRID: AB_2629806
<i>Staining Panel 6: Bone Marrow Chimera experiment: Bone marrow B lineage progenitors</i>		
Purified anti-mouse CD16/32 Antibody (Fc receptor blocker)	BioLegend	Cat#101302 ; RRID: AB_312801
Biotin anti-mouse CD3e Antibody	BioLegend	Cat#100304 ; RRID: AB_312669
Biotin anti-mouse CD8a Antibody	BioLegend	Cat#100704 ; RRID: AB_312743
Biotin anti-mouse F4/80 Antibody	BioLegend	Cat#123106 ; RRID: AB_893501
Biotin anti-mouse Ly-6G/Ly-6C (Gr-1) Antibody	BioLegend	Cat#108404 ; RRID: AB_313369
Biotin anti-mouse/human CD11b Antibody	BioLegend	Cat#101204 ; RRID: AB_312787
Biotin anti-mouse CD49b (pan-NK cells) Antibody	BioLegend	Cat#108904 ; RRID: AB_313411
Biotin anti-mouse TER-119/Erythroid Cells Antibody	BioLegend	Cat#116204 ; RRID: AB_313705
Brilliant Violet 510™ Streptavidin	BioLegend	Cat#405234 ; N/A
FITC anti-mouse CD45.2 Antibody	BioLegend	Cat#109806 ; RRID: AB_313443
PE anti-mouse IgD Antibody	BioLegend	Cat#405706 ; RRID: AB_315028
PE/Dazzle™ 594 anti-mouse IgM Antibody	BioLegend	Cat#406530 ; RRID: AB_2566586
CD249 (BP-1) Monoclonal Antibody (6C3), PerCP-eFluor 710, eBioscience™	Invitrogen	Cat#46-5891-82 ; RRID: AB_2573797
PE/Cy7 anti-mouse CD43 Antibody	BioLegend	Cat#143210 ; RRID: AB_2564349

APC anti-mouse/human CD45R/B220 Antibody	BioLegend	Cat#103212 ; RRID: AB_312997
APC/Fire™ 750 anti-mouse CD24 Antibody	BioLegend	Cat#101840 ; RRID: AB_2650876
Brilliant Violet 711™ anti-mouse CD45.1 Antibody	BioLegend	Cat#110739 ; RRID: AB_2562605
<i>Staining Panel 7: Analysis on apoptotic cell population: Bone marrow B lineage progenitors</i>		
Purified anti-mouse CD16/32 Antibody (Fc receptor blocker)	BioLegend	Cat#101302 ; RRID: AB_312801
PE anti-mouse CD3ε Antibody	BioLegend	Cat#100308 ; RRID: AB_312673
CD8a Monoclonal Antibody (53-6.7), PE, eBioscience™	Invitrogen	Cat#12-0081-83 ; RRID: AB_465531
PE anti-mouse F4/80 Antibody	BioLegend	Cat#123110 ; RRID: AB_893486
CD11b Monoclonal Antibody (M1/70), PE, eBioscience™	Invitrogen	Cat#12-0112-83 ; RRID: AB_2734870
PE anti-mouse Ly-6G/Ly-6C (Gr-1) Antibody	BioLegend	Cat#108408 ; RRID: AB_313373
PE anti-mouse CD49b (pan-NK cells) Antibody	BioLegend	Cat#108908 ; RRID: AB_313415
PE anti-mouse TER-119/Erythroid Cells Antibody	BioLegend	Cat#116208 ; RRID: AB_313709
PE/Dazzle™ 594 anti-mouse IgM Antibody	BioLegend	Cat#406530 ; RRID: AB_2566586
CD249 (BP-1) Monoclonal Antibody (6C3), PerCP-eFluor 710, eBioscience™	Invitrogen	Cat#46-5891-82 ; RRID: AB_2573797
PE/Cy7 anti-mouse CD43 Antibody	BioLegend	Cat#143210 ; RRID: AB_2564349
APC anti-mouse/human CD45R/B220 Antibody	BioLegend	Cat#103212 ; RRID: AB_312997
APC/Fire™ 750 anti-mouse CD24 Antibody	BioLegend	Cat#101840 ; RRID: AB_2650876
Brilliant Violet 605™ anti-mouse IgD Antibody	BioLegend	Cat#405727 ; RRID: AB_2562887
<i>Staining Panel 8: Intracellular staining on Ki-67: Bone marrow B lineage progenitors</i>		
Purified anti-mouse CD16/32 Antibody (Fc receptor blocker)	BioLegend	Cat#101302 ; RRID: AB_312801
PE anti-mouse CD3ε Antibody	BioLegend	Cat#100308 ; RRID: AB_312673
CD8a Monoclonal Antibody (53-6.7), PE, eBioscience™	Invitrogen	Cat#12-0081-83 ; RRID: AB_465531
PE anti-mouse F4/80 Antibody	BioLegend	Cat#123110 ; RRID: AB_893486
CD11b Monoclonal Antibody (M1/70), PE, eBioscience™	Invitrogen	Cat#12-0112-83 ; RRID: AB_2734870
PE anti-mouse Ly-6G/Ly-6C (Gr-1) Antibody	BioLegend	Cat#108408 ; RRID: AB_313373
PE anti-mouse CD49b (pan-NK cells) Antibody	BioLegend	Cat#108908 ; RRID: AB_313415

PE anti-mouse TER-119/Erythroid Cells Antibody	BioLegend	Cat#116208 ; RRID: AB_313709
PE/Dazzle™ 594 anti-mouse IgM Antibody	BioLegend	Cat#406530 ; RRID: AB_2566586
CD249 (BP-1) Monoclonal Antibody (6C3), PerCP-eFluor 710, eBioscience™	Invitrogen	Cat#46-5891-82 ; RRID: AB_2573797
PE/Cy7 anti-mouse CD43 Antibody	BioLegend	Cat#143210 ; RRID: AB_2564349
APC anti-mouse/human CD45R/B220 Antibody	BioLegend	Cat#103212 ; RRID: AB_312997
APC/Fire™ 750 anti-mouse CD24 Antibody	BioLegend	Cat#101840 ; RRID: AB_2650876
Brilliant Violet 605™ anti-mouse IgD Antibody	BioLegend	Cat#405727 ; RRID: AB_2562887
Brilliant Violet 421™ anti-mouse Ki-67 Antibody	BioLegend	Cat#652411 ; RRID: AB_2562663
<i>Staining Panel 9: Enrichment and sorting for common lymphoid progenitors</i>		
Biotin anti-mouse CD3e Antibody	BioLegend	Cat#100304 ; RRID: AB_312669
Biotin anti-mouse CD8a Antibody	BioLegend	Cat#100704 ; RRID: AB_312743
Biotin anti-mouse F4/80 Antibody	BioLegend	Cat#123106 ; RRID: AB_893501
Biotin anti-mouse Ly-6G/Ly-6C (Gr-1) Antibody	BioLegend	Cat#108404 ; RRID: AB_313369
Biotin anti-mouse/human CD11b Antibody	BioLegend	Cat#101204 ; RRID: AB_312787
Biotin anti-mouse CD49b (pan-NK cells) Antibody	BioLegend	Cat#108904 ; RRID: AB_313411
Biotin anti-mouse TER-119/Erythroid Cells Antibody	BioLegend	Cat#116204 ; RRID: AB_313705
Biotin anti-mouse/human CD45R/B220 Antibody	BioLegend	Cat#103204 ; RRID: AB_312989
Brilliant Violet 421™ Streptavidin	BioLegend	Cat#405225; N/A
PE anti-mouse CD117 (c-Kit) Antibody	BioLegend	Cat#105808 ; RRID: AB_313217
PE/Dazzle™ 594 anti-mouse CD127 (IL-7R $\alpha$ ) Antibody	BioLegend	Cat#135032 ; RRID: AB_2564217
CD135 (Flt3) Monoclonal Antibody (A2F10), PerCP-eFluor 710, eBioscience™	Invitrogen	Cat#46-1351-82 ; RRID: AB_10733393
PE/Cy7 anti-mouse Ly-6A/E (Sca-1) Antibody	BioLegend	Cat#108114 ; RRID: AB_493596
CD34 Monoclonal Antibody (RAM34), eFluor 660, eBioscience™	Invitrogen	Cat#50-0341-82 ; RRID: AB_10596826
APC/Cyanine7 anti-mouse CD16/32 Antibody	BioLegend	Cat#101328 ; RRID: AB_2104158
<i>Staining Panel 10: B cell progenitors/precursors in OP9 feeder culture</i>		

CD3e Monoclonal Antibody (145-2C11), FITC, eBioscience™	Invitrogen	Cat#11-0031-85 ; RRID: AB_464883
CD8a Monoclonal Antibody (53-6.7), FITC, eBioscience™	Invitrogen	Cat#11-0081-85 ; RRID: AB_464916
FITC anti-mouse F4/80 Antibody	BioLegend	Cat#123108 ; RRID: AB_893502
FITC anti-mouse Ly-6G/Ly-6C (Gr-1) Antibody	BioLegend	Cat#108406 ; RRID: AB_313371
FITC anti-mouse/human CD11b Antibody	BioLegend	Cat#101206 ; RRID: AB_312789
TER-119 Monoclonal Antibody (TER-119), FITC, eBioscience™	Invitrogen	Cat#11-5921-85 ; RRID: AB_465312
APC anti-mouse/human CD45R/B220 Antibody	BioLegend	Cat#103212 ; RRID: AB_312997
IgM Monoclonal Antibody (II/41), PE-Cyanine7, eBioscience™	Invitrogen	Cat#25-5790-82 ; RRID: AB_469655
CD43 Monoclonal Antibody (eBioR2/60), PE, eBioscience™	Invitrogen	Cat#12-0431-82 ; RRID: AB_465659
CD24 Monoclonal Antibody (M1/69), APC-eFluor 780, eBioscience™	Invitrogen	Cat#47-0242-82 ; RRID: AB_10853172
CD249 (BP-1) Monoclonal Antibody (6C3), PerCP-eFluor 710, eBioscience™	Invitrogen	Cat#46-5891-82 ; RRID: AB_2573797
IgD Monoclonal Antibody (11-26c (11-26)), eFluor 450, eBioscience™	Invitrogen	Cat#48-5993-82 ; RRID: AB_1272202
<i>Staining Panel 11: Enrichment and sorting staining panel for early B cell progenitor populations for scRNAseq</i>		
Purified anti-mouse CD16/32 Antibody (Fc receptor blocker)	BioLegend	Cat#101302 ; RRID: AB_312801
Biotin anti-mouse CD3e Antibody	BioLegend	Cat#100304 ; RRID: AB_312669
Biotin anti-mouse CD8a Antibody	BioLegend	Cat#100704 ; RRID: AB_312743
Biotin anti-mouse F4/80 Antibody	BioLegend	Cat#123106 ; RRID: AB_893501
Biotin anti-mouse Ly-6G/Ly-6C (Gr-1) Antibody	BioLegend	Cat#108404 ; RRID: AB_313369
Biotin anti-mouse/human CD11b Antibody	BioLegend	Cat#101204 ; RRID: AB_312787
Biotin anti-mouse CD49b (pan-NK cells) Antibody	BioLegend	Cat#108904 ; RRID: AB_313411
Biotin anti-mouse TER-119/Erythroid Cells Antibody	BioLegend	Cat#116204 ; RRID: AB_313705
Brilliant Violet 510™ Streptavidin	BioLegend	Cat#405234 ; N/A
PE anti-mouse IgD Antibody	BioLegend	Cat#405706 ; RRID: AB_315028
PE/Dazzle™ 594 anti-mouse IgM Antibody	BioLegend	Cat#406530 ; RRID: AB_2566586

CD249 (BP-1) Monoclonal Antibody (6C3), PerCP-eFluor 710, eBioscience™	Invitrogen	Cat#46-5891-82 ; RRID: AB_2573797
PE/Cy7 anti-mouse CD43 Antibody	BioLegend	Cat#143210 ; RRID: AB_2564349
APC anti-mouse/human CD45R/B220 Antibody	BioLegend	Cat#103212 ; RRID: AB_312997
APC/Fire™ 750 anti-mouse CD24 Antibody	BioLegend	Cat#101840 ; RRID: AB_2650876
<i>Immunohistochemistry staining</i>		
Rabbit polyclonal anti-CD3 antibody	Agilent	Cat#A045201-2 ; RRID: N/A
Purified Rat Anti-Mouse CD45R, Clone RA3-6B2	BD Biosciences	Cat#550286 ; RRID: AB_393581
Rat Anti-Mouse CD11b Monoclonal antibody, Unconjugated, Clone M1/70.15	BioRad	Cat#MCA74G ; RRID: AB_321293
Purified Rat Anti-Mouse Ly-6G, Clone 1A8	BD Biosciences	Cat#551459 ; RRID: AB_394206
Chemicals, Peptides, and Recombinant Proteins		
DAPI (4',6-Diamidino-2-Phenylindole, Dilactate)	Invitrogen	Cat#D3571 ; RRID: AB_2307445
eBioscience™ Fixable Viability Dye eFluor™ 506	Invitrogen	Cat#50-246-097 ; N/A
Critical Commercial Assays		
7-AAD Viability Staining Solution	BioLegend	Cat#420404 ; N/A
Annexin V Apoptosis Detection Kit eFluor™ 450	Invitrogen	Cat#88-8006-74 ; RRID: AB_2575164
FIX & PERM™ Cell Permeabilization Kit	Invitrogen	Cat#GAS004 ; N/A
IC fixation buffer	Invitrogen	Cat#00-8222-49 ; N/A
UltraComp eBeads™ Compensation Beads	Invitrogen	Cat#01-2222-41 ; N/A
Dakocytomation Envision+ System Labelled Polymer HRP anti-rabbit antibody	Agilent	PN#K4003 ; RRID: AB_2630375
MagniSort™ Streptavidin Negative Selection Beads	Invitrogen	Cat#MSNB-6002- 74 ; N/A
Chromium Single Cell 5' Library & Gel Bead Kit	10X Genomics	PN#1000014 ; N/A
Chromium Single Cell A Chip Kit	10X Genomics	PN#1000009 ; N/A
Chromium i7 Multiplex Kit	10X Genomics	PN#120262 ; N/A
Chromium Single Cell 5' Library Construction Kit	10X Genomics	PN#1000020 ; N/A
Chromium Single Cell V(D)J Enrichment Kit, Mouse B Cell	10X Genomics	PN#1000072 ; N/A
SPRIselect Reagent Kit	Beckman Coulter	PN#B23318 ; N/A
Deposited Data		
Single-cell RNA sequencing analysis data	This manuscript	GSE137966
Experimental Models: Cell Lines		
OP9-M2	Mikkola Lab UCLA	N/A
Experimental Models: Organisms/Strains		

Mouse: C57BL/6J	The Jackson Laboratory	JAX: 000664 ; RRID: IMSR_JAX:000664
Mouse: B6.SJL- <i>Ptprca</i> <sup>a</sup> <i>Pepcb</i> <sup>b</sup> /BoyJ	The Jackson Laboratory	JAX: 002014 ; RRID: IMSR_JAX:002014
Mouse: C57BL/6: RelA-mVenus	This manuscript	N/A
Mouse: C57BL/6: <i>Nfkbie</i> <sup>-/-</sup> <i>Nfkbib</i> <sup>-/-</sup> <i>Nfkbia</i> <sup>+/-</sup>	This manuscript	N/A
Mouse: C57BL/6: <i>Nfkbie</i> <sup>-/-</sup> <i>Nfkbib</i> <sup>-/-</sup> <i>Nfkbia</i> <sup>+/-</sup> <i>Rela</i> <sup>+/-</sup>	This manuscript	N/A
Oligonucleotides		
NFκB-EMSA probe	This manuscript	(5'GCTACAAGGG ACTTTCGCTG GGGACTTCCA GGGAGG-3')
Software and Algorithms		
ImageQuant TL	GE Healthcare Life Sciences	N/A
FlowJo	FlowJo, LLC	v10.6 ; N/A
Seaborn	Github	v0.9 ; <a href="https://github.com/mwaskom/seaborn">https://github.com/mwaskom/seaborn</a>
Scipy	Github	v1 ; <a href="https://github.com/scipy/scipy">https://github.com/scipy/scipy</a>
GraphPad Prism	GraphPad	Version 6 ; RRID:SCR_002798
MathWorks MATLAB	MathWorks, Inc	R2014a ; RRID: SCR_001622
Cell Ranger	10X Genomics	3.0 ; N/A
Loupe Cell Browser	10X Genomics	3.1.1 ; N/A
Scrublet	Github	Wolock et al., 2019 ; <a href="https://github.com/AllonKleinLab/scrublet">https://github.com/AllonKleinLab/scrublet</a>
DoubletDetection	Github	Gayoso et al., 2018 ; N/A <a href="https://github.com/JonathanShor/DoubletDetection">https://github.com/JonathanShor/DoubletDetection</a>
Pandas	Github	0.24.0 ; <a href="https://github.com/pandas-dev/pandas">https://github.com/pandas-dev/pandas</a>
HOMER Motif Analysis	Benner Lab, University of California, San Diego	<a href="http://homer.ucsd.edu/homer/motif/">http://homer.ucsd.edu/homer/motif/</a>
All Mathematical Modeling Code	This manuscript	<a href="https://www.signaling-systems.ucla.edu/models-and-code/">https://www.signaling-systems.ucla.edu/models-and-code/</a>

## **Acknowledgement**

The work presented in this chapter was a result of collaboration from different colleagues and is currently unpublished. Yi Liu has provided major contribution on assisting all the experiments and providing feedback on data analysis. Ying Tang and Arnav Mehta have contributed to the mathematical modeling establishment and modeling-associated data analysis. Jennifer K. King, May Paing, and Prof. Dinesh Rao have provided support in the bone marrow chimera experiments. Prof. Dinesh Rao also contributed the analysis on histochemistry samples based on his expertise.

In addition to all the co-authors and corresponding author, I would also like to acknowledge Prof. Harry Leighton Grimes and Dr. Andre Olsson from Cincinnati Children's Hospital Medical Center on the help in designing and performing single-cell RNA sequencing analysis. I would like to personally thank my wife, Li Lei, for providing the artistic feedback and illustration of the mice for the figures.

I want to acknowledge UCLA Janis V. Giorgi Flow Cytometry Core Laboratory for providing the instrument and support for majority of the flow cytometry experiments, UCLA Translational Pathology Core Laboratory (TPCL) for providing the service on histochemistry analysis, and UCLA Technology Center for Genomics & Bioinformatics (TCGB) for the single-cell RNA sequencing assistance.

The dissertation author is the primary researcher and author of this study. Yi Liu, Ying Tang, Arnav Mehta, Jennifer K King, May Paing, and Dinesh S. Rao are co-authors. Alexander Hoffmann is the corresponding author.

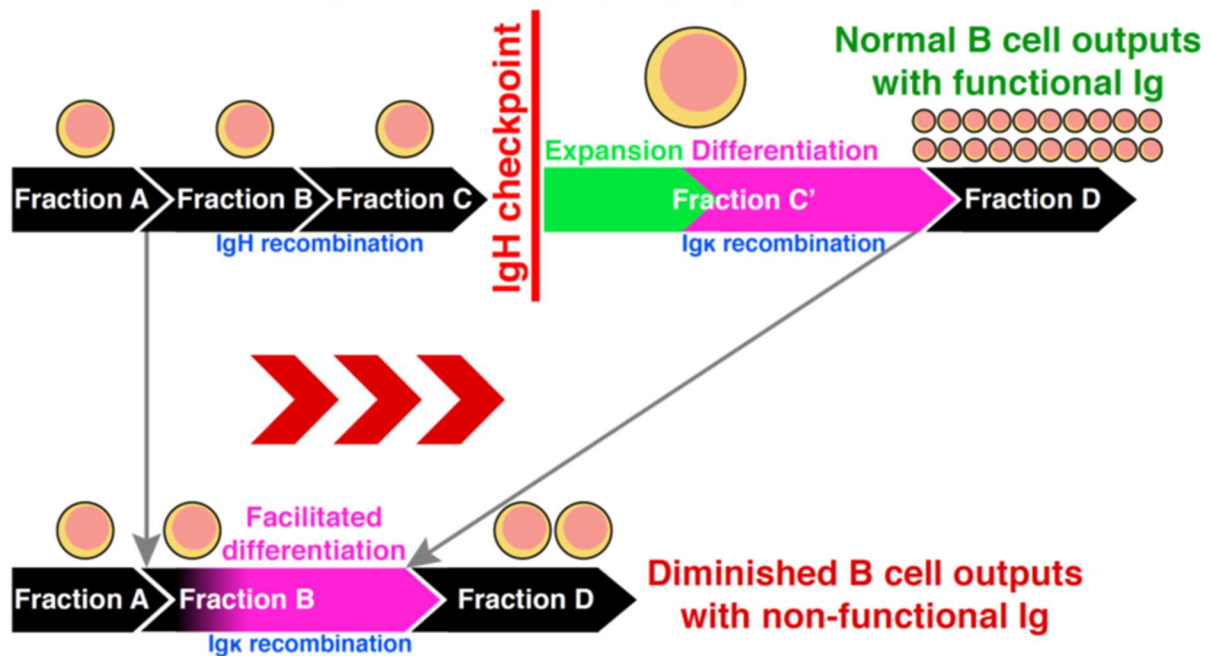
## **Chapter 3: Conclusion and Future Directions**

## Conclusion

Aging and inflammation are known to impact lymphoid repertoire while the prevailing explanation is due to myeloid-biased hematopoiesis. By using NF $\kappa$ B reporter mice, we uncovered dramatic dynamics in RelA control during early B lymphopoiesis while the dysregulation of RelA dynamics correlates with diminished bone marrow B cell outputs in aging. Through the genetic perturbation, we found that dysregulated RelA dynamics lead to severe B lymphopenia in a cell-intrinsic manner. By using mathematical modeling of the differentiation pathway, we described the paradoxical phenomenon that a differentiation hypermorph leads to diminished downstream precursor cells. Single-cell transcriptomic analysis suggested RelA dynamic dysregulation resulted in accelerated transcriptomic states not in sync with the defined progenitor cell types and a preBCR checkpoint override, which consequently resulted in nonfunctional immunoglobulin expression. Our findings establish a new paradigm for how aging and inflammation impact humoral immunity via dysregulation of RelA dynamics: accelerated differentiation diminishes the B-cell repertoire.

# Normal B lymphopoiesis

when  $\text{NF}\kappa\text{B}/\text{RelA}$  dynamics are properly regulated



# Rush-through B lymphopoiesis

when  $\text{NF}\kappa\text{B}/\text{RelA}$  dynamics are dysregulated

Figure 19. Schematics demonstrating how dysregulation in  $\text{RelA}$  dynamic controls impacts early B lymphopoiesis by rushing the Fraction B to Fraction D transition and results in diminished B cell repertoire.

## Future Directions

### Investigating the roles of NFκB dynamics control in the transition between fetal and adult B lymphopoiesis

Previous literature suggested that in fetal B lymphopoiesis, some of the pro-B cell population are able to bypass the preBCR checkpoint by premature κ-light chain recombination, which is similar to what we observed in the *IκBε<sup>-/-</sup>IκBβ<sup>-/-</sup>IκBα<sup>+/-</sup>* mice for immunoglobulin recombination analysis. Additionally, in the spleen of *IκBε<sup>-/-</sup>IκBβ<sup>-/-</sup>IκBα<sup>+/-</sup>RelA<sup>+/-</sup>* mice, we have repetitively observed a robust B220<sup>+</sup>CD19<sup>+</sup> population, which suggested there can be more B-1 cell progenitor cells by the induction of partial dysregulation of NFκB dynamic control. Therefore, it would be interesting to observe whether there is correlation between NFκB dynamic control and the formation of B-1 B cells in fetal and adult B lymphopoiesis.

### NFκB dynamic control and cell fate decision in early lymphoid progenitor cells

Based on what we observed in scRNAseq analysis, in the gene ontology analysis on upregulated genes across different clusters we found frequent enrichment on antigen-presenting mechanisms and MHC-associated GO terms. Additionally, in the Cluster A of IκB-mutant group, we have also identified a distinct cluster that is enriched in Sox-family binding motifs. In our CLP ex vivo experiments, we have also observed more non-B lineage cell emerged from the CLP differentiation, which suggested the *IκBε<sup>-/-</sup>IκBβ<sup>-/-</sup>IκBα<sup>+/-</sup>* genetic background may have altered the cell fate decision. As previous literature has indicated Fraction A still retain the potential of committing to non-B lineage (Welner et al., 2008), it would be interesting to investigate whether the dysregulation in RelA dynamics would alter the decision on cell fate, including lineage commitment and self-renewal capacity.

## **NFκB dynamic control as therapeutic target for B acute lymphoblastic leukemia treatment (B-ALL)**

According to the motif enrichment analysis in the mice with dysregulated NFκB dynamic control, the genes enriched with Elk transcription factor binding motif is downregulated in Cluster B and C'. As enhanced Elk activation account for ~30% of the mutant in B-ALL patients (Irving et al., 2014; Knight and Irving, 2014), reducing Elk transcriptional activities may be beneficial to the B-ALL treatment. Additionally, since dysregulated RelA can accelerate the transition from Fraction B to Fraction D, it is possible that by targeting the dynamic control of NFκB in the pro-B cell of pro-B-ALL, we will be able to drive the cell exiting the proliferative state and enter differentiation toward the downstream population.

## **Dysregulated NFκB dynamics mutant mice as a potential inflammation-associated aging model**

As chronic inflammation is known to constitutively activating NFκB canonical signaling and alter the outputs of hematopoiesis (Lawrence, 2009; Orkin et al., 2008; Chung and Park, 2017; Pietras, 2017; Haas et al., 2018 ), we wonder whether our current mice model with genetic abrogation of major canonical IκBs may serve as an alternative and less variable model than the current low-dose LPS injected murine experimental model to study the impact of inflammation-associated aging on hematopoietic stem and progenitors.

# References

- Alcamo, E., Hacohen, N., Schulte, L.C., Rennert, P.D., Hynes, R.O., and Baltimore, D. (2002). Requirement for the NF- $\kappa$ B Family Member RelA in the Development of Secondary Lymphoid Organs. *J. Exp. Med.* *195*, 233–244.
- Almaden, J.V, Liu, Y.C., Yang, E., Otero, D.C., Birnbaum, H., Davis-Turak, J., Asagiri, M., David, M., Goldrath, A.W., Hoffmann, A. (2016). B-cell survival and development controlled by the coordination of NF- $\kappa$ B family members RelB and cRel. *Blood* *127*, 1276–1286.
- Balistreri, C.R., Candore, G., Accardi, G., Colonna-Romano, G., and Lio, D. (2013). NF- $\kappa$ B pathway activators as potential ageing biomarkers: targets for new therapeutic strategies. *Immun. Ageing* *10*, 24.
- Balkhi, M.Y., Willette-Brown, J., Zhu, F., Chen, Z., Liu, S., Guttridge, D.C., Karin, M., and Hu, Y. (2012). IKK $\alpha$ -mediated signaling circuitry regulates early B lymphopoiesis during hematopoiesis. *Blood* *119*, 5467–5477.
- Beerman, I., Bhattacharya, D., Zandi, S., Sigvardsson, M., Weissman, I.L., Bryder, D., and Rossi, D.J. (2010a). Functionally distinct hematopoietic stem cells modulate hematopoietic lineage potential during aging by a mechanism of clonal expansion. *Proc. Natl. Acad. Sci.* *107*, 5465–5470.
- Beerman, I., Maloney, W.J., Weissmann, I.L., and Rossi, D.J. (2010b). Stem cells and the aging hematopoietic system. *Curr. Opin. Immunol.* *22*, 500–506.
- Beg, A.A., Sha, W., Bronsont, R.T., Ghosh, S., and Baltimore, D. (1995). Embryonic lethality and liver degeneration in mice lacking the RelA component of NF- $\kappa$ B. *Nature* *376*, 167–170.
- Busch, K., Klapproth, K., Barile, M., Flossdorf, M., Holland-Letz, T., Schlenner, S.M., Reth, M., Höfer, T., and Rodewald, H.-R. (2015). Fundamental properties of unperturbed haematopoiesis from stem cells in vivo. *Nature* *518*, 542–546.
- Cain, D., Kondo, M., Chen, H., and Kelsoe, G. (2009). Effects of acute and chronic inflammation on B-cell development and differentiation. *J. Invest. Dermatol.* *129*, 266–277.

Carrà, G., Torti, D., Crivellaro, S., Panuzzo, C., Taulli, R., Cilloni, D., Guerrasio, A., Saglio, G., and Morotti, A. (2016). The BCR-ABL/NF- $\kappa$ B signal transduction network: A long lasting relationship in Philadelphia positive Leukemias. *Oncotarget* *7*, 66287–66298.

Chien, Y., Scuoppo, C., Wang, X., Fang, X., Balgley, B., Bolden, J.E., Premrirut, P., Luo, W., Chicas, A., Lee, C.S., Kogan S.C., Lowe S.W., (2011). Control of the senescence-associated secretory phenotype by NF- $\kappa$ B promotes senescence and enhances chemosensitivity. *Genes Dev.* *25*, 2125–2136.

Chung, S.S., and Park, C.Y. (2017). Aging, hematopoiesis, and the myelodysplastic syndromes. *Hematology* *2017*, 73–78.

Ciabattini, A., Nardini, C., Santoro, F., Garagnani, P., Franceschi, C., and Medaglini, D. (2018). Vaccination in the elderly: The challenge of immune changes with aging. *Semin. Immunol.* *40*, 83–94.

Clark, M.R., Mandal, M., Ochiai, K., and Singh, H. (2013). Orchestrating B cell lymphopoiesis through interplay of IL-7 receptor and pre-B cell receptor signalling. *Nat. Rev. Immunol.* *14*, 69–80.

Claudio, E., Saret, S., Wang, H., and Siebenlist, U. (2009). Cell-autonomous role for NF- $\kappa$ B in immature bone marrow B cells. *J. Immunol.* *182*, 3406–3413.

Dorshkind, K., and Montecino-Rodriguez, E. (2007). Fetal B-cell lymphopoiesis and the emergence of B-1-cell potential. *Nat. Rev. Immunol.* *7*, 213–219.

Dorshkind, K., Montecino-Rodriguez, E., and Signer, R.A.J. (2009). The ageing immune system: is it ever too old to become young again? *Nat. Rev. Immunol.* *9*, 57–62.

Doulatov, S., Notta, F., Laurenti, E., and Dick, J.E. (2012). Hematopoiesis: A human perspective. *Cell Stem Cell* *10*, 120–136.

Feng, B., Cheng, S., Pear, W.S., and Liou, H.-C. (2004). NF- $\kappa$ B inhibitor blocks B cell development at two checkpoints. *Med. Immunol.* *3*, 1.

Franceschi, C., and Campisi, J. (2014). Chronic inflammation (inflammaging) and its potential contribution to age-associated diseases. *J. Gerontol. A. Biol. Sci. Med. Sci.* *69 Suppl 1*, S4-9.

- Frasca, D., Diaz, A., Romero, M., Landin, A.M., and Blomberg, B.B. (2011). Age effects on B cells and humoral immunity in humans. *Ageing Res. Rev.* *10*, 330–335.
- Gayoso, A. and Shor, J. (2018) DoubletDetection (Version v2.4). Zenodo. <http://doi.org/10.5281/zenodo.2678042>
- Geier, J.K., and Schlissel, M.S. (2006). Pre-BCR signals and the control of Ig gene rearrangements. *Semin. Immunol.* *18*, 31–39.
- Gerondakis, S., Grumont, R., Gugasyan, R., Wong, L., Isomura, I., Ho, W., and Banerjee, A. (2006). Unravelling the complexities of the NF- $\kappa$ B signalling pathway using mouse knockout and transgenic models. *Oncogene* *25*, 6781–6799.
- Goudeau, B., Huetz, F., Samson, S., DiSanto, J.P., Cumano, A., Beg, A., Israël, A., and Mémet, S. (2003). I $\kappa$ B $\alpha$ /I $\kappa$ B $\beta$  deficiency reveals that a critical NF- $\kappa$ B dosage is required for lymphocyte survival. *Proc. Natl. Acad. Sci. U. S. A.* *100*, 15800–15805.
- Grossmann, M., Metcalf, D., Merryfull, J., Beg, A., Baltimore, D., and Gerondakis, S. (2002). The combined absence of the transcription factors Rel and RelA leads to multiple hemopoietic cell defects. *Proc. Natl. Acad. Sci.* *96*, 11848–11853.
- Guerrettaz, L.M., Johnson, S.A., and Cambier, J.C. (2008). Acquired hematopoietic stem cell defects determine B-cell repertoire changes associated with aging. *Proc. Natl. Acad. Sci.* *105*, 11898–11902.
- Guo, F., Tänzer, S., Busslinger, M., Weih, F., De, W., and Ta, S. (2012). Lack of nuclear factor- $\kappa$ B2 / p100 causes a RelB-dependent block in early B lymphopoiesis. *112*, 551–559.
- Guzman, M.L., Neering, S.J., Upchurch, D., Grimes, B., Howard, D.S., Rizzieri, D.A., Luger, S.M., and Jordan, C.T. (2001). Nuclear factor- $\kappa$ B is constitutively activated in primitive human acute myelogenous leukemia cells. *Blood* *98*, 2301–2307.
- Haas, S., Trumpp, A., and Milsom, M.D. (2018). Causes and Consequences of Hematopoietic Stem Cell Heterogeneity. *Cell Stem Cell* *22*, 627–638.

Hardy R.R., Carmack C.E., Shinton S.A., Kemp J.D., and Hayakawa K. (1991). Resolution and Characterization of Pro-B and Pre-Pro-B Cell Stages in Normal Mouse Bone Marrow. *Imaging* 173.

Hardy, R.R., and Hayakawa, K. (2001). B cell development pathways. 595–621.

Hendriks, R.W., and Middendorp, S. (2004). The pre-BCR checkpoint as a cell-autonomous proliferation switch. *Trends Immunol.* 25, 249–256.

Hoffmann, A., Levchenko, A., Scott, M.L., and Baltimore, D. (2002). The I $\kappa$ B-NF- $\kappa$ B signaling module: Temporal control and selective gene activation. *Science* (80-. ). 298, 1241–1245.

Holmes, M.L., Carotta, S., Corcoran, L.M., and Nutt, S.L. (2006). Repression of Flt3 by Pax5 is crucial for B-cell lineage commitment. *Genes Dev.* 20, 933–938.

Horwitz, B.H., Scott, M.L., Cherry, S.R., Bronson, R.T., and Baltimore, D. (1997). Failure of lymphopoiesis after adoptive transfer of NF- $\kappa$ B-deficient fetal liver cells. *Immunity* 6, 765–772.

Irving, J., Matheson, E., Minto, L., Blair, H., Case, M., Halsey, C., Swidenbank, I., Ponthan, F., Kirschner-Schwabe, R., Groeneveld-Krentz, S., Hof J., Allan J., Harrison C., Vormoor J., von Stackelberg A., Eckert C. (2014). Ras pathway mutations are prevalent in relapsed childhood acute lymphoblastic leukemia and confer sensitivity to MEK inhibition. *Blood* 124, 3420–3430.

Isobe, K., Nishio, N., and Hasegawa, T. (2017). Immunological aspects of age-related diseases. *World J. Biol. Chem.* 8, 129.

Jimi, E., Phillips, R.J., Rincon, M., Voll, R., Karasuyama, H., Flavell, R., and Ghosh, S. (2005). Activation of NF- $\kappa$ B promotes the transition of large, CD43<sup>+</sup> pre-B cells to small, CD43<sup>-</sup> pre-B cells. *Int. Immunol.* 17, 815–825.

Jung, D., and Alt, F.W. (2004). Review Unraveling V(D)J Recombination: Insights into Gene Regulation Mendelian fashion. Based on these and other observations, Dreyer and Bennett described a theoretical basis for the generation of antigen receptors through an un. *Cell* 116, 299–311.

- Keenan, R.A., DeRiva, A., Corleis, B., Hepburn, L., Licence, S., Winkler, T.H., and Mårtensson, I.L. (2008). Censoring of autoreactive B cell development by the pre-B cell receptor. *Science* *321*, 696–699.
- Kordes, U., Krappmann, D., Heissmeyer, V., Ludwig, W.D., and Scheidereit, C. (2000). Transcription factor NF- $\kappa$ B is constitutively activated in acute lymphoblastic leukemia cells. *Leukemia* *14*, 399–402.
- Koushik, S.V., Chen, H., Thaler, C., Puhl, H.L., and Vogel, S.S. (2006). Cerulean, venus, and venusY67C FRET reference standards. *Biophys. J.* *91*, L99–L101.
- Knight, T., and Irving, J.A.E. (2014). Ras/Raf/MEK/ERK Pathway Activation in Childhood Acute Lymphoblastic Leukemia and Its Therapeutic Targeting. *Front. Oncol.* *4*, 1–12.
- Larbi, A., Franceschi, C., Mazzatti, D., Solana, R., Wikby, A., and Pawelec, G. (2008). Aging of the Immune System as a Prognostic Factor for Human Longevity. *Physiology* *23*, 64–74.
- Lawrence, T. (2009). The nuclear factor NF- $\kappa$ B pathway in inflammation. *Cold Spring Harb. Perspect. Biol.* *1*.
- Linton, P.J., and Dorshkind, K. (2004). Age-related changes in lymphocyte development and function. *J.* *5*, 133–139.
- Liu, G.J., Cimmino, L., Jude, J.G., Hu, Y., Witkowski, M.T., McKenzie, M.D., Kartal-Kaess, M., Best, S.A., Tuohey, L., Liao, Y., Shi W., Mullighan C.G., Farrar M.A., Nutt S.L., Smyth G.K., Zuber J., Dickins R.A. (2014). Pax5 loss imposes a reversible differentiation block in B-progenitor acute lymphoblastic leukemia. *Genes Dev.* *28*, 1337–1350.
- Liu, Z., Hazan-Halevy, I., Harris, D.M., Li, P., Ferrajoli, A., Faderl, S., Keating, M.J., and Estrov, Z. (2011). STAT-3 activates NF- $\kappa$ B in chronic lymphocytic leukemia cells. *Mol. Cancer Res.* *9*, 507–515.
- Lopez-Guerra, M., and Colomer, D. (2010). NF- $\kappa$ B as a therapeutic target in chronic lymphocytic leukemia. *Expert Opin. Ther. Targets* *14*, 275–288.
- Mårtensson, I.L., and Ceredig, R. (2000). Role of the surrogate light chain and the pre-B-cell receptor in mouse B-cell development. *Immunology* *101*, 435–441.

- Melamed, D., and Scott, D.W. (2012). Aging and neoteny in the B lineage. *Blood* *120*, 4143–4149.
- Melchers, F. (2015). Checkpoints that control B cell development. *125*, 2203–2210.
- Mitchell, S., Mercado, E.L., Adelaja, A., Ho, J.Q., Cheng, Q.J., Ghosh, G., and Hoffmann, A. (2019). An NF $\kappa$ B activity calculator to delineate signaling crosstalk: Type I and II interferons enhance NF $\kappa$ B via distinct mechanisms. *Front. Immunol.* *10*, 1–16.
- Montecino-Rodriguez, E., Dorshkind, K., Clark, R.G., and Powell-Braxton, L. (1997). Primary B cell development is impaired in mice with defects of the pituitary/thyroid axis. *J. Immunol.* *159*, 2712–2719.
- O’Dea, E., and Hoffmann, A. (2009). NF- $\kappa$  B signaling. *Wiley Interdiscip. Rev. Syst. Biol. Med.* *1*, 107–115.
- Ratliff, M., Alter, S., Mcavoy, K., Frasca, D., Wright, J.A., Zinkel, S.S., Khan, W.N., Blomberg, B.B., and Riley, R.L. (2015). In aged mice, low surrogate light chain promotes pro-B-cell apoptotic resistance, compromises the PreBCR checkpoint, and favors generation of autoreactive, phosphorylcholine-specific B cells. 382–390.
- Orkin S.H., and Zon L.I. (2008). Hematopoiesis: an evolving paradigm for stem cell biology. *Cell* *132*, 631–644.
- Pera, A., Campos, C., López, N., Hassouneh, F., Alonso, C., Tarazona, R., and Solana, R. (2015). Immunosenescence: Implications for response to infection and vaccination in older people. *Maturitas* *82*, 50–55.
- Pietras, E.M., Reynaud, D., Kang, Y.A., Carlin, D., Calero-Nieto, F.J., Leavitt, A.D., Stuart, J.A., Göttgens, B., and Passegué, E. (2015). Functionally Distinct Subsets of Lineage-Biased Multipotent Progenitors Control Blood Production in Normal and Regenerative Conditions. *Cell Stem Cell* *17*, 35–46.
- Pietras, E.M. (2017). Inflammation: A key regulator of hematopoietic stem cell fate in health and disease. *Blood* *130*, 1693–1698.
- Prendes, M., Zheng, Y., and Beg, A.A. (2003). Regulation of Developing B Cell Survival by RelA-Containing NF- $\kappa$ B Complexes. *J. Immunol.* *171*, 3963–3969.

Riley, R.L., Khomtchouk, K., and Blomberg, B.B. (2018). Inflammatory Immune Cells May Impair the PreBCR Checkpoint, Reduce New B Cell Production, and Alter the Antibody Repertoire in Old Age. *Exp. Gerontol.* *105*, 87–93.

Salminen, A., Huuskonen, J., Ojala, J., Kauppinen, A., Kaarniranta, K., and Suuronen, T. (2008). Activation of innate immunity system during aging: NF- $\kappa$ B signaling is the molecular culprit of inflamm-aging. *Ageing Res. Rev.* *7*, 83–105.

Shih, V.F.S., Tsui, R., Caldwell, A., and Hoffmann, A. (2011). A single NF $\kappa$ B system for both canonical and non-canonical signaling. *Cell Res.* *21*, 86–102.

Smith, E., and Sigvardsson, M. (2004). The roles of transcription factors in B lymphocyte commitment, development, and transformation. *J. Leukoc. Biol.* *75*, 973–981.

Sung, M.H., Li, N., Lao, Q., Gottschalk, R.A., Hager, G.L., and Fraser, I.D.C. (2014). Switching of the relative dominance between feedback mechanisms in lipopolysaccharide-induced NF- $\kappa$ B signaling. *Sci. Signal.* *7*, 1–12.

Terwilliger, T., and Abdul-Hay, M. (2017). Acute lymphoblastic leukemia: a comprehensive review and 2017 update. *Blood Cancer J.* *7*, e577.

Van der Put, E., Sherwood, E.M., Blomberg, B.B., and Riley, R.L. (2003). Aged mice exhibit distinct B cell precursor phenotypes differing in activation, proliferation and apoptosis. *Exp. Gerontol.* *38*, 1137–1147.

Van Epps, H.L. (2006). Bringing order to early B cell chaos. *J. Exp. Med.* *203*, 1389.

Velten, L., Haas, S.F., Raffel, S., Blaszkiewicz, S., Islam, S., Hennig, B.P., Hirche, C., Lutz, C., Buss, E.C., Nowak, D., et al. (2017). Human haematopoietic stem cell lineage commitment is a continuous process. *Nat. Cell Biol.* *19*, 271–281.

Werner, S.L., Barken, D., and Hoffmann, A. (2005). Stimulus specificity of gene expression programs determined by temporal control of IKK activity. *Science* (80-. ). *309*, 1857–1861.

Welner, R.S., Pelayo, R., and Kincade, P.W. (2008). Evolving views on the genealogy of B cells. *Nat Rev Immunol* *8*, 95–106.

Wolock S.L., Lopez R., Klein A.M. (2019). Scrublet: Computational Identification of Cell Doublets in Single-Cell Transcriptomic Data. *Cell Syst.* *8*(4):281-291.

Wong, Jason B. and Hewitt, Susannah L. and Heltemes-Harris, Lynn M. and Mandal, Malay and Johnson, Kristen and Rajewsky, Klaus and Koralov, Sergei B. and Clark, Marcus R. and Farrar, Michael A. and Skok, Jane, B-1a Cells Acquire Their Unique Characteristics by Bypassing the Pre-BCR Selection Stage (April 30, 2019). Available at SSRN: <https://ssrn.com/abstract=3380258> or <http://dx.doi.org/10.2139/ssrn.3380258>

Zhang, Q., Lenardo, M.J., and Baltimore, D. (2017). 30 Years of NF- $\kappa$ B: A Blossoming of Relevance to Human Pathobiology. *Cell* 168, 37–57.

Zhou, J., Ching, Y.Q., and Chng, W.J. (2015). Aberrant nuclear factor-kappa B activity in acute myeloid Leukemia: From molecular pathogenesis to therapeutic target. *Oncotarget* 6, 5490–5500.